

CONTROLLING CATALYST ACTIVE SITES USING SELF-ASSEMBLED MONOLAYERS

by

Carolyn Schoenbaum

B.S., University of Washington, 2009

A thesis submitted to the

Faculty of the Graduate School of the

University of Colorado in partial fulfillment

of the requirement for the degree of

Doctor of Philosophy

Department of Chemical and Biological Engineering

2014

This thesis entitled:
Controlling Catalyst Active Sites Using Self-Assembled Monolayers
written by Carolyn Ann Schoenbaum
has been approved for the Department of Chemical and Biological Engineering

J. Will Medlin

Daniel K. Schwartz

Date _____

The final copy of this thesis has been examined by the signatories, and we find that both the content and the form meet acceptable presentation standards of scholarly work in the above mentioned discipline.

ABSTRACT

Schoenbaum, Carolyn A. (Ph.D., Chemical and Biological Engineering)

Controlling Catalyst Active Sites Using Self-Assembled Monolayers

Thesis directed by Associate Professor J. Will Medlin and Daniel K. Schwartz

Elucidating the site requirements for reactions over heterogeneous catalysts can be challenging since, unlike their homogenous counterparts, the surfaces of these materials are comprised of a variety of diverse features where reactions can occur. Because there is strong evidence suggesting that reactions will occur at a specific type (or group) of active site(s), significant effort has been put forth in the field to try to determine the site requirements for particular reactions. Here, we report a new approach for controlling the availability of specific active sites on supported Pd/Al₂O₃ catalysts using alkanethiolate self-assembled monolayers (SAMs). SAMs form consistent and ordered structures on metal surfaces; these features were exploited to form monolayers that preferentially block or expose specific types of sites on catalyst particles.

The structure of the tail moiety played an important role in the overall organization of the resulting monolayer and was tuned to control the types of active sites that were exposed on metal particle surfaces. Infrared spectroscopy using CO as a probe molecule was used to characterize site availability on the catalysts. A monolayer formed from a bulky caged molecule like 1-adamantanethiol (AT) restricted the availability of contiguous active sites on particle terraces with respect to the uncoated catalyst. Increasing the density of the monolayer using a linear alkanethiol like 1-octadecanethiol (C18) further restricted adsorption on terraces. For both of

these monolayers, adsorption at particle edges and steps was nearly unaffected but could be blocked by forming a high coverage monolayer from 1,2-benzene dithiol (BDT).

The relationship between monolayer spacing and reactivity dramatically depended on the structure of the reactant, even for small species. For example, employing a C18 monolayer reduced the rate of epoxybutane hydrogenation by nearly 3 orders of magnitude with respect to the unmodified catalyst, whereas hydrogenation of propionaldehyde was only reduced by a single order of magnitude. These results suggested 1) that site requirements for conversion of these two species were substantially different and 2) this modification approach could potentially be utilized to direct selectivity of more complex reactants where competing reaction pathways have different site requirements.

To demonstrate the feasibility of the latter hypothesis, this approach was utilized for the hydrogenation of furfural. On palladium catalysts, furfural tends to decarbonylate to produce furan and carbon monoxide. A competing process involves hydrogenation of the aldehyde to produce furfuryl alcohol and subsequent hydrodeoxygenation producing methylfuran. Site requirements for each pathway were investigated by comparing reactivity on uncoated, C18-coated and BDT-coated catalysts. Comparison between reaction rates and site availability suggested that decarbonylation occurred primarily on terrace sites while hydrodeoxygenation occurred on particle steps and edges. Aldehyde hydrogenation, and its reverse process of alcohol dehydrogenation, was found to occur on both terrace or edge sites, with the dominant pathway dependent on surface coverage as determined by reaction conditions.

ACKNOWLEDGEMENTS

I would first like to thank both of my advisors, Will Medlin and Dan Schwartz, for their tremendous guidance and support over the past five years. They have always encouraged me to pursue interesting and challenging scientific questions and have provided the tools to allow me to achieve my goals. They have both taught me so much, and I feel truly fortunate to have had the opportunity to work with both of them. I would also like to thank the members of my committee: Charles Musgrave, Joel Kaar, and Garry Rumbles. They not only provided helpful feedback directly pertaining to the work presented in this thesis, but they also provided significant mentorship and guidance toward my overall professional development.

Next, I would like to thank all of the past and present members of both the Schwartz and Medlin groups that I have had the pleasure of working with. It has been amazing to have such a wonderful group of colleagues to work alongside every day. I'd particularly like to acknowledge the Medliners who have been on this journey with me from the beginning: Rhea Williams, Simon Pang, and Matt Montemore. It has truly been an amazing trip with you all. I want to say a special thank you to Simon whom I've collaborated with on much of the work presented here and worked closely with over the past several years. Thank you for your thoughtful discussion, diligence, and friendship throughout this project. I'd like to thank Marykate O'Brien and Charles Hartman who performed a number of the experiments for this work and spent significant time maintaining and helping to improve equipment for the lab. I'd also like to thank Tania Tauer, Troy Gould, and Mike Griffin for their mentorship and friendship throughout this experience.

There are a number of individuals who spent considerable time providing guidance and instruction for different aspects of this work. I would like to thank Steve Marshall for teaching

me how to use and maintain all of the lab equipment and for showing me the tricks of the trade. I'd like to thank Rob Walder for all of his help teaching me how to design, build and automate equipment, a skill I will undoubtedly use in my future. I'd like to thank Hans Funke for his unwavering willingness to share his expertise (and equipment) with me whenever he could help. I'd also like to thank Dragan Mejic, Dana Hauschulz, and Maria Toscano-Leary for all of their patience and help in designing and building a number of complimentary pieces of equipment for the lab.

This work would not have been possible without the financial support from the US Department of Energy, Office of Science, Basic Energy Sciences Program, Chemical Sciences, Geosciences, and Biosciences Division (DE-FG02-10ER16206), and the US National Science Foundation (CHE-1149752). I'd also like to thank Phillips 66 and the Department of Education (GAANN) for partial financial support through graduate fellowships. In addition, I'd like to thank Samuel Tenney and Peter Sutter at Brookhaven National Laboratory Center for Functional Nanomaterials for beamtime and assistance at the National Synchrotron Light Source.

Finally, I would like to thank all of my friends and family for their incredible support. To my friends, the experiences we have shared together have resulted in friendships that will undoubtedly last a lifetime. To my fiancé, Kevin, thank you for your patience, support, and perspective which have been invaluable throughout the duration of this experience. And lastly to my parents, Gary and Kathy, I want to thank you for a lifetime of unconditional love and support. You have taught me that if you want something badly enough, and you try hard enough, you can achieve anything.

CONTENTS

CHAPTER

1. INTRODUCTION.....	1
1.1 Concepts in catalysis.....	1
1.2 Catalyst modifiers.....	6
1.3 Self-assembled monolayers.....	10
1.4 SAMs for enhancing catalytic performance.....	18
1.5 Experimental Methods.....	26
1.6 Thesis goals.....	34
1.7 References.....	34
2. CONTROLLING SURFACE CROWDING ON PD CATALYSTS WITH THIOLATE SELF-ASSEMBLED MONOLAYERS	42
2.1 Abstract.....	42
2.2 Introduction.....	43
2.3 Experimental methods.....	45
2.4 Results and discussion.....	46
2.5 Conclusions.....	64
2.6 References.....	65
3. DIRECTING REACTION PATHWAYS BY CATALYST ACTIVE-SITE SELECTION USING SELF-ASSEMBLED MONOLAYERS.....	69
3.1 Abstract.....	69

3.2	Introduction.....	70
3.3	Experimental methods.....	72
3.4	Results and discussion.....	77
3.5	Conclusions.....	85
3.6	References.....	85
4.	EFFECTS OF THIOL MODIFIERS ON THE KINETICS OF FURFURAL HYDROGENATION OVER PD CATALYSTS.....	89
4.1	Abstract.....	89
4.2	Introduction.....	90
4.3	Experimental methods.....	93
4.4	Results and discussion.....	97
4.5	Conclusions.....	113
4.6	References.....	114
5.	CONCLUSIONS AND FUTURE DIRECTIONS.....	117
5.1	Summary.....	117
5.2	Future directions.....	119
5.3	References.....	124
	BIBLIOGRAPHY.....	124
	APPENDIX A: LANGMUIR-HINSHELWOOD MODEL OF FURFURAL REACTION NETWORK.....	137

LIST OF TABLES

- 2-1. CO frequency assignments for uncoated, C18-modified, and AT-modified catalysts.....54
- 3-1. Selectivity to furfuryl alcohol enhanced at lower temperature and smaller conversion; selectivity to methylfuran enhanced at higher conversion. WHSV is reported in units of $(\text{mg furfural fed}) (\text{mg Pd})^{-1} \text{h}^{-1}$ 78
- 4-1. Apparent activation energies for processes involved in Scheme 4-1. DC and AH activation energies were determined using furfural as the reactant; ADH and HDO activation energies were determined using furfuryl alcohol as the reactant. The error reported is the standard error of the slope of the Arrhenius plot using a weighted linear regression.....107
- 4-2. Reaction orders for processes depicted in Scheme 4-1. Reaction order experiments for DC and AH were performed with furfural; experiments for ADH and HDO were performed with furfuryl alcohol. The numbers in parentheses represent the uncertainty in the least significant digit. The uncertainty is the standard error of the slope of the power law plot using a weighted linear regression.....108

LIST OF SCHEMES

2-1.	Proposed adsorption mechanism on thiol-modified surfaces. On C18 catalysts, adsorption primarily occurs in three-fold hollow and a single type of atop site at saturation coverage. On AT-coated catalysts, adsorption occurs on these same types of sites but has additional access to bridging and a second type of reactive, linear site upon increasing coverage....	60
3-1.	Reaction pathways for furfural hydrogenation.....	70
4-1.	Furfural hydrogenation pathways over Pd.....	92
4-2	Proposed reaction pathways for furfural and furfuryl alcohol on uncoated and thiol-coated catalysts. On uncoated catalysts, the reactants adsorbed in a flat-lying conformation on terraces or in an upright conformation on both terraces and edges; reactants were restricted to the upright conformation on both terraces and edges when the thiol coating was present.....	113

LIST OF FIGURES

1-1.	Structure of an fcc metal. a) Each layer shows hexagonal symmetry and sequentially sits in the hollows of the underlying metal layer creating a repeating “ABC-ABC” structure. b) The resulting structure has cubic symmetry.....	3
1-2.	Depictions of the (100) and (111) planes for a cubo-octahedron shaped fcc metal particle. The Miller Indices, (xyz), are used for specifying the crystal plane. These numbers refer to the vector normal to the plane in reciprocal space. Sites located at particle edges and terraces are also highlighted.....	5
1-3.	Different classes of organic modification techniques including dendrimer encapsulated, polymer protected, and ligand-protected.....	8
1-4.	Basic structure of alkanethiolate monolayer on a supported metal surface.....	11
1-5.	Simplified schematic of SAM formation involving a “vapor” phase, striped or disordered liquid-like phase, and a solid, high density phase.....	13
1-6.	$(\sqrt{3}\times\sqrt{3})R30$ adsorption geometry of sulfur (red) on metal fcc(111) surface. The length of the adsorbed sulfur unit cell is $\sqrt{3} \times$ and is rotated 30° with respect to the underlying metal unit cell.....	14
1-7.	Recent approaches for tuning catalytic particles using SAMs.....	19
1-8.	a) Proposed adsorption geometry of cinnamaldehyde (ball-and-stick) on Pt_3Co (100) modified with oleylamine (line). b) Selectivity for cinnamyl alcohol (white), hydrocinnamaldehyde (crosshatch), and hydrocinnamyl alcohol (gray) at nearly 100% conversion in the hydrogenation of cinnamaldehyde with different amine-capped Pt_3Co catalysts shown in order from longest (left) to shortest (right) tail length.....	20
1-9.	a) Plots of the adsorption energies of 4-octyne, cis-4-octene, trans-4-octene, and 1-octylamine on clean and 1-octylamine modified Pt (111) surface as a function of octylamine coverage. Dash red circle highlights that at high enough amine coverage, alkylamines adsorb more readily than the alkenes. b) Depiction of the structures used in DFT calculations.....	24
1-10.	Examples of mixed monolayers and SAM-based substrates.....	26
1-11.	DRIFTS cell used for gas dosing applications including a) the gas-tight dome, b) inside praying mantis accessory showing the light path of IR and c) the whole system orientation.....	28

1-12.	Gas-phase reactor system. Both feed and product streams could be monitored using gas chromatography (Agilent 7890A) equipped with a flame ionization detector.....	30
1-13.	Comparison of hydrocarbon stretching regime of two C18-modified catalysts prepared via different methods. (Bottom) The previously used method involved pouring thiolate solution directly over dilute catalyst in the reactor tube without mixing. (Top) The revised method involved removing catalyst from reactor tube to deposit in a beaker of thiol solution with an additional wash step to remove loosely bound thiol species from the catalyst.....	33
2-1.	DRIFT spectra and structure of (a) 1-adamantanethiol and (b) 1-octadecanethiol on a Pd surface.....	48
2-2.	Hydrogenation rates of acetylene and ethylene on uncoated, AT, and C18 coated Pd/Al ₂ O ₃ catalysts.....	49
2-3.	DRIFT spectra for samples before and after (a) acetylene and (b) ethylene hydrogenation on (i) C18 (ii) AT (iii) and unmodified catalysts. Solid and dashed lines are shown for samples before and after 1 hour of hydrocarbon exposure, respectively.....	50
2-4.	Unit cells for (a) C18 and (b) AT monolayers on fcc(111) surfaces.....	51
2-5.	CO DRIFTS on (a) unmodified (b) AT modified, and (c) C18 modified Pd/Al ₂ O ₃ catalysts. The series of spectra were obtained at constant temperature (298 K) with CO pressure increasing from 0.15 to 300 torr (solid black line). (d) Integrated peak areas for multi-coordinated and linear bound species for AT and C18 surfaces.....	53
2-6.	Linearized Langmuir isotherms for AT and C18 surfaces.....	57
2-7.	Reaction rates for mono- and bi-functional reactants on C18 and AT surfaces. Rates have been normalized to rate on unmodified surface. Circled functional groups indicate that rates are reported for the hydrogenation of the specified group.....	61
3-1.	Representative TEM image and particle size distribution for 5 wt% (top) and 1 wt% (bottom) Pd/Al ₂ O ₃	73
3-2.	Representative kinetic plots of conversion and selectivity as a function of time on stream for uncoated 5 wt% Pd/Al ₂ O ₃ (left), and C18-coated 5 wt% Pd/Al ₂ O ₃ (right). Uncoated catalysts deactivate quickly; on the other hand, the SAM coating stabilizes conversion..	75
3-3.	Left: Selectivity to furan does not significantly increase for the C18-coated 5 wt% Pd/Al ₂ O ₃ catalyst, indicating that the SAM layer is still intact. Furfural conversion for the uncoated catalyst at 4 hours and 15 hours are 12.0% and 0.5%, respectively. Furfural conversion for the C18-coated catalyst at 4 hours and 15 hours are 12.2% and 4.9%, respectively. Right: DRIFT spectra for the methylene stretching region on the C18-coated	

	5 wt% Pd/Al ₂ O ₃ catalyst, before (dashed) and after (solid) 15 hours under reaction conditions.....	76
3-4.	Gas phase hydrogenation of furfural. a) Product selectivity for furfural hydrogenation over uncoated and alkanethiolate SAM coated Pd/Al ₂ O ₃ catalysts. b) Rate of production normalized by number of surface sites on the uncoated catalyst. Hydrogenations were carried out continuously at 190°C at a 25:1 molar ratio of H ₂ to furfural. Selectivity and rate are reported at (13 ± 1.8)% conversion of furfural fed. Error bars indicate s.d. of 12 repeated measurements of product concentration.....	77
3-5.	DRIFT spectra for uncoated and SAM coated catalysts. CO stretch region for uncoated and alkanethiolate SAM coated a) 5 wt% (adapted from ref. 15) and b) 1 wt% Pd/Al ₂ O ₃ catalysts. For linear adsorption on top sites, the lower wavenumber features are associated with adsorption at steps and edges whereas higher wavenumber features are indicative of adsorption on terrace sites. ²⁵ DRIFT spectra for samples after furfural exposure. c) Hydrocarbon stretching region for uncoated, AT, and C18 catalysts. Dashed and solid lines are shown for samples before and after exposure, respectively. d) CO production on the uncoated, AT, and C18 catalysts after exposure to furfural.....	81
3-6.	CO DRIFTS for unmodified 1% Pd/Al ₂ O ₃ showing the evolution of peaks associated with CO binding in three-fold and linear configurations.....	82
3-7.	Proposed schematic depicting <i>active-site selection</i> using self-assembled monolayers of octadecanethiol and adamantanethiol. On C18-modified surfaces, furfural binds upright on step edges and defects while on AT-modified surfaces, furfural can lie flat on a terrace.....	83
4-1.	Infrared spectra of the hydrocarbon stretching region for C18 and BDT monolayers on 5 wt% Pd/Al ₂ O ₃ catalysts. The feature found at 2923 cm ⁻¹ for the C18 catalyst was attributed to a CH ₂ methylene stretch. The feature at 3050 cm ⁻¹ for BDT was attributed to a CH stretch of the phenyl moiety.....	94
4-2.	Infrared spectra of bound CO (2,000 mTorr exposure) on (top) 5 wt% Pd/Al ₂ O ₃ particles used in previous study compared to (bottom) new 5 wt% Pd/Al ₂ O ₃ particles used in this study.....	98
4-3.	X-ray photoelectron spectra (open circles) in the S 2p region taken in situ under reaction conditions for: (a), (b) the C18-coated catalyst and (c), (d) the BDT-coated catalyst. Spectra (a) and (c) were taken upon introduction of gases and heating to 190°C. Spectra (b) and (d) were obtained after exposure to reaction conditions for two hours. S 2p _{3/2} /2p _{1/2} doublet separation = 1.19 ± 0.02 eV (solid/dashed colored lines).....	99
4-4.	Turnover frequencies for various products from (a) furfural hydrogenation (y _F = 0.010 and y _{H₂} = 0.250) and (b) furfuryl alcohol hydrogenation (y _{FA} = 0.001 and y _{H₂} = 0.300) over uncoated, C18-coated and BDT-coated 5 wt% Pd/Al ₂ O ₃ . Turnover frequencies are reported per surface Pd atom (site ⁻¹ s ⁻¹) where the number of surface atoms was determined from the clean, uncoated catalyst. Selectivity and rate are reported under 10%	

	conversion of reactant fed. Error bars indicate the standard deviation of five repeated measurements of product concentration over the course of an hour.....	101
4-5.	CO stretching region for uncoated, C18- and BDT-modified 5 wt% Pd/Al ₂ O ₃ after exposure to reaction conditions for two hours.....	103
4-6.	Differential rates of (a) decarbonylation and aldehyde hydrogenation of furfural and (b) alcohol dehydrogenation and hydrodeoxygenation of furfuryl alcohol. For the furfural reactions, the mole fractions of furfural and hydrogen were $y_F = 0.010$ and $y_{H_2} = 0.400$, respectively. For the furfuryl alcohol reactions, the mole fractions of furfuryl alcohol and hydrogen were $y_{FA} = 0.001$ and $y_{H_2} = 0.400$, respectively.....	104
5-1.	The relative distribution of the adsorption sites for an idealized cubo-octahedron Pd particle as a function of particle diameter.....	119
5-2.	Additional caged modifiers that could potentially be used to control modifier density..	121
5-3.	Schematic of RAIRS setup. S- polarized radiation is oriented perpendicular to the plane of incidence whereas p- polarized radiation is oriented parallel to this plane.....	122
5-4.	Dosing system built for RAIRS.....	123
A-1.	Best fit rate parameters for ϕ terms. ϕ_{AH} and ϕ_{HDO} have units of ($s^{-1} \times atm^{-3/2}$) and ϕ_{ADH} and ϕ_{DC} have units of ($s^{-1} \times atm^{-1}$).....	140

CHAPTER 1

Introduction

1.1 Concepts in catalysis

The role of catalysis in our society is crucial. In fact, it is estimated that over 90% of all commercially produced chemical products require the use of catalysts at some point during their manufacture¹. The major benefit of these materials is their ability to accelerate the rate of a reaction by providing an alternative pathway with a lower activation barrier. For example, a gaseous mixture of hydrogen and oxygen may be stable for years at room temperature; however, in the presence of platinum, the mixture can explode². The rate at which a catalyst transforms chemical species is referred to as the *activity* of the catalyst. While catalysts enhance the overall rate of conversion of a reactant species, several pathways are often attainable under particular reaction conditions. Thus, reactants with multiple functional groups can react to produce several different products. A catalyst that improves the rate of the desired reaction product over the undesirable ones is said to be *selective*, where selectivity is more specifically defined as the rate of a reaction along a particular pathway divided by the sum of the rates along all reaction pathways³. A major aim of the field of heterogeneous catalysis is to design and synthesize catalytic materials that exhibit both high activity and high selectivity.

Typically, catalysts are classified as either homogeneous or heterogeneous depending on the phase of the reactant with respect to the catalytic material. For a homogeneous catalyst, the catalyst is present in the same phase as the reactants. A wide variety of homogeneous catalysts are known, including metal complexes, metal ions, organometallic complexes, organic molecules, and enzymes. However, the term homogeneous catalyst is most commonly associated with organometallic or coordination complexes. A heterogeneous catalytic process involves more than one phase; often the catalyst is a solid and the reactants are either in the liquid or gas phases. Although many reactions can be promoted with either homogeneous or heterogeneous catalysts, the latter generally allows for less waste, fewer toxic reagents, and easier retrieval and recycling of the catalyst⁴ and are the focus of the work presented in this thesis.

In heterogeneous catalysis, the material chosen depends strongly on the application. However, transition metals are active materials for a number of important hydrogenation reactions⁵. The transition metal outermost d-orbitals are incompletely filled so they can easily donate or withdraw electrons, a property that is very important with regards to the inherent activity of the material. In particular, reactant molecules tend to bind very strongly to transition metals that have few filled d orbitals. Thus, the strength of adsorption tends to decrease from left to right along the Periodic Table as d-orbitals become filled. At some intermediate point, the molecules bind “just the right amount” such that they are mobile and strongly interacting with the surface, but not so strongly that products cannot desorb from the surface following reaction. This concept is known as the “Sabatier principle”, and while it is indeed an oversimplification of a complex concept, it provides a helpful initial framework for thinking about catalytic activity.

The crystalline structure of the metal is another (related) aspect that plays a central role in governing catalytic performance. For transition metals, the most common bulk structures exist as

body-centered cubic (bcc), face-centered cubic (fcc), or hexagonal close packed (hcp) crystals. Many of the commonly used transition metal catalysts form an fcc bulk structure. This structure can be envisioned as stacked layers of atoms arranged in a close-packed hexagonal array; where the atoms of each additional layer preferentially sit in hollows of the first layer in what is commonly referred to as an “ABC-ABC” packing sequence. The resulting three-dimensional structure has cubic symmetry and is shown in Figure 1-1.

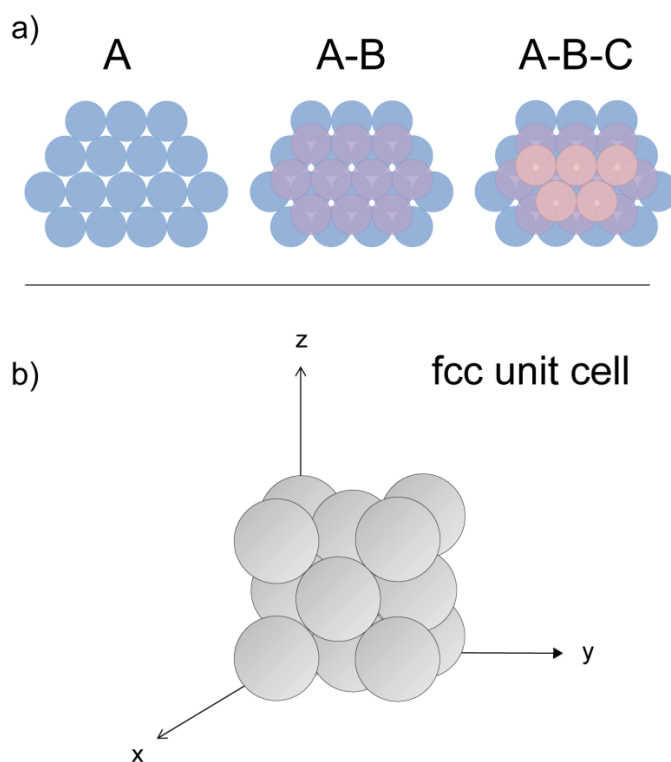


Figure 1-1. Structure of an fcc metal. a) Each layer shows hexagonal symmetry and sequentially sits in the hollows of the underlying metal layer creating a repeating “ABC-ABC” structure. b) The resulting structure has cubic symmetry.

An fcc metal particle will then exhibit different types of surface facets based on this crystalline structure. These different facets can be thought of as the resulting planes that would be exposed

if the bulk crystal were to be sliced in a particular planar direction. The most commonly studied are typically the (111) and (100) due to their thermodynamic stability.

Because catalytic reactions occur on the *surface* of the metal, and not generally within the bulk of the material, enhancing the surface area of the catalyst is of practical importance for most industrial applications. This is typically achieved by depositing small metal particles on an inert, high surface area support. The resulting shape of the supported metal particles is generally governed by a compromise between exposing the lowest energy surface planes, which for an fcc metal is the (111), and minimizing the surface area of the particle, which would result in a particle of spherical shape⁵. The relative surface energies of different crystal planes determine the equilibrium shape which can be predicted from knowledge of the energy terms by use of the Wulff construction⁶. One possibility that offers a compromise between exposing the lower surface energy planes and minimizing the particle surface area is generated by truncating the vertices of an octahedron forming what is referred to as a cubo-octahedron. This shape is often used as a conceptual model for particles on catalyst supports. As the size of the particle decreases, a higher fraction of the exposed sites are located at particle edges and steps whereas the opposite is true for atoms located on particle terraces⁷. The structure of a cubo-octahedral metal cluster and the relative positions of the (100) and (111) planes for this particle shape are shown together in Figure 1-2.

A number of studies have demonstrated that certain reaction pathways preferentially occur on a specific type (or group) of sites commonly referred to as the “active site” for the particular reaction pathway^{8,9}. For example, during the decomposition of methanol on well-ordered Pd crystallites, two competing decomposition pathways exist including 1) dehydrogenation to CO and 2) C-O bond scission to form CH_x species. Schauerman *et al.*

demonstrated using kinetic measurement studies that the activity for C-O scission is significantly enhanced at the particle defect sites, whereas this was not found to be the case for the dehydrogenation pathway¹⁰. Determining the specific active site associated with a particular reaction pathway in heterogeneous catalysis is an especially challenging endeavor since these complex systems are inherently dynamic and there exist relatively few *in-situ* characterization techniques to provide direct characterization of the active surface. Since particular sites are associated with specific reaction pathways, and because knowledge of this structure/reactivity relationship can aid in designing highly selective catalysts, significant effort has been put forth in the field to try to determine the site requirements for particular reactions.

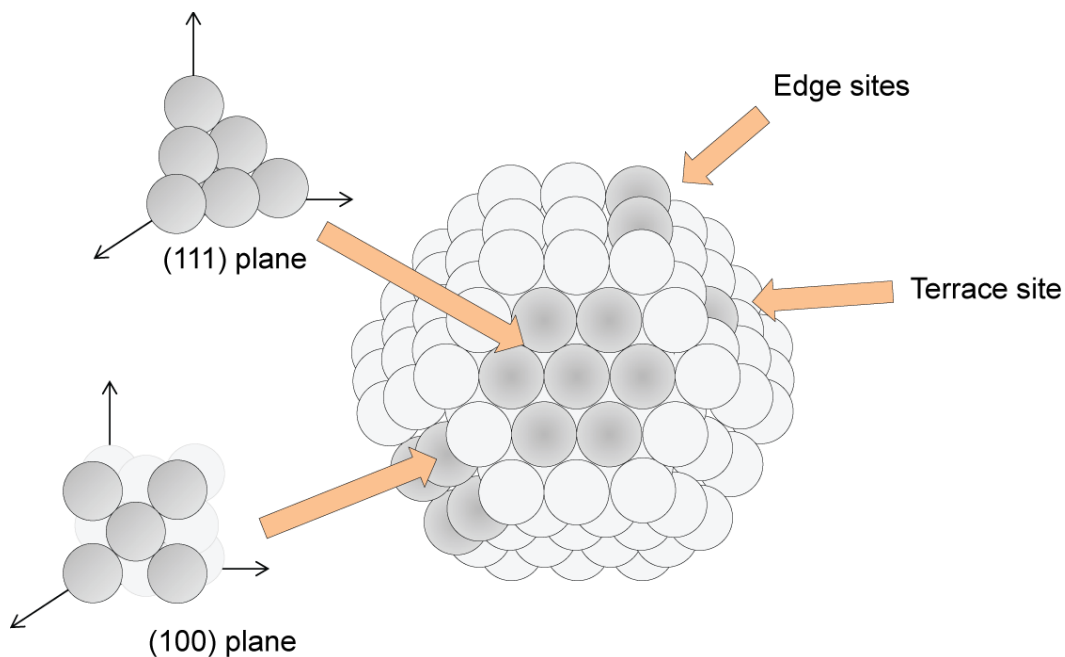


Figure 1-2. Depictions of the (100) and (111) planes for a cubo-octahedron shaped fcc metal particle. The Miller Indices, (xyz) , are used for specifying the crystal plane. These numbers refer to the vector normal to the plane in reciprocal space. Sites located at particle edges and terraces are also highlighted.

1.2 Catalyst modifiers

One potential approach for modifying adsorption characteristics and/or site availability is by using reaction modifiers, a technique that has been ubiquitous in catalysis for decades. Ideally, the added species interacts strongly with the active surface sites in such a way that induces a favorable outcome for the reaction.¹¹ Modifiers are typically either continuously added to the system during the reaction (*process* modifier), or used to modify the catalytic material during its synthesis (*reaction* modifier). A wide variety of modifiers have been employed in catalysis due to the relative ease of varying the nature and quantity used for each particular application, but the most frequently utilized can be divided into two major groups: 1) metal ions and strongly-adsorbing anions, and 2) organic species containing a sulfur, phosphorous, oxygen, or nitrogen heteroatom.

One of the earliest and most extensively investigated reaction modifiers is the Lindlar catalyst, which employs a combination of both inorganic (Pb) and organic (quinoline) modifiers on a palladium/CaCO₃ catalyst. The Lindlar catalyst is often used during the hydrogenation of alkynes to enhance selectivity to the *cis*-alkene without further hydrogenation to the undesirable alkane¹². Although it is widely used in laboratory and industrial synthesis, the specific role of the modifier components is still poorly-understood, demonstrating the difficulty associated with characterizing these complex systems. Pb has been shown to favor alloy formation with Pd, with the composition Pd₃Pb, which has been suggested as the active species.¹³ McEwen *et al.* suggested that the presence of the Pb serves to rearrange Pd particles in a favorable way¹⁴. More recent computational studies have suggested that Pb modifies the thermodynamic factor by reducing alkene adsorption and by hindering the formation of hydrides¹⁴. The organic quinoline component has been proposed to be a site blocking effect to impede the formation of C-C bonds

(oligomerization)¹⁵ or as an electronic effect due to the donation of electrons from the N-atom to the surface metal atom¹¹.

Inorganic modifiers are often utilized in heterogeneous catalysis to induce enhancement in activity, selectivity, or lifetime, or to protect the structural integrity of the catalyst¹⁶; these benefits are typically referred to as “promotional” effects which are generally thought to improve catalytic performance through either *structural* and/or *electronic* mechanisms. The former describes materials that are added to help stabilize materials, for example by preventing undesirable degradation of the catalytic material. Al₂O₃ has been added to Fe catalysts during ammonia synthesis because the alumina preferentially segregates to crystallite grain boundaries thereby preventing crystallite growth through sintering. Ultimately, this promotional effect serves to enhance the activity and lifetime of the catalyst. Electronic promoters are typically associated with strong electron transfer (either withdrawing or donating), which serves to alter the strength of bonds formed between the metal atoms and subsequently-adsorbing reactants. Alkali metals are often used as electronic promoters since they influence the bonding, and thus reactivity, of co-adsorbed molecules¹⁷. For example, K is an important promoter in ammonia synthesis because it weakens the bonding of the NH₃ product to the metal, thereby reducing its surface concentration which otherwise would block important reaction sites. Potassium also aids in the dissociation of N₂. Halogen species can also dramatically affect metal electronic properties. Chloride ions are often used in the silver catalyzed epoxidation of ethylene^{18,19} where the promoting effect has been attributed to changes in electronic structure^{20,21}, surface restructuring²², and ensemble/site-blocking^{21,23} effects.

A number of different types of organic modifiers have also been extensively utilized and studied in heterogeneous catalysis. Typically, the species involved is either some kind of

polymer, dendrimer, or ligand. A general depiction of organic modification approaches is shown in Figure 1-3.

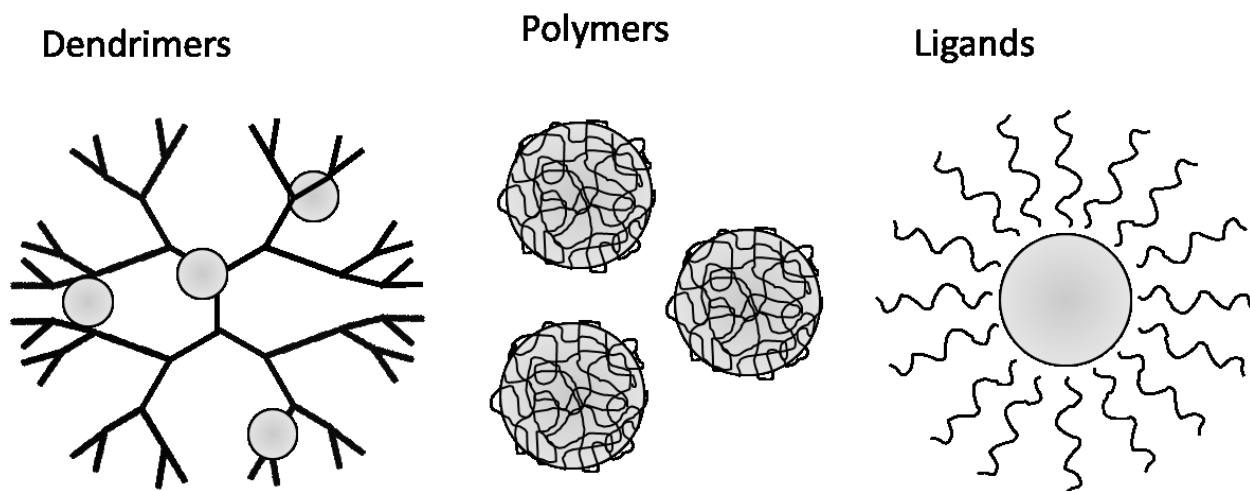


Figure 1-3. Different classes of organic modification techniques including dendrimer encapsulated, polymer protected, and ligand-protected.

Dendrimer encapsulated metal nanoparticles (DEMNs) are synthesized using a template approach in which metal ions are sorbed into the interior of the dendrimers and then reduced to yield metallic nanoparticles ranging from ~1-10 nm in diameter. In addition to serving as a template for the nanoparticle synthesis, the structure of the dendrimers can be employed to stabilize the nanoparticle, tune important practical properties including reactivity/solubility, and in some cases enhance selectivity for catalytic reactions²⁴. One of the major approaches for enhancing selectivity involves the ability to tune the dendrimers to promote size-selective catalysis. Because higher-generation dendrimers have more crowded peripheries, these kinds of modifiers have been used to exclude larger reactants from reaching nanoparticle surfaces. For

example, Niu *et al.* used hydroxyl-terminated poly(amidoamine) dendrimers for the hydrogenation of allyl alcohol and 4 related species containing increasing amounts of bulky substituents. They showed that increasing the DEMN generation excluded the bulkier reactants and thus could be used to selectively react smaller species²⁵. In addition, the dendrimer cage can easily be functionalized or tuned in order to facilitate solubility or specific interaction with solvents and reactants²⁶.

During synthesis, nanoparticles are often protected or “capped” with a polymer layer. These layers act to stabilize the nanoparticles (e.g. against agglomeration) through the steric bulk of their framework, but also by binding to the particle’s surface through heteroatoms that act as ligands. Poly(N-vinyl-2-pyrrolidone) (PVP) is commonly used because it is non-toxic and soluble in many polar solvents²⁷. It has been suggested that part of the PVP adsorbs on the nanoparticle surface, while the other part dissolves freely in the suspension, creating a second protective shell. The densities of both of these layers are thought to be important for controlling size²⁸. The effect of size on catalytic activity of these kinds of polymer stabilized nanoparticles has been examined and has been shown for a number of examples that smaller particles tend to show higher activity for Suzuki reactions²⁹ and aerobic oxidation of alcohols^{30,31}.

One of the more sophisticated approaches utilizes chiral ligands for application in asymmetric catalysis^{32,33}. The approach involves adsorption of a chiral ligand to a metal surface, creating highly enantioselective catalytic materials. The most common chiral modifiers used are the naturally occurring cinchona alkaloids and tartaric acid. Although these modifiers have been shown for a number of applications involving Pd, Pt, and Ni to dramatically improve enantiomeric selectivity, the mechanisms for improvement are still poorly understood due to the difficulty with performing in-situ measurements. Even the structure of the adsorbed ligands on

the surface has been a topic of debate, although surface science and scanning tunneling microscopy (STM) studies have suggested that cinchonidine and related modifiers do not form ordered structures on Pt^{34,35}.

1.3 Self-Assembled Monolayers (SAMs)

A class of organic modifiers that has recently been considered for controlling selectivity in heterogeneous catalysis is self-assembled monolayer (SAM) coatings. SAMs are organic assemblies comprised of molecules containing a head-group that interacts strongly with a solid surface^{36,37}. These modifiers provide versatility as a modification platform due to the tunability of their tail-group structure. Moreover, SAM preparation is robust and consistent because monolayer formation is both spontaneous and self-limiting, and therefore does not, in theory, depend on the details of the deposition process. These characteristics lead to the formation of organized structures that are thin and uniform, unlike polymer layers that tend to have more defects, are not as well ordered, and provide less control of the resulting surface chemical environment. For these reasons, SAMs have found numerous applications as thin films in a number of different areas including coatings for controlling wetting³⁸ and adhesion³⁹, biocompatibility⁴⁰, sensor⁴¹ and electronics⁴² applications, and more recently catalysis⁴³.

There are a variety of SAM types, but by far the most commonly studied include systems involving thiolates on metal surfaces and silanes on hydroxyl-terminated substrates (e.g. silicon and glass). The work in this thesis relies heavily on the organization of the monolayer for applications of catalysis on metal surfaces. Therefore, the following discussion will focus primarily on the formation and structure of monolayers formed from thiol precursors. The general structure of an alkanethiolate monolayer is shown in Figure 1-4.

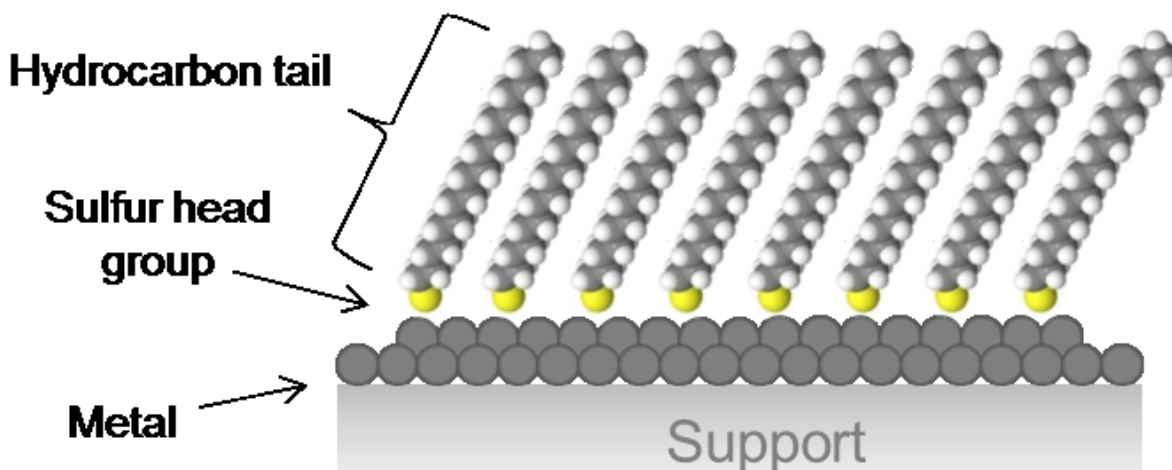


Figure 1-4. Basic structure of alkanethiolate monolayer on a supported metal surface.

Mechanisms of assembly of thiolate SAMs

Thiol molecules are comprised of a sulfur head group and a hydrocarbon tail group. When exposed to metal surfaces, the sulfur group covalently binds to the metal and a highly-ordered monolayer spontaneously assembles. The formation of alkanethiolate SAMs have been studied primarily on Au surfaces, however SAMs have been shown to form well-ordered structures on a number of other metals including Ag^{44,45}, Cu⁴⁴, and Pd⁴⁶. While Au is not the only metal substrate known to form well-ordered SAMs, it has historically been the metal of choice because it is easy to obtain both as a thin film and as a colloid, is relatively inert (does not oxidize easily), and is compatible with many biological systems³⁷. The first step of the formation process is thought to involve physisorption of the thiol in which the S-H bond remains intact. It

has been suggested that increasing the length of the alkane chain stabilizes both the initial physisorbed state as well as the transition state for S-H bond scission⁴⁷. At chain lengths with enough carbons ($n > \sim 6$) the barrier for S-H scission appears to be lower than energy for molecular desorption and what is likely a dissociative chemisorption process occurs readily.

From this physisorbed state, the growth process is thought to occur via several phase transitions before final monolayer formation is reached. While this process is indeed complex, and there remains some disagreement in the literature regarding the details, there are some general commonalities that have been agreed upon. It seems that initially, a 2D disordered “vapor” phase forms comprised of isolated, mobile adsorbates at low densities on the surface. With increasing density, a transition occurs toward a higher density state involving thiolates that are either disordered (liquid-like) or form a more ordered, lying down “striped” phase. Nucleation and island growth of a high density, solid-like state then begins to form and grow until high coverage is achieved and the adsorption process is more-or-less complete.^{36,37} While, full monolayer formation is expected to occur over the course of ~12-24 hours, it is generally thought that ~90% of the total monolayer adsorbs in the first couple of minutes. A second, slower step then involves restructuring and removal of defects within the monolayer. Figure 1-5 demonstrates this simplified view of SAM formation from low to high density where phase transitions involving island growth and coalescence are expected between each phase. While this is a simplified picture of a complex process that may undergo additional phase transitions and structures, it serves as a useful starting point for understanding monolayer growth.

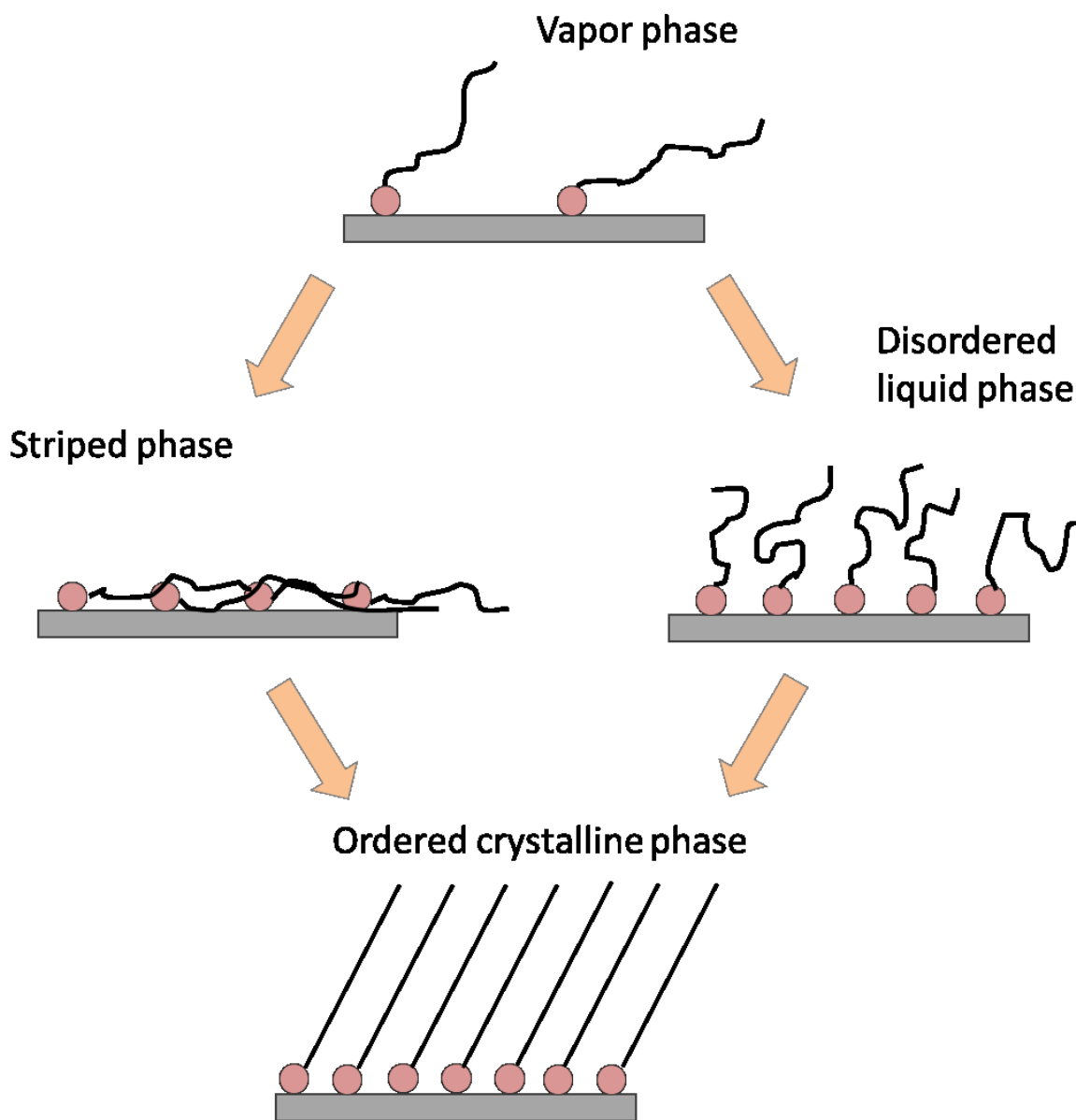


Figure 1-5. Simplified schematic of SAM formation involving a “vapor” phase, striped or disordered liquid-like phase, and a solid, high density phase.

The resulting density of the monolayer is governed by a compromise between the geometry preferred by the sulfur heteroatoms on the metal and maximizing lateral interactions

between the tail moieties. For a well-ordered alkanethiol monolayer, the resulting sulfur coverage has been shown to be $\theta_s \approx 0.33$ where the sulfur adsorbs in what is referred to as a $(\sqrt{3} \times \sqrt{3})R30$ adsorption geometry. This coverage specifies that for every three metal atoms, there is one adsorbed sulfur atom. The $(\sqrt{3} \times \sqrt{3})R30$ nomenclature indicates that the length of the unit cell of the adsorbed overlayer is a factor of $\sqrt{3}$ x greater with respect to the unit cell of the underlying metal. The R30 indicates that the adsorbed overlayer structure is rotated 30 degrees relative to the support. Figure 1-6 depicts the structure of a $(\sqrt{3} \times \sqrt{3})R30$ adsorption geometry.

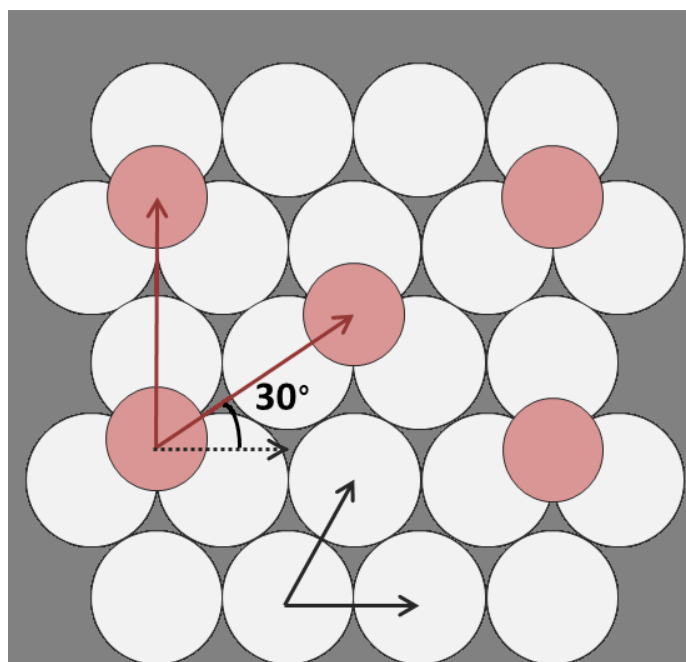


Figure 1-6. $(\sqrt{3} \times \sqrt{3})R30$ adsorption geometry of sulfur (red) on metal fcc(111) surface. The length of the adsorbed sulfur unit cell is $\sqrt{3} \times$ and is rotated 30° with respect to the underlying metal unit cell.

The spacing between adsorbed sulfur species is not typically the same spacing anticipated to maximize lateral interactions between the tail moieties. In fact, the minimized free energy of

the hydrocarbon tails would result in a higher density $c(4 \times 2)$ packing structure comprised of four thiolate molecules in a unit cell⁴⁸. Because of these density mismatches, thiolate monolayers tend to exhibit a “tilted” conformation so that the compromise between the sulfur arrangement and tail spacing can be met. Thioliates with bulky tail groups will similarly arrange in order to maximize lateral interactions which (depending on this spacing) may tend to decrease the coverage of the sulfur on the surface. For these lower density monolayers, the organic tail group then dictates the ultimate density of the monolayer on the surface. This is the case for bulky 1-adamantanethiol (AT) which has a caged hydrocarbon tail moiety which will be discussed in further detail throughout the work presented here.

Defects and other facets

While SAM monolayers are often depicted as consistent structures having long-range order, these films more realistically have a number of types of defects that can readily occur owing to the structure of the substrate and preparation conditions under which monolayer deposition occurs. Variations in the structure of the substrate can cause irregularities in SAM formation. Even flat metal surfaces exhibiting largely (111) facets contain grain boundaries, dislocations, steps, and some fraction of low-index facets that can lead to irregularities in the resulting monolayer⁴⁹. In addition, there is evidence suggesting that formation of alkanethiol SAMs on Au can cause a restructuring to the underlying surface upon adsorption. For example, Au “pits” have been observed by a number of groups to form upon addition of the modifiers using STM^{50,51}. It is thought that during adsorption, the thiols induce a relaxation of the surface in such a way that changes the underlying atomic density. Consequently, single-atom vacancies form and then nucleate into larger vacancy “islands”. In addition to the inherent structure of the

substrate, surface cleanliness also plays a role in both kinetics and potentially final structure since strongly-bound contaminants compete with thiols for adsorption sites. For this reason, the cleanliness of the support and purity of the solvent used are important for reducing defects.

While the majority of studies of SAMs have been performed on (111) single crystals or polycrystalline substrates largely exhibiting (111) character, a few studies have investigated SAM formation on other well defined facets. It is generally found that SAMs form with higher density on Au(100) facets, and while a $c(2 \times 2)$ geometry has been observed⁴⁷, the exact adsorption geometry remains unclear⁵². In a comparative study between Au(111), (100), and (110), the more stepped Au(110) surface was found to have the lowest density of docosyl mercaptan⁵³; however adsorption at these kinds of under-coordinated sites is generally found to be stronger. For SAMs formed on curved nanoparticles with a high radius of curvature, the chain density can change substantially with the length of the alkyl chain⁵⁴ which leads to enhanced mobility of the terminal methyl groups. Luedtke *et al.* showed computationally that SAM formation on 4.4 nm particles, where the majority of the particle comprise flat (111) terraces rather than edges and corners, led to “bundles” of ordered alkanethiolates with gaps at the corners and vertexes at low temperatures⁵⁵. The contribution of these different types of sites plays an important role in the context of this thesis and will be discussed in later chapters in further detail.

Role of sulfur

Sulfur has historically been considered an unwelcome poison for a number of catalytic applications. For example, reactant gases entering a Fischer-Tropsch reactor must be desulfurized since sulfur impurities dramatically deactivate the catalysts for this process⁵⁶. On

the other hand, sulfide catalysts have been used commercially for some major industrial processes such as hydrodesulphurization, a process used to remove sulfur from natural gas and refined petroleum products. Consequently, a number of studies have investigated how the presence of adsorbed sulfur affects catalytic reactivity. Considering the extensive amount of work and relative simplicity of these systems, it is somewhat surprising that the precise role of the sulfur species still remains unclear. It has been proposed that the mechanism of poisoning may be due to simple site-blocking from potential adsorption species. This effect is commonly referred to as a “steric” or local effect. Another possibility is that the sulfur induces longer-range perturbations of the electronic surface structure which would extend beyond nearest neighboring sites and is commonly referred to as an “electronic” effect. Both experimental and theoretical methods have been utilized to investigate this question.

While it is generally agreed that sulfur changes the electronic structure of the metal atoms *directly* bound to it, it remains unclear how far this effect extends into neighboring metal atoms. A number of UHV studies have investigated how the presence of sulfur affects hydrogen adsorption. The saturation coverage of hydrogen was shown to decrease linearly with increasing sulfur coverage both on Ru(001)⁵⁷ and Pd(100)⁵⁸. These results complemented calculations that predicted the presence of randomly distributed site-blocking agents, suggesting that the sulfur poisoning effect was primarily due to steric effects. For these studies, each sulfur atom was found to block 3.7-4.0 binding sites and no hydrogen adsorption was observed for sulfur coverages greater than ~0.25 monolayers. A theoretical study investigating the poisoning effect of sulfur on hydrogen adsorption for Pd(111) found that the sulfur increased the hydrogen diffusion barrier and dissociation energy, and significantly altered the electronic nature of the palladium, but that these effects were only associated with Pd atoms that were directly bonded to

the sulfur atom consistent with short-range site blocking effects⁵⁹. While many groups have suggested that the effect of sulfur poisoning was most likely due to local, steric changes in the surface, other studies have suggested that longer-range, electronic effects were the dominating effect⁶⁰. A number of theoretical studies have suggested that the electronic perturbations extend beyond Pd atoms bound to sulfur atoms^{61,62}.

1.4 SAMs for enhancing selectivity in heterogeneous catalysis

As mentioned previously, organic species have been utilized as reaction modifiers in heterogeneous catalysis; however, creating consistent surfaces has remained a challenge due to variations arising from different preparation techniques. Even in studies where the same organic species and nominal preparation techniques were used, significant differences have been observed⁶³⁻⁶⁵, presumably due to subtle variances in the final modifier state. With increasing attention being paid to organic modifiers, there has been growing interest in developing more consistent, highly-ordered structures that can provide a systematic approach for mechanistic studies. Toward this end, self-assembled monolayers (SAMs) have recently been used to modify catalysts in a more consistent and rational way. The successful use of SAMs in controlling activity of supported metal catalysts was first demonstrated by Marshall *et al.*, where different alkanethiolate coatings were used to dramatically improve the selectivity of the hydrogenation of 1-epoxy-3-butene to 1-epoxybutane⁶⁶. The enhanced selectivity was found to be independent of the tail functionality and attributed to an electronic effect induced by the presence of the sulfur attachment group and selective poisoning of the epoxide moiety⁶⁷.

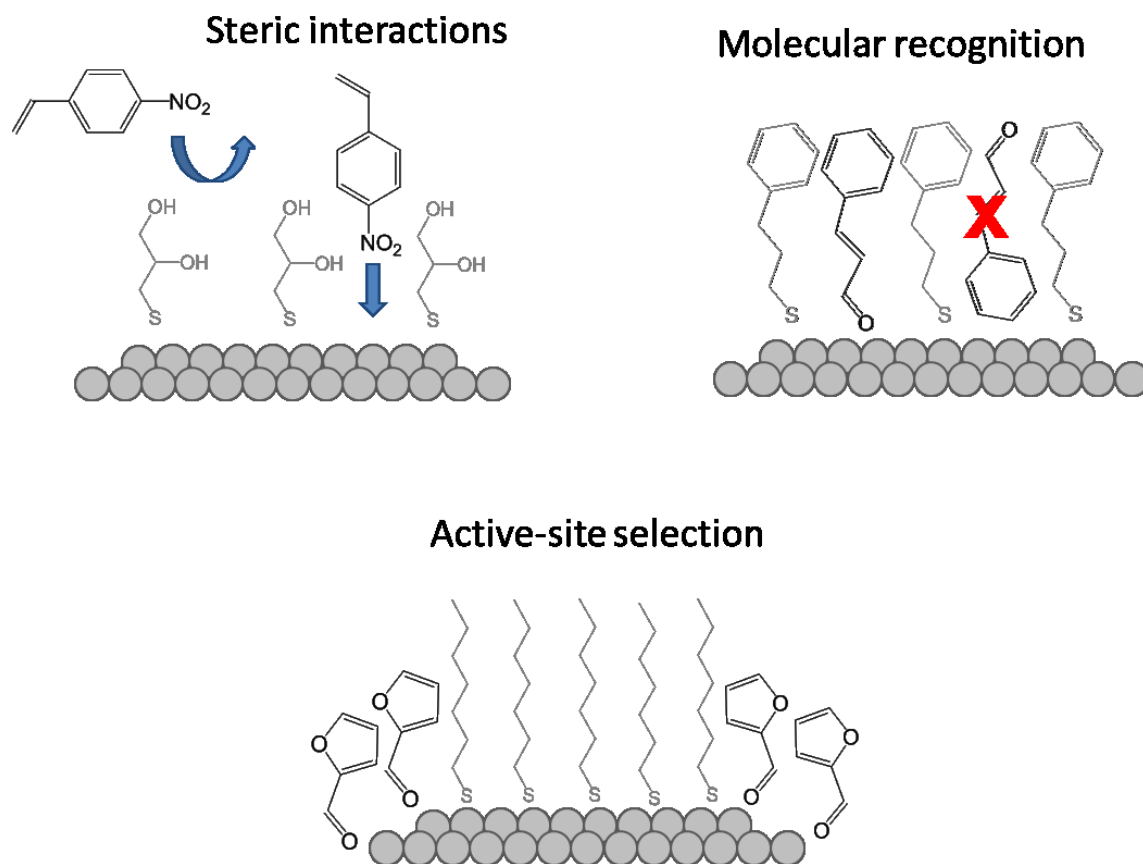


Figure 1-7. Recent approaches for tuning catalytic particles using SAMs.

Since their introduction in heterogeneous catalysis, SAMs have been utilized to enhance catalytic performance via several apparent mechanisms, as illustrated in Figure 1-7. One commonly-attributed effect of the organic modifiers has been to prevent a particular “lying-down” orientation of the reactant molecule due to *steric interactions* (Figure 1-7). For example, during the hydrogenation of 4-nitrostyrene, two reducible functional groups on either side of a benzene moiety have equal access to the surface in a “lying-down” conformation. Makosch *et al.* demonstrated that SAM-modification of Pt/TiO₂ catalysts induced a complete change in

selectivity from 4-ethylnitrobenzene and 4-ethylaniline (uncoated) to 4-aminostyrene on modified catalysts at conversion levels close to 100%. The presence of the monolayer was thought to inhibit the nitrostyrene molecule from lying flat on the catalyst, resulting in preferential interaction of the nitro group⁶⁸. Similarly, Wu *et al.* recently demonstrated that a sufficiently long-tailed amine capping layer on Pt₃Co nanocatalysts prevented α,β -unsaturated aldehydes from lying flat on the surface, preventing direct contact of the C=C bonds with the catalyst⁶⁹. The result was a dramatic enhancement in selectivity to cinnamyl alcohol (desired) which was found to improve with increasing tail length. Figure 1-8 shows the proposed adsorption geometry of cinnamaldehyde on oleylamine-modified surfaces and selectivity to cinnamyl alcohol (white) as a function of modifier tail length.

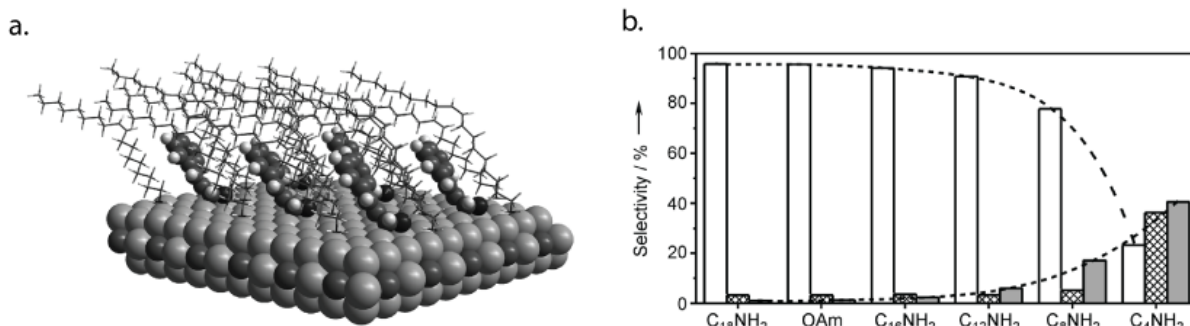


Figure 1-8. a) Proposed adsorption geometry of cinnamaldehyde (ball-and-stick) on Pt₃Co (100) modified with oleylamine (line). b) Selectivity for cinnamyl alcohol (white), hydrocinnamaldehyde (crosshatch), and hydrocinnamyl alcohol (gray) at nearly 100% conversion in the hydrogenation of cinnamaldehyde with different amine-capped Pt₃Co catalysts shown in order from longest (left) to shortest (right) tail length. Figure adapted from ref. [69].

Kahsar *et al.* found that an organized monolayer of alkanethiols facilitated hydrogenation of polyunsaturated to monounsaturated fatty acids, but inhibited further hydrogenation to the completely saturated species due to the sterically-hindered, single “kink” shape of the monounsaturated product⁷⁰. It has been shown that even small molecules, like ethylene, can be physically blocked from active catalyst sites using a bulky diphenyl-modified Pd/TiO₂ catalysts during acetylene hydrogenation⁷¹.

A more sophisticated approach for modifying selectivity on SAM-coated catalysts involves *molecular recognition* (Figure 1-7) by exploiting non-covalent intermolecular interactions between the surface modifier and reactant molecules to orient the reactant in a desirable way. Kahsar *et al.* recently demonstrated that the orientation of cinnamaldehyde, which contains an aromatic phenyl moiety, can be controlled using a suitable SAM modifier that can engage in aromatic pi-pi stacking interactions⁷². By using an appropriately spaced benzene-containing SAM modifier, >90% selectivity toward reaction of the aldehyde group was achieved. In contrast, employing a SAM where the benzene moiety was closer to the catalyst surface switched selectivity to hydrogenation of the C=C bond due to reorienting the molecule to a more “lying down” conformation bringing this moiety much closer to the surface. In another contribution, Taguchi *et al.* suggested that alkanethiol-SAMs on Au nanoparticles show molecular recognition properties based on intermolecular hydrophobic interactions for *n*-butanolysis of dimethylphenylsilane⁷³. In a related approach, SAMs have been exploited to study reactions conventionally difficult to observe because of unfavorable reaction geometries. Kim *et al.* used SAMs to anchor photocatalytic reactants in a specific orientation, geometrically unfavorable in solution, to study the resulting complex photochemical transformations⁷⁴. While

this approach is in its infancy, it has great potential for mimicking the function of enzymes in an effort to move toward biomimetic catalyst systems.

The major focus of the work presented in this thesis involves developing a third type of selectivity enhancement; *active-site selection* involves exploiting SAM monolayers that preferentially expose specific types of reactive sites, associated with a desirable reaction pathway, while simultaneously blocking sites, or groups of sites, related to undesirable products (Figure 1-7). In the work to be discussed, the tail structure of alkanethiol SAMs was tuned to either expose or block particle edge sites and to control the availability of contiguous active sites on particle terraces. A few related studies have recently investigated the possibility of using organized monolayers to probe the relationship between catalyst structure and reactivity. Nigra *et al.* demonstrated the kinetic contribution of three distinct types of sites during reduction of resazurin to resorufin where site availability was controlled by the fractional surface coverage of two organic ligands: dodecanethiol, shown to form a significantly d-charge depleted metal surface, and triphenylphosphine, which produces an electron-rich surface⁷⁵. Interestingly, the catalytic rate was found to be independent of the electronic state of the metal and only dependent on the ligand surface coverage. While it is not often a trivial matter to determine the exact SAM overlayer structure, which likely affects where and how reactants can adsorb, Jiang *et al.* suggested experimentally that with increasing alkyl length, the sulfur headgroup occupies sites with increasing coordination numbers⁷⁶. Thus, it may be possible to control the preference for specific terrace sites by controlling SAM length.

Ligand Density, Solvent Effects, and Particle Characterization

It is well-established that the size of nanoparticles can be controlled by varying either the tail length or concentration of modifier in solution during nanoparticle formation^{77,78}. When chemoselectivity is not of particular importance, but organic ligands are required to stabilize nanoparticles, the catalytic activity of an organically-modified surface is generally increased by reducing the density of the ligands on the surface. While alkanethiol SAMs are densely packed, by altering the attachment geometry or tail moiety, the modifiers can be spaced more sparsely on the surface. Lu *et al.* demonstrated that SH-POSS (polyhedral oligomeric silsesquioxane) ligands afford larger gaps between ligand molecules than 1-dodecanethiol, which resulted in significantly higher turnover rates for Pd nanoparticle-catalyzed Heck coupling⁷⁹. Similarly, Sadeghmoghaddam *et al.* showed that a monolayer formed from S-dodecylthiosulfate created a sparser coating than dodecanethiol, resulting in increased catalytic activity for the isomerization of allyl alcohols^{80,81}. In a follow up study, these authors controlled the surface ligand density (and core size) of the thiolate ligand-capped Pd nanoparticles where the larger, less-dense NPs exhibited higher activity⁸². The relationship between modifier density and reactant binding energy has also been investigated. Kwon *et al.* found, during the hydrogenation of 4-octyne, that the binding energy of the intermediate octene was reduced with increasing concentration of primary alkylamine modifiers⁸³. At high enough modifier coverage, the alkylamines won the competition for adsorption sites, preventing further hydrogenation of alkenes into alkanes. Figure 1-9 shows the DFT calculated adsorption energies for the alkyne, alkenes, and amines as a function of modifier coverage along with the corresponding adsorption structures used in this study.

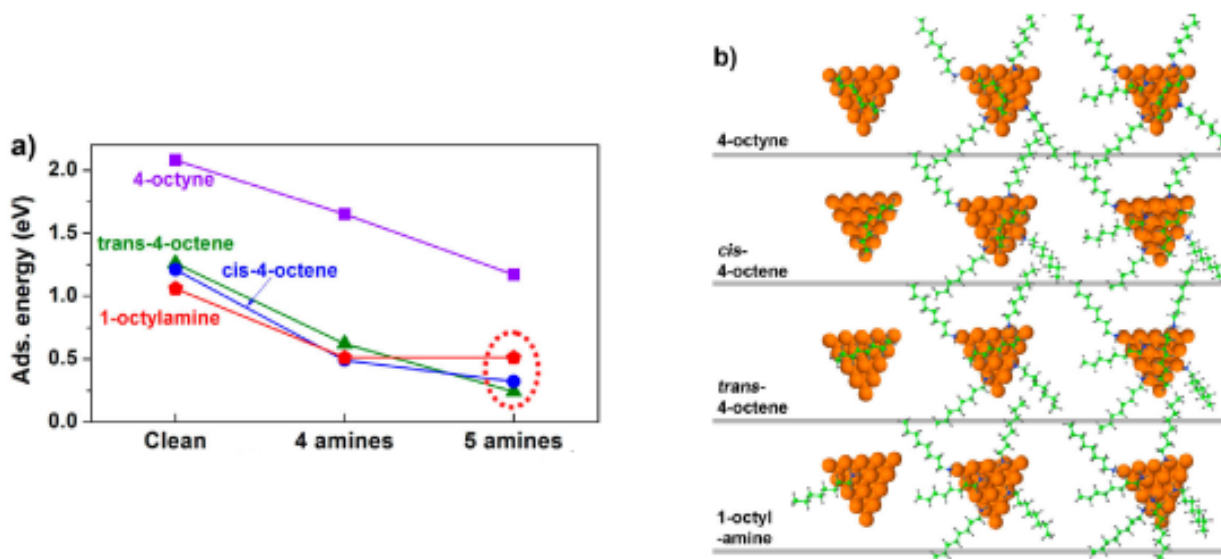


Figure 1-9. a) Plots of the adsorption energies of 4-octyne, cis-4-octene, trans-4-octene, and 1-octylamine on clean and 1-octylamine modified Pt (111) surface as a function of octylamine coverage. Dash red circle highlights that at high enough amine coverage, alkylamines adsorb more readily than the alkenes. b) Depiction of the structures used in DFT calculations. Figure adapted from ref. [83].

Sadeghmoghaddam *et al.* also investigated the effect of solvent on the isomerization or hydrogenation of allyl alcohols⁸⁴. Nonpolar solvents promoted the isomerization pathway where a branched Pd-alkyl intermediate formed on the surface. In contrast, polar solvents caused alkanethiolate-capped Pd nanoparticles to aggregate, resulting in increased surface density of ligands. The increased steric crowding caused a switch in selectivity toward the hydrogenated product instead of isomerization, presumably because the reactant did not have enough room to form the branched intermediate on the surface. Kahsar *et al.* also found a significant solvent effect during the hydrogenation of 1-epoxybutene to the desirable product epoxybutane⁸⁵. The most selective conditions were found using a hydrophilic monolayer (thioglycerol) and a hydrophobic solvent (heptane) where competing hydrophobic interactions from the solvent and the hydrophilic nature of the SAM environment were hypothesized to create a more stabilized

monolayer. The effects of a solvent phase can be complex; in addition to changes in selectivity, the nature of the solvent also has been shown to play a large role in particle solubility and stability^{84,86}.

Mixed Monolayers and SAM-based Substrates

Enzymatic catalysts commonly orient reactant molecules by exploiting non-covalent interactions between reactants and amino acids residues adjacent to an active site. To more accurately mimic these biological catalysts, mixed monolayers may be useful for creating specific surface environments. Examples of mixed monolayer systems are shown in Figure 1-10. Moreno *et al.* investigated the effect of mixing nitrogen and sulfur headgroup based monolayers and found that nitrogen-based monolayers showed higher reactivity with H₂ gas but were less stable and showed a tendency toward agglomeration during H₂ exposure⁸⁷. Sulfur based monolayers, on the other hand, demonstrated higher stability but were less reactive with H₂. Another mixed-monolayer study by Cargnello *et al.* synthesized particles with mixed monolayers containing alkyl, alcohol, and acidic terminations⁸⁸. These monolayers were easily prepared and, as seen previously⁸⁹, the resulting nanoparticles were very stable and showed good recyclability for Suzuki cross-coupling reactions. SAMs have also been utilized as part of the substrate platform to subsequently immobilize catalytically-active surface metals⁹⁰. This technique generally requires a well-ordered SAM grafted onto a flat support which is subsequently functionalized with an active surface metal (Figure 1-10). In a number of recent reports, the SAM-grafted heterogeneous catalysts were found to prevent deactivation of the active metal and actually showed enhanced catalytic properties for their homogeneous counterparts.⁹¹⁻⁹⁴

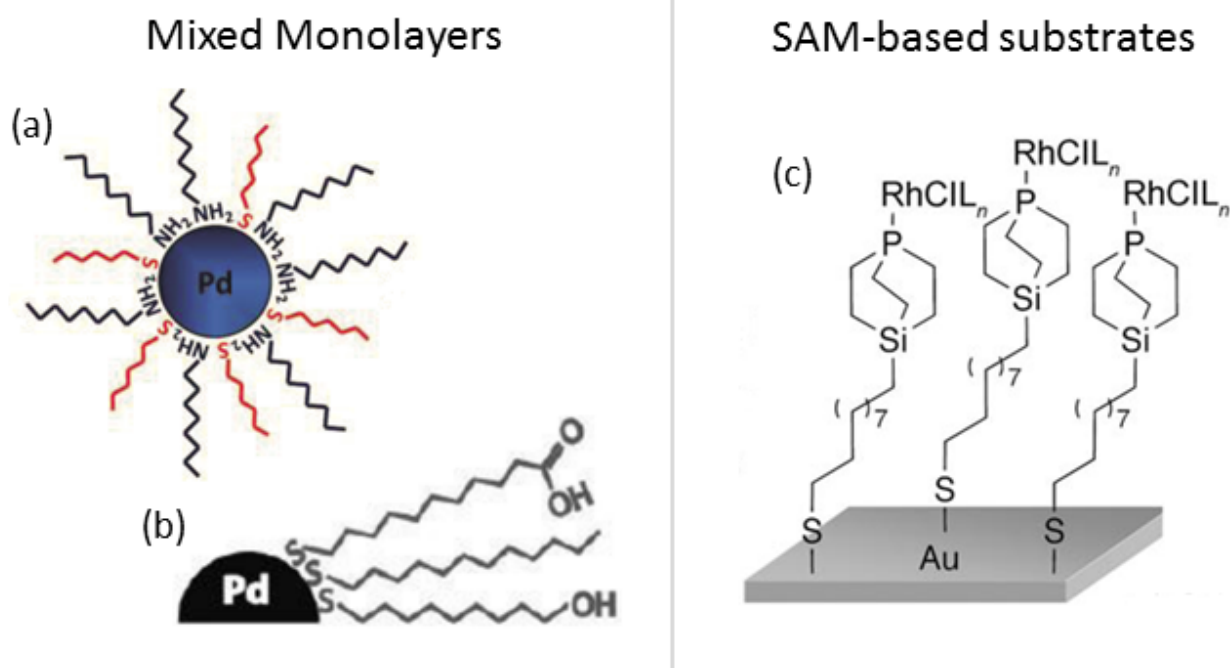


Figure 1-10. Examples of mixed monolayers and SAM-based substrates adapted from references a) 89 b) 90 and c) 94.

1.5 Experimental Methods

Infrared spectroscopy

Infrared (IR) spectroscopy was performed for all experiments using a Thermo-Fisher Nicolet 6700 FT-IR. The primary technique used was diffuse reflectance infrared Fourier transform spectroscopy (DRIFTS) which is commonly employed for characterization of powder samples. Experiments were performed using the Praying Mantis DRIFTS cell design from Harrick Scientific. In this technique, the IR radiation directed toward a powder sample can undergo a number of different reflection or absorption processes including: 1) *specular reflection* where radiation reflects off the surface without interacting with the sample, 2) *diffuse reflection* where radiation reflects off the surface of a powdered surface without undergoing interaction

with the sample, and 3) *true diffuse* where the radiation actually interacts with and is absorbed by the sample. Only this third process provides information about the chemical species present in the sample.

The setup used for the experiments presented in this thesis is shown in Figure 1-11. The catalyst is placed inside a small, dome-shaped cell that forms a gas-tight seal. Gas ports allow either for the dosing or pumping down of gases inside the cell. Three windows exist within the walls of the dome; two are IR transmissive windows that allow the infrared beam to enter and exit the dome after interacting with the sample while the third is a glass viewing port. While theoretically any IR transmissive material can be chosen for the windows in-line with the IR radiation, ZnSe was chosen which can withstand greater pressure differentials and will not dissolve in the presence of water unlike salt windows (e.g. KBr). This is particularly important if oxidation/reduction will be performed using the IR dosing cell which will result in the formation of water.

A dosing system was designed in order to introduce reactants into the system. Lecture bottles containing the desired gases (Sigma Aldrich) were connected to a stainless steel manifold and controlled via a needle valve. The manifold was isolated from the dosing cell using a leak valve/ball valve combination (injection) and a ball valve (exhaust/pumping). The leak valve was necessary in order to introduce very small, controlled amounts of gas into the system. The inherent design of the leak valve is such that it cannot be closed entirely; for this reason the second ball valve was added to inhibit small amounts of gas from leaking into the system. Pressure gauges were added to the manifold to simultaneously monitor pressure in the manifold and in the dome.

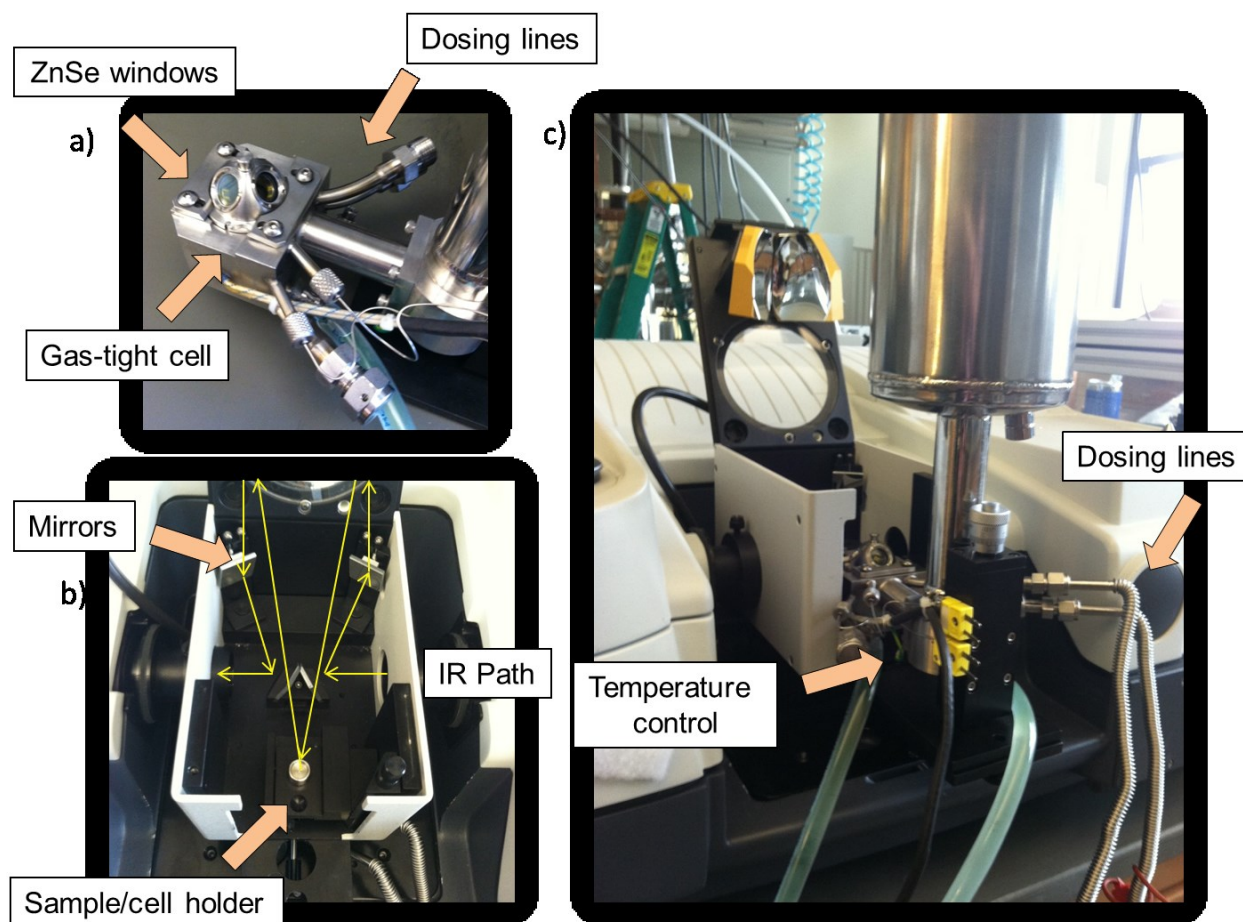


Figure 1-11. DRIFTS cell used for gas dosing applications including a) the gas-tight dome, b) inside praying mantis accessory showing the light path of IR and c) the whole system orientation.

For applications involving high vacuum, uncoated samples were typically left to pump down under vacuum for over two hours. At this point, a low baseline pressure was obtained and stabilized (usually ~ 80 mtorr) such that closing off the dome system to the pump did not result in rising pressure. For cases where the pressure rose by closing off the pump, this typically indicated either the system was not fully pumped down or there was a leak in the system. For coated samples, longer evacuation times were typically required for stabilizing the baseline pressure (~ 4 hours). This longer stabilization period was presumably due to a longer time

needed to remove the more-loosely bound organics that were deposited on the catalysts. After samples were fully evacuated, background spectra were acquired such that the all absorbing species would be subtracted except for changes in the material due to the dosed compounds. When the structure of the SAMs was under investigation, a background of the uncoated catalyst under vacuum was used. While atmospheric samples could serve as a potential background for these applications, undesirable species present under these conditions (e.g water/hydroxyl groups adsorbed on catalyst supports) could significantly complicate spectra.

Gas-phase reactor system

All catalytic reactions were carried out in a tubular gas-phase packed bed flow reactor and were monitored using an Agilent 7890A gas chromatograph (GC) equipped with a flame ionization detector. The setup of the reactor system is shown in Figure 1-12. Gas cylinders (Airgas) were controlled individually by mass flow controllers (Tylan). The gases were then combined into a single feed stream and directed toward a valve and injector system interfaced with the GC to test the feed composition. The feed stream was then directed to the reactor system comprised of a 0.25" inner diameter glass reactor tube and cylindrical temperature-controlled furnace. The catalyst was diluted using an appropriate amount of inert Al_2O_3 powder (~300 mg) and placed in the reactor tube sandwiched between packed glass wool. The furnace temperature was monitored separately from the temperature at the catalyst bed. For particularly exothermic reactions like acetylene hydrogenation, the temperature at the bed could increase significantly. For this reason, it was necessary to monitor the bed temperature closely. After the gas stream passed through the reactor system, the product stream was then directed to the GC for analysis.

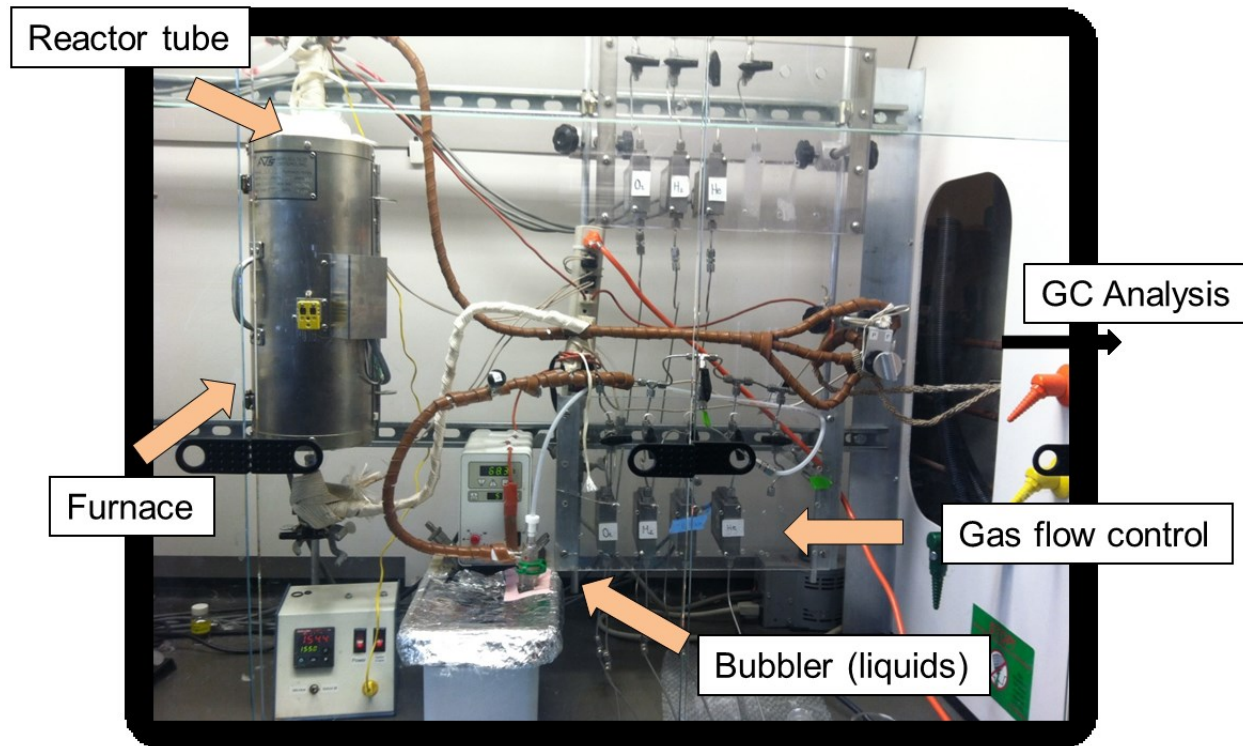


Figure 1-12. Gas-phase reactor system. Both feed and product streams could be monitored using gas chromatography (Agilent 7890A) equipped with a flame ionization detector.

For reactions where the reactant was a liquid, a bubbler system was used. Just downstream of the mass flow controller but before recombining with other reactant flow, a flow of helium was directed toward a bubbler containing the liquid. The bubbler was immersed in a temperature controlled water bath and heated to the temperature required to produce the particular vapor pressure desired for the reaction. This saturated helium/reactant flow mixture was then combined with original gas flow and permitted to flow through the reactor system. In order to inhibit the condensation of the reactant in the lines, heating tape was thoroughly wrapped around all tubing in the system. For this reason, and for general stability/inert purposes, stainless steel was used for all tubing that did not need to be flexible. When flexible tubing was required, the tubing was first wrapped in glass wool before applying heating tape.

Catalytic reactions

All catalytic reactions were carried out in the gas-phase plug flow reactor and GC detection system described in the previous section. The specific flow conditions and amount of catalyst used for each application will be described in the subsequent sections, but typically a high ($>10 \times$) hydrogen to hydrocarbon ratio was used for all hydrogenation reactions. Originally, reactions were run for shorter time intervals (~ 1 hour) to determine initial activities of catalyst. Subsequent studies were performed over longer time periods where catalysts performance had stabilized, typically for at least 4 hours. Reactions run for longer periods of time demonstrated higher reproducibility and were preferred over more transient studies. Rates are reported per metal site on the uncoated catalysts as determined by CO chemisorption, even for catalysts with thiol coatings. In order to determine the true turnover frequencies on coated catalysts, knowledge of the number of active sites on modified catalysts would be needed. This is notoriously a difficult feature to measure, and we have found that assumptions about the number of active sites dramatically effects the interpretation of results. Therefore, in the absence of reliable knowledge of true active site density, normalizing rates to the total sites on the uncoated catalyst is the most appropriate and consistent approach for comparing reactivity.

Preparation of SAM-modified catalysts

Originally, before depositing alkanethiols, the 5wt% Pd/Al₂O₃ was oxidized in 20% oxygen (balance He) for > 3 hours at 300 °C and then reduced in 20% hydrogen (balance He) in a glass reactor tube diluted with ~ 300 mg Al₂O₃. After the oxidation/reduction cleaning, a dilute solution (~ 1 mM) of thiol dissolved in 200-proof HPLC-grade ethanol (Sigma Aldrich) was poured over the catalyst in the reactor tube. The tube was then capped with parafilm and the

mixture allowed to deposit for at least 12 hours at which point the solution was poured off. The modified catalyst was then allowed to dry in a low flow (~10 sccm) of nitrogen for ~12 hours. While this procedure allowed for some thiolate adsorption, IR spectroscopy of the hydrocarbon stretching regime demonstrated that the resulting monolayer was poorly-formed, perhaps due to mass transfer problems. A spectrum of the SAMs formed using this procedure is shown in Figure 1-13.

The procedure was altered in order to improve mixing between catalyst particles and thiols in solution. For this procedure, ~300 mg of pure catalyst (no dilutant Al_2O_3) was cleaned under the same oxidation and reduction conditions in the reactor tube, but was then removed entirely from the tube and transferred to a beaker (~40mL) containing the dilute ethanol solution. The mixture was stirred together for ~10 seconds to promote mixing and was then allowed to deposit for at least 12 hours. After deposition, the ethanol solution was decanted and the slurry was allowed to dry in air. For some types of thiols, particularly for less soluble thiols like 1-octadecanethiol (C18), precipitate formation was observed presumably due to crystalized thiol. Thus, a wash step was introduced; after the 12 hour deposition step, the ethanolic solution was decanted, fresh ethanol was added, the mixture was stirred, allowed to settle, decanted, and then allowed to dry in air. This procedure eliminated the formation of thiol precipitate and was found to produce a well-ordered monolayer. An IR spectrum of the hydrocarbon stretching regime for C18 SAMs formed from this new technique is shown in Figure 1-13.

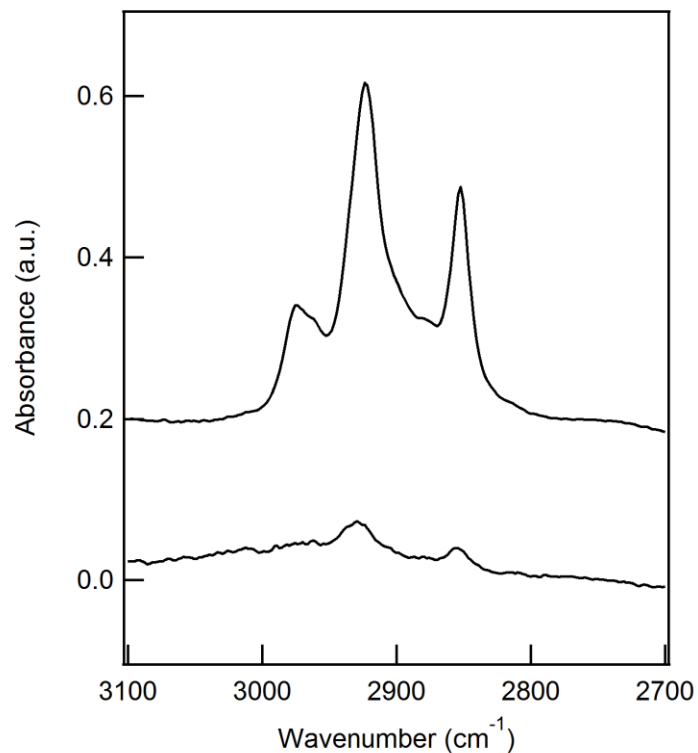


Figure 1-13. Comparison of hydrocarbon stretching regime of two C18-modified catalysts prepared via different methods. (Bottom) The previously used method involved pouring thiolate solution directly over dilute catalyst in the reactor tube without mixing. (Top) The revised method involved removing catalyst from reactor tube to deposit in a beaker of thiol solution with an additional wash step to remove loosely bound thiol species from the catalyst.

Palladium films

Thin palladium films were prepared for XPS studies at the Colorado Nanofabrication Laboratory user facility at the University of Colorado. Films were obtained by depositing ~1.0 nm chromium onto 2” prime grade silicon wafers as an adhesion layer, followed by ~200 nm of palladium. The evaporation was conducted using a CVC 3-boat thermal evaporator. Originally, a titanium adhesion layer was used, however oxide formation by rapid heating often resulted in broken boats. The titanium was thus replaced with a chromium rod.

1.6 Thesis Goals

The ultimate goal of this thesis is to describe a new and convenient approach for exposing specific types of active sites on palladium catalysts using thiolate self-assembled monolayers. First, the development of the modification technique is described whereby the density of the thiolates is controlled through systematically changing the bulkiness of the thiol tail moiety. It will be shown that increasing thiol density restricts the availability of contiguous adsorption sites on particle terraces while leaving adsorption at edge and step sites largely unaffected. Second, the modification approach is employed to control selectivity for the hydrogenation of a reactive and highly functionalized molecule, furfural. Third, a detailed kinetic treatment of this system is described to identify how the presence of the modifiers affects the individual reaction processes for this reaction.

1.7 References

- 1 Recognizing the Best in Innovation: Breakthrough Catalyst. . *R&D Magazine* (2005).
- 2 Masel, R. I. *Chemical Kinetics and Catalysis*. 28 (John Wiley & Sons, Inc., 2001).
- 3 Somorjai, G. A. & Kliewer, C. J. Reaction selectivity in heterogeneous catalysis. *React Kinet Catal L* **96**, 191-208 (2009).
- 4 Zaera, F. Mechanisms of hydrocarbon conversion reactions on heterogeneous catalysts: analogies with organometallic chemistry. *Top Catal* **34**, 129-141 (2005).
- 5 Bond, G. C. *Metal-Catalysed Reactions of Hydrocarbons*. (Springer Science+Business Media, Inc., 2005).
- 6 Ponc, V. & Bond, G. C., *Catalysis by Metals and Alloys*, Elsevier: Amsterdam (1995).
- 7 Bond, G. C. Small Particles of the Platinum Metals. *Platinum Metals Review* **19**, 126-134 (1975).

- 8 Norskov, J. K. *et al.* The nature of the active site in heterogeneous metal catalysis. *Chem Soc Rev* **37**, 2163-2171 (2008).
- 9 Freund, H. J., Libuda, J., Baumer, M., Risse, T. & Carlsson, A. Cluster, facets, and edges: Site-dependent selective chemistry on model catalysts. *Chem Rec* **3**, 181-200 (2003).
- 10 Schauermann, S. *et al.* Catalytic activity and poisoning of specific sites on supported metal nanoparticles. *Angew Chem Int Edit* **41**, 2532-+ (2002).
- 12 Mallat, T. & Baiker, A. Selectivity enhancement in heterogeneous catalysis induced by reaction modifiers. *Appl Catal a-Gen* **200**, 3-22 (2000).
- 12 Lindlar, H. *Ein Neuer Katalysator Fur Selektive Hydrierungen. *Helv Chim Acta* **35**, 446-456 (1952).
- 13 Palczewska, W., Jablonski, A., Kaszkur, Z., Zuba, G. & Wernisch, J. Study on Lead Additives in Modified Palladium Catalysts. *J Mol Catal* **25**, 307-316 (1984).
- 14 Mcewen, A. B., Guttieri, M. J., Maier, W. F., Laine, R. M. & Shvo, Y. Metallic Palladium, the Actual Catalyst in Lindlar and Rosenmund Reductions. *J Org Chem* **48**, 4436-4438 (1983).
- 15 Garcia-Mota, M. *et al.* A density functional theory study of the 'mythic' Lindlar hydrogenation catalyst. *Theor Chem Acc* **128**, 663-673 (2011).
- 16 Hutchings, G. J. Promotion in heterogeneous catalysis: a topic requiring a new approach? *Catal Lett* **75**, 1-12 (2001).
- 17 Joyner, R. W. & Santen, R. A. *Elementary Reaction Steps in Heterogeneous Catalysis*. (Kluwer Academic Publishers, 1993).
- 18 Campbell, C. T. Chlorine Promoters in Selective Ethylene Epoxidation over Ag(111) - a Comparison with Ag(110). *J Catal* **99**, 28-38 (1986).
- 19 Meisenheimer, R. G. & Wilson, J. N. Interaction of Oxygen and of Ethylene Dichloride with Silver Surfaces. *J Catal* **1**, 151-155 (1962).
- 20 Kershen, K., Celio, H., Lee, I. & White, J. M. Chlorine-modified properties of Ag(111) probed by C₂H₄, C₃H₆, C₃H₅Cl, and CO. *Langmuir* **17**, 323-328 (2001).
- 21 Monnier, J. R., Stavinoha, J. L. & Hartley, G. W. Effects of chlorine and chlorine dynamics during silver-catalyzed epoxidation of butadiene. *J Catal* **226**, 321-333 (2004).
- 22 Frank, E. R. & Hamers, R. J. Chlorine-induced restructuring of Ag(111) films observed by scanning tunneling microscopy. *J Catal* **172**, 406-413 (1997).
- 23 Campbell, C. T. & Paffett, M. T. The Role of Chlorine Promoters in Catalytic Ethylene Epoxidation over the Ag(110) Surface. *Appl Surf Sci* **19**, 28-42 (1984).

- 24 Niu, Y. H. & Crooks, R. M. Dendrimer-encapsulated metal nanoparticles and their applications to catalysis. *Cr Chim* **6**, 1049-1059 (2003).
- 25 Niu, Y. H., Yeung, L. K. & Crooks, R. M. Size-selective hydrogenation of olefins by dendrimer-encapsulated palladium nanoparticles. *J Am Chem Soc* **123**, 6840-6846 (2001).
- 26 Vogtle, F., Gestermann, S., Hesse, R., Schwierz, H. & Windisch, B. Functional dendrimers. *Prog Polym Sci* **25**, 987-1041 (2000).
- 27 He, B. L., Ha, Y., Liu, H. F., Wang, K. M. & Liew, K. Y. Size control synthesis of polymer-stabilized water-soluble platinum oxide nanoparticles. *J Colloid Interf Sci* **308**, 105-111 (2007).
- 28 Hirai, H. & Yakura, N. Protecting polymers in suspension of metal nanoparticles. *Polym Advan Technol* **12**, 724-733 (2001).
- 29 Li, Y., Boone, E. & El-Sayed, M. A. Size effects of PVP-Pd nanoparticles on the catalytic Suzuki reactions in aqueous solution. *Langmuir* **18**, 4921-4925 (2002).
- 30 Kanaoka, S. *et al.* Thermosensitive gold nanoclusters stabilized by well-defined vinyl ether star polymers: Reusable and durable catalysts for aerobic alcohol oxidation. *J Am Chem Soc* **129**, 12060-+ (2007).
- 31 Feng, B. *et al.* Functionalized Poly(ethylene glycol)-Stabilized Water-Soluble Palladium Nanoparticles: Property/Activity Relationship for the Aerobic Alcohol Oxidation in Water. *Langmuir* **26**, 2505-2513 (2010).
- 32 Mallat, T., Orglmeister, E. & Baiker, A. Asymmetric catalysis at chiral metal surfaces. *Chem Rev* **107**, 4863-4890 (2007).
- 33 Studer, M., Blaser, H. U. & Exner, C. Enantioselective hydrogenation using heterogeneous modified catalysts: An update. *Adv Synth Catal* **345**, 45-65 (2003).
- 34 von Arx, M., Wahl, M., Jung, T. A. & Baiker, A. Adsorption and surface mobility of cinchonidine on Pt(111) studied by STM. *Phys Chem Chem Phys* **7**, 273-277 (2005).
- 35 Simons, K. E. *et al.* A Model for the Enantioselective Hydrogenation of Pyruvate Catalyzed by Alkaloid-Modified Platinum. *Recl Trav Chim Pay B* **113**, 465-474 (1994).
- 36 Schwartz, D. K. Mechanisms and kinetics of self-assembled monolayer formation. *Annu Rev Phys Chem* **52**, 107-137 (2001).
- 37 Love, J. C., Estroff, L. A., Kriebel, J. K., Nuzzo, R. G. & Whitesides, G. M. Self-assembled monolayers of thiolates on metals as a form of nanotechnology. *Chem. Rev.* **105**, 1103-1169 (2005).
- 38 Abbott, N. L., Gorman, C. B. & Whitesides, G. M. Active control of wetting using applied electrical potentials and self-assembled monolayers. *Langmuir* **11**, 16-18 (1995).

- 39 Ederth, T. *et al.* Resistance of galactoside-terminated alkanethiol self-assembled monolayers to marine fouling organisms. *ACS Appl. Mater. Interfaces* **3**, 3890-3901 (2011).
- 40 Tiwari, P. M., Vig, K., Dennis, V. A. & Singh, S. R. Functionalized gold nanoparticles and their biomedical applications. *Nanomaterials* **1**, 31-63 (2011).
- 41 Crooks, R. M. & Ricco, A. J. New organic materials suitable for use in chemical sensor arrays. *Acc. Chem. Res.* **31**, 219-227, (1998).
- 42 Edsger, P. C. *et al.* Bottom-up organic integrated circuits. *Nature* **455**, 956-959 (2008).
- 43 Schoenbaum, C. A., Schwartz, D. K. & Medlin, J. W. Controlling the Surface Environment of Heterogeneous Catalysts using Self-Assembled Monolayers. *Acc. Chem. Res.* **47**, 1438-1445, (2014).
- 44 Laibinis, P. E. *et al.* Comparison of the structures and wetting properties of self-assembled monolayers of normal-alkanethiols on the coinage metal-surfaces, Cu, Ag, Au. *J. Am. Chem. Soc.* **103**, 7152-7167 (1991).
- 45 Sellers, H., Ulman, A., Shnidman, Y. & Eilers, J. E. Structure and binding of alkanethiolates on gold and silver surfaces - implications for self-assembled monolayers. *J. Am. Chem. Soc.* **115**, 9389-9401 (1993).
- 46 Love, J. C. *et al.* Formation and structure of self-assembled monolayers of alkanethiolates on palladium. *J Am Chem Soc* **125**, 2597-2609 (2003).
- 47 Dubois, L. H., Zegarski, B. R. & Nuzzo, R. G. Molecular Ordering of Organosulfur Compounds on Au(111) and Au(100) - Adsorption from Solution and in Ultrahigh-Vacuum. *J Chem Phys* **98**, 678-688 (1993).
- 48 Poirier, G. E. & Tarlov, M. J. The C(4x2) Superlattice of N-Alkanethiol Monolayers Self-Assembled on Au(111). *Langmuir* **10**, 2853-2856 (1994).
- 49 Sun, L. & Crooks, R. M. Indirect Visualization of Defect Structures Contained within Self-Assembled Organomercaptan Monolayers - Combined Use of Electrochemistry and Scanning-Tunneling-Microscopy. *Langmuir* **9**, 1951-1954 (1993).
- 50 Poirier, G. E. Mechanism of formation of Au vacancy islands in alkanethiol monolayers on Au(111). *Langmuir* **13**, 2019-2026 (1997).
- 51 Yang, G. H. & Liu, G. Y. New insights for self-assembled monolayers of organothiols on Au(111) revealed by scanning tunneling microscopy. *J Phys Chem B* **107**, 8746-8759 (2003).
- 52 Strong, L. & Whitesides, G. M. Structures of Self-Assembled Monolayer Films of Organosulfur Compounds Adsorbed on Gold Single-Crystals - Electron-Diffraction Studies. *Langmuir* **4**, 546-558 (1988).

- 53 Camillone, N., Chidsey, C. E. D., Liu, G. & Scoles, G. Substrate Dependence of the Surface-Structure and Chain Packing of Docosyl Mercaptan Self-Assembled on the (111), (110), and (100) Faces of Single-Crystal Gold. *J Chem Phys* **98**, 4234-4245 (1993).
- 54 Hostetler, M. J. *et al.* Alkanethiolate gold cluster molecules with core diameters from 1.5 to 5.2 nm: Core and monolayer properties as a function of core size. *Langmuir* **14**, 17-30 (1998).
- 55 Luedtke, W. D. & Landman, U. Structure and thermodynamics of self-assembled monolayers on gold nanocrystallites. *J Phys Chem B* **102**, 6566-6572 (1998).
- 56 Anderson, R. B., Karn, F. S. & Shultz, J. F. Factors in Sulfur Poisoning of Iron Catalysts in Fischer-Tropsch Synthesis. *J Catal* **4**, 56-& (1965).
- 57 Schwarz, J. A. & Kelemen, S. R. Adsorption - Desorption-Kinetics of Co from Clean and Sulfur Covered Ru(001). *Surf Sci* **87**, 510-524 (1979).
- 58 Burke, M. L. & Madix, R. J. Hydrogen on Pd(100)-S - the Effect of Sulfur on Precursor Mediated Adsorption and Desorption. *Surf Sci* **237**, 1-19 (1990).
- 59 Gravil, P. A. & Toulhoat, H. Hydrogen, sulphur and chlorine coadsorption on Pd(111): a theoretical study of poisoning and promotion. *Surf Sci* **430**, 176-191 (1999).
- 60 Kiskinova, M. & Goodman, D. W. Modification of Chemisorption Properties by Electronegative Adatoms - H-2 and Co on Chlorided, Sulfided, and Phosphided Ni(100). *Surf Sci* **108**, 64-76 (1981).
- 61 Feibelman, P. J. & Hamann, D. R. Modification of Transition-Metal Electronic-Structure by P, S, Cl, and Li Adatoms. *Surf Sci* **149**, 48-66 (1985).
- 62 Wilke, S. & Scheffler, M. Poisoning of Pd(100) for the Dissociation of H-2 - a Theoretical-Study of Coadsorption of Hydrogen and Sulfur. *Surf Sci* **329**, L605-L610 (1995).
- 63 Hutchings, G. J., King, F., Okoye, I. P., Padley, M. B. & Rochester, C. H. Selectivity Enhancement in the Hydrogenation of Alpha,Beta-Unsaturated Aldehydes and Ketones Using Thiophene-Modified Catalysts. *J. Catal.* **148**, 453-463 (1994).
- 64 Hutchings, G. J., King, F., Okoye, I. P. & Rochester, C. H. Influence of Sulfur Poisoning of Copper Alumina Catalyst on the Selective Hydrogenation of Crotonaldehyde. *Appl. Catal. A-Gen.* **83**, L7-L13 (1992).
- 65 Marinelli, T. B. L. W. & Ponc, V. A Study on the Selectivity in Acrolein Hydrogenation on Platinum Catalysts - a Model for Hydrogenation of Alpha,Beta-Unsaturated Aldehydes. *J. Catal.* **156**, 51-59 (1995).

- 66 Marshall, S. T. *et al.* Controlled selectivity for palladium catalysts using self-assembled monolayers. *Nat. Mater.* **9**, 853-858 (2010).
- 67 Marshall, S. T., Schwartz, D. K. & Medlin, J. W. Adsorption of Oxygenates on Alkanethiol-Functionalized Pd(111) Surfaces: Mechanistic Insights into the Role of Self-Assembled Monolayers on Catalysis. *Langmuir* **27**, 6731-6737 (2011).
- 68 Makosch, M. *et al.* Organic Thiol Modified Pt/TiO₂ Catalysts to Control Chemoselective Hydrogenation of Substituted Nitroarenes. *ACS Catal.* **2**, 2079-2081 (2012).
- 69 Wu, B. H., Huang, H. Q., Yang, J., Zheng, N. F. & Fu, G. Selective Hydrogenation of alpha,beta-Unsaturated Aldehydes Catalyzed by Amine-Capped Platinum-Cobalt Nanocrystals. *Angew. Chem.-Int. Edit.* **51**, 3440-3443 (2012).
- 70 Kahsar, K. R., Schwartz, D. K. & Medlin, J. W. Selective Hydrogenation of Polyunsaturated Fatty Acids Using Alkanethiol Self-Assembled Monolayer-Coated Pd/Al₂O₃ Catalysts. *ACS Catal.* **3**, 2041-2044 (2013).
- 71 McKenna, F. M. & Anderson, J. A. Selectivity enhancement in acetylene hydrogenation over diphenyl sulphide-modified Pd/TiO₂ catalysts. *J. Catal.* **281**, 231-240 (2011).
- 72 Kahsar, K. R., Schwartz, D. K. & Medlin, J. W. Control of Metal Catalyst Selectivity through Specific Noncovalent Molecular Interactions. *J. Am. Chem. Soc.* **136**, 520-526 (2014).
- 73 Taguchi, T., Isozaki, K. & Miki, K. Enhanced Catalytic Activity of Self-Assembled-Monolayer-Capped Gold Nanoparticles. *Adv. Mater.* **24**, 6462-6467 (2012).
- 74 Kim, M. *et al.* Creating Favorable Geometries for Directing Organic Photoreactions in Alkanethiolate Monolayers. *Science* **331**, 1312-1315 (2011).
- 75 Nigra, M. M., Arslan, I. & Katz, A. Gold nanoparticle-catalyzed reduction in a model system: Quantitative determination of reactive heterogeneity of a supported nanoparticle surface. *J. Catal.* **295**, 115-121 (2012).
- 76 Jiang, Y. *et al.* Modifying the Atomic and Electronic Structures of Gold Nanocrystals via Changing the Chain Length of n-Alkanethiol Ligands. *J. Phys. Chem. C* **116**, 24999-25003 (2012).
- 77 Li, Z. P. *et al.* Synthesis and Characterization of n-Alkylamine-Stabilized Palladium Nanoparticles for Electrochemical Oxidation of Methane. *J. Phys. Chem. C* **114**, 723-733 (2010).
- 78 Xian, J. Y., Hua, Q., Jiang, Z. Q., Ma, Y. S. & Huang, W. X. Size-Dependent Interaction of the Poly(N-vinyl-2-pyrrolidone) Capping Ligand with Pd Nanocrystals. *Langmuir* **28**, 6736-6741 (2012).

- 79 Lu, C. H. & Chang, F. C. Polyhedral Oligomeric Silsesquioxane-Encapsulating Amorphous Palladium Nanoclusters as Catalysts for Heck Reactions. *ACS Catal.* **1**, 481-488 (2011).
- 80 Sadeghmoghaddam, E., Lam, C., Choi, D. & Shon, Y. S. Synthesis and catalytic properties of alkanethiolate-capped Pd nanoparticles generated from sodium S-dodecylthiosulfate. *J Mater Chem* **21**, 307-312 (2011).
- 81 Sadeghmoghaddam, E., Gaieb, K. & Shon, Y. S. Catalytic isomerization of allyl alcohols to carbonyl compounds using poisoned Pd nanoparticles. *Appl. Catal. A-Gen.* **405**, 137-141 (2011).
- 82 Gavia, D. J. & Shon, Y. S. Controlling Surface Ligand Density and Core Size of Alkanethiolate-Capped Pd Nanoparticles and Their Effects on Catalysis. *Langmuir* **28**, 14502-14508 (2012).
- 83 Kwon, S. G. *et al.* Capping Ligands as Selectivity Switchers in Hydrogenation Reactions. *Nano Lett.* **12**, 5382-5388 (2012).
- 84 Sadeghmoghaddam, E., Gu, H. M. & Shon, Y. S. Pd Nanoparticle-Catalyzed Isomerization vs Hydrogenation of Allyl Alcohol: Solvent-Dependent Regioselectivity. *ACS Catal.* **2**, 1838-1845 (2012).
- 85 Kahsar, K. R., Schwartz, D. K. & Medlin, J. W. Liquid-and vapor-phase hydrogenation of 1-epoxy-3-butene using self-assembled monolayer coated palladium and platinum catalysts. *Appl. Catal. A-Gen.* **445**, 102-106 (2012).
- 86 Kim, J. H., Park, J. S., Chung, H. W., Boote, B. W. & Lee, T. R. Palladium nanoshells coated with self-assembled monolayers and their catalytic properties. *RSC Adv.* **2**, 3968-3977 (2012).
- 87 Moreno, M., Ibanez, F. J., Jasinski, J. B. & Zamborini, F. P. Hydrogen Reactivity of Palladium Nanoparticles Coated with Mixed Monolayers of Alkyl Thiols and Alkyl Amines for Sensing and Catalysis Applications. *J. Am. Chem. Soc.* **133**, 4389-4397 (2011).
- 88 Cargnello, M. *et al.* A Versatile Approach to the Synthesis of Functionalized Thiol-Protected Palladium Nanoparticles. *Chem. Mat.* **23**, 3961-3969 (2011).
- 89 Lu, F., Ruiz, J. & Astruc, D. Palladium-dodecanethiolate nanoparticles as stable and recyclable catalysts for the Suzuki-Miyaura reaction of aryl halides under ambient conditions. *Tetrahedron Lett.* **45**, 9443-9445 (2004).
- 90 Gross, E. *et al.* Asymmetric Catalysis at the Mesoscale: Gold Nanoclusters Embedded in Chiral Self-Assembled Monolayer as Heterogeneous Catalyst for Asymmetric Reactions. *J. Am. Chem. Soc.* **135**, 3881-3886 (2013).

- 91 Fernandes, A. *et al.* Increased Catalytic Activity of Surface-Immobilized Palladium Complexes in the Fluorogenic Deprotection of an Alloc-Derivatized Coumarin. *Chem.-Eur. J.* **18**, 788-792 (2012).
- 92 Hara, K. *et al.* Self-assembled monolayers of compact phosphanes with alkanethiolate pendant groups: Remarkable reusability and substrate selectivity in Rh catalysis. *Angew. Chem.-Int. Edit.* **47**, 5627-5630 (2008).
- 93 Berner, S. *et al.* Activity boost of a biomimetic oxidation catalyst by immobilization onto a gold surface. *J. Catal.* **244**, 86-91 (2006).
- 94 Paluti, C. C. & Gawalt, E. S. Immobilized aza-bis(oxazoline) copper catalysts on alkanethiol self-assembled monolayers on gold: Selectivity dependence on surface electronic environments. *J. Catal.* **275**, 149-157 (2010).

CHAPTER 2

Controlling surface crowding on Pd catalysts with thiolate self-assembled monolayers

2.1 Abstract

The relationship between surface crowding and catalytic activity was investigated using thiolate self-assembled monolayers (SAMs) on Pd/Al₂O₃ catalysts. The surface density of the thiolate modifier was controlled by varying the steric bulk of the organic substituent. A straight-chain alkanethiol 1-octadecanethiol (C18), with a nearest-neighbor spacing of ~4.7 Å on Pd(111) surfaces, created a denser SAM coating than 1-adamantanethiol (AT) with a nearest-neighbor spacing of ~6.4 Å. Diffuse reflectance infrared spectroscopy revealed that CO adsorbate molecules adsorbed only on three-fold hollow and atop sites on C18-modified surfaces. On AT-modified surfaces, however, access to bridging and additional linear sites was also observed. Analysis of adsorption isotherms suggested that CO adsorption energies were comparable on AT-modified and C18-modified catalysts. Acetylene hydrogenation, which results in uncontrolled crowding due to carbonaceous “coke” formation on the catalyst, was found to be insensitive to modification by the thiols. For hydrogenation reactions less associated with uncontrolled coking, crowding – and therefore reactivity – could be controlled systematically using SAMs. In particular, ethylene hydrogenation was 17 times faster on AT-coated surfaces than on C18-coated surfaces, consistent with the additional accessibility to specific sites

unavailable on C18-modified surfaces. The effect of modifier density on reactivity was found to be dramatically different for several mono- and bi- functional reactants in a manner consistent with previous literature reports, suggesting that controlled crowding with SAMs can be used to understand reaction structure sensitivity and active site requirements in catalysis.

2.2 Introduction

Self-assembled monolayers (SAMs) have recently been utilized as modifiers to control reactivity in heterogeneous catalysis¹⁻⁵. For example, alkanethiol SAMs improved the selectivity of 1-epoxybutane formation from 1-epoxy-3-butene (EpB) on supported Pd catalysts from 11 to 94% under equivalent reaction conditions. One of the major advantages of SAM based modifiers is their ability to form highly-ordered, consistent structures on metal surfaces. This consistency is presumably attributable to the thermodynamically limited assembly process, which also facilitates connections between catalysis and surface science studies. In addition, both the attachment chemistry and tail groups can easily be tailored to create monolayers with desirable surface properties. These features potentially make SAMs useful modifiers for studying the effect of controlled surface modification on catalytic reactivity. However, though a previous surface science study has shown that well-ordered SAMs on Pd(111) inhibit epoxide ring-opening while permitting olefin adsorption⁶, the detailed effect of SAMs on the nature of available active sites has not been explored in detail. This is particularly true for supported nanoparticle catalysts, where the presence of significant numbers of corner, edge, and defect sites may create uncertainties in the effect on active sites.

The effect of surface crowding, i.e. modifier density, on catalytic reactivity is of significant practical importance. *Uncontrolled* surface crowding in the form of carbonaceous

coke can occur when reactant molecules strongly adsorb and decompose on a catalyst surface. This process is prevalent in a number of important industrial applications⁷ including hydrogenation⁸, steam reforming^{9,10}, and dehydrogenation¹¹. In addition, sulfur, which is often naturally present in hydrocarbon feedstocks¹², has the ability to essentially poison a reaction when present at high coverage, but has been used as a modifier at lower coverage to drive selectivity of reactions toward more desired products^{13,14}. Despite the prevalence of this modification technique, a deep understanding of the effect of modifier density on catalytic reactivity is lacking. Given that subtle changes in surface density can dramatically affect the electronic and steric interactions between reactants and the surface, it is important to develop systematic methods to examine these phenomena.

In this chapter, we demonstrate the ability to control modifier surface density systematically by tuning the thiol tail chemistry to form monolayers with varying sulfur coverage. As expected, in situations where an irreversibly-adsorbed coke layer forms (e.g. acetylene hydrogenation), the SAM coating does not affect the reactivity. However, in the absence of coking, crowding can be systematically controlled using SAMs. This is achieved by using a densely-packed, straight-chain alkanethiol 1-octadecanethiol (C18) and a bulky caged hydrocarbon thiol 1-adamantanethiol (AT) to control thiol density on the surface via differences in the steric bulk of the organic substituent of the thiol modifier. Kinetic measurements were performed in conjunction with IR spectroscopy to develop a deeper understanding of the ways in which surface crowding affects adsorption and reactivity, which can be rationalized in terms of specific surface site availability. This knowledge provides insight that could lead to improved catalyst modification and could be a useful technique for directing selectivity for other reactions.

2.3 Experimental methods

Pd/Al₂O₃ (5 wt%), 1-octadecanethiol (98%), 1-adamantanethiol (95%), 1-2-epoxybutane (99%), and 200-proof HPLC-grade ethanol were obtained from Sigma Aldrich. CO chemisorption (Quantachrome Autosorb-1) was previously used to determine a metal surface area of 3.74 m²g⁻¹ on the uncoated catalyst¹. The palladium metal dispersion was 16.8% and the average metal particle diameter was 6.7 nm. Propionaldehyde (97%) was obtained from Fisher Scientific. Acetylene and ethylene (10% hydrocarbon, balance helium) and all other gases were obtained from Airgas. Before testing, all catalyst samples were oxidized at 573 K in 20% oxygen for two hours, subsequently reduced at 473 K in 20% hydrogen for at least two hours, and then allowed to cool to room temperature before deposition and/or testing. For thiol deposition, modified catalysts were then placed in 1mM ethanolic solution for between 12 and 24 hours. After deposition, samples were washed once with ethanol, decanted, and then dried under vacuum for at least two hours before characterization to confirm complete SAM formation.

All catalytic reactions were carried out in a gas-phase plug flow reactor and were monitored using an Agilent 5890A gas chromatograph equipped with a flame ionization detector, DB-FFAP capillary column, and Agilent software. Hydrogenation reactions were performed at 323K using a 10:1 hydrogen to reactant feed ratio where total flow rates for each reaction were between 50-100 sccm. Liquid reactants were temperature controlled and bubbled through the system using helium carrier gas where Antoine parameters were used to determine reactant vapor pressure. The amount of catalyst used for both modified and unmodified surfaces was dependent on the specific reactivity of each reaction but was chosen to achieve < 5% conversion in all cases. All samples were diluted to 300 mg using inert Al₂O₃. Rates are reported per gram of catalyst as opposed to turnover frequencies in order to

make comparisons about activity between modified and unmodified catalysts. In order to determine the true turnover frequencies on coated catalysts, knowledge of the number of active sites on modified catalysts would be needed. While this is still a subject of debate, turnover frequencies normalized to the known surface area of the *uncoated* system can be calculated from the reported rates. These TOFs are reported in the discussion below, so that rates for all reactions and catalysts can be interpreted on a per-surface metal atom basis.

FTIR analysis was performed using a Thermo Scientific Nicolet 6700 FT-IR with a closed cell attachment (Harrick) for Diffuse Reflectance Infrared Fourier Transform Spectroscopy (DRIFTS). Fifty scans at 4 cm⁻¹ resolution were used for each spectrum. The quality of all coated samples was characterized in the C-H stretching region (2,800 – 3,000 cm⁻¹) to confirm monolayer formation prior to catalytic testing. For CO DRIFT experiments, catalyst samples were placed in a gas tight cell that was evacuated to achieve an initial baseline pressure of <0.10 Torr. Successive doses of CO were then introduced into the cell at CO pressures of 0.15, 0.27, 0.50, 1.20, 2.00, and 300 torr. After each dose, spectra were taken after at least 10 minutes to allow the system to come to equilibrium. At pressures above 300 torr, gas phase CO was observed indicating the surface was at CO saturation.

2.4 Results and discussion

The formation and structure of straight-chain alkanethiol monolayers has been studied extensively on metal surfaces¹⁵. When thiol molecules are exposed to metal surfaces the sulfur head groups bind covalently to the metal producing a highly ordered monolayer that forms a ($\sqrt{3} \times \sqrt{3}$)R30 adsorption geometry on fcc(111) surfaces. The spacing between sulfur atoms on Au and Pd surfaces has been determined to be $\sim 5.0 \text{ \AA}$ ^{16,17} and $\sim 4.7 \text{ \AA}$ ¹⁸,

respectively. Monolayers formed using 1-adamantanethiol have also been investigated on Au surfaces. For these types of monolayers, the spacing between sulfur groups has been found to be $\sim 6.9 \text{ \AA}$ with a proposed (7X7) unit cell structure¹⁹. This spacing corresponds to a nearest neighbor distance of $\sim 6.4 \text{ \AA}$ on Pd. Figure 2-1 shows the DRIFT spectra in the C-H stretching regime and structure of the molecules used to form monolayers in this study. For the C18 coated catalyst, the methylene *d*- stretching mode was observed at $2,921 \text{ cm}^{-1}$, consistent with an ordered SAM on polycrystalline palladium¹⁷. AT monolayers have not been studied previously on Pd using IR spectroscopy. Here, the asymmetric and symmetric methylene stretches were observed at $2,918 \text{ cm}^{-1}$ and $2,854 \text{ cm}^{-1}$, respectively. This is compared to Au(111) surfaces where these peaks were observed at $2,911 \text{ cm}^{-1}$ and $2,850 \text{ cm}^{-1}$, respectively²⁰. Peak positions of characteristic C-H stretches can, in general, be used only to gain a broad sense of monolayer structure and provide minimal information about absolute monolayer coverage. Additional information about coverage can be determined from the CO “titration” technique described in this work.

Controlled vs. Uncontrolled Crowding: Ethylene vs. Acetylene

Uncontrolled surface crowding can occur when reactant molecules decompose on the surface to form irreversibly adsorbed coke species; this process is known to occur during acetylene hydrogenation²¹. For uncontrolled crowding conditions where significant coking occurs, the irreversibly adsorbed reactants produce their own surface environment with a unique chemical character. In this situation, it is expected that the SAMs will have less effect on the reactivity of the catalyst because of the layer produced by the reactants, i.e. the modified and unmodified surfaces become less distinguishable to adsorbed reactants. In situations where

significant coking does not occur (e.g. ethylene hydrogenation²²), we hypothesize that surface crowding can be controlled systematically using SAMs.

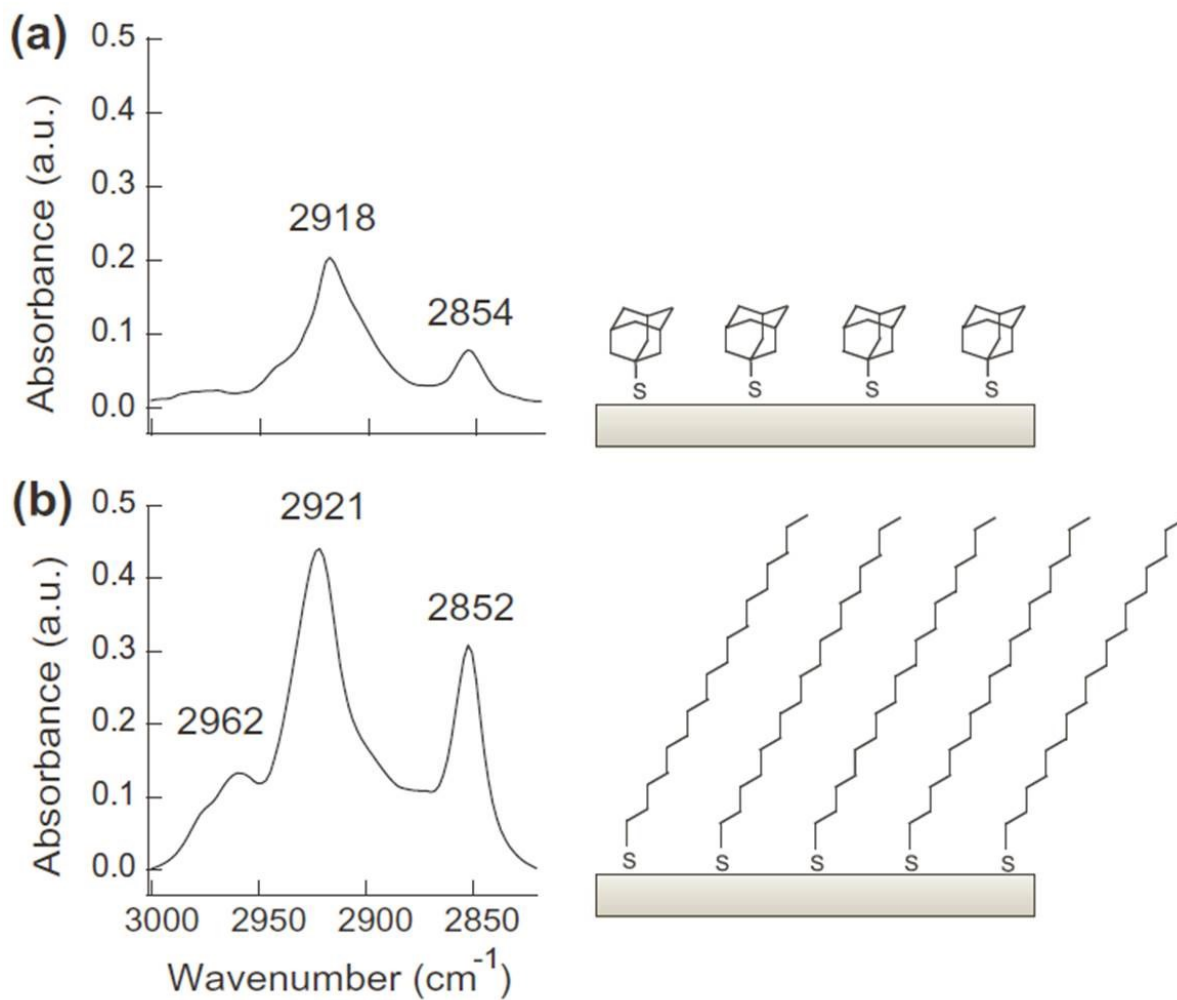


Figure 2-1. DRIFT spectra and structure of (a) 1-adamantanethiol and (b) 1-octadecanethiol on a Pd surface.

To demonstrate the effects of uncontrolled vs. controlled crowding, hydrogenation rates were measured on unmodified, AT-, and C18-modified surfaces for the hydrogenation of acetylene and ethylene. Results are shown in Figure 2-2. Results are presented after ~1 hour

time-on-stream after which steady-state conditions were achieved for this reaction. As expected, the rate of acetylene hydrogenation was indistinguishable on coated or uncoated Pd surfaces at steady-state. For the initial time-on-stream, the thiol coated catalysts showed slightly lower activity than the uncoated catalyst. This difference in activity remained more-or-less constant over the first ~40 minutes at which point the uncoated catalyst reached steady-state. Afterward, typically within ~10-20 minutes, thiol coated catalysts achieved steady-state. During this initial period, thiol coated catalysts showed improved selectivity over uncoated catalysts toward ethylene formation (~20%). However, this improvement was no longer observed after steady-state conditions were achieved. Unlike the case with acetylene, the rate of ethylene hydrogenation, which occurs in the absence of significant coking, systematically decreased with increasing sulfur coverage.

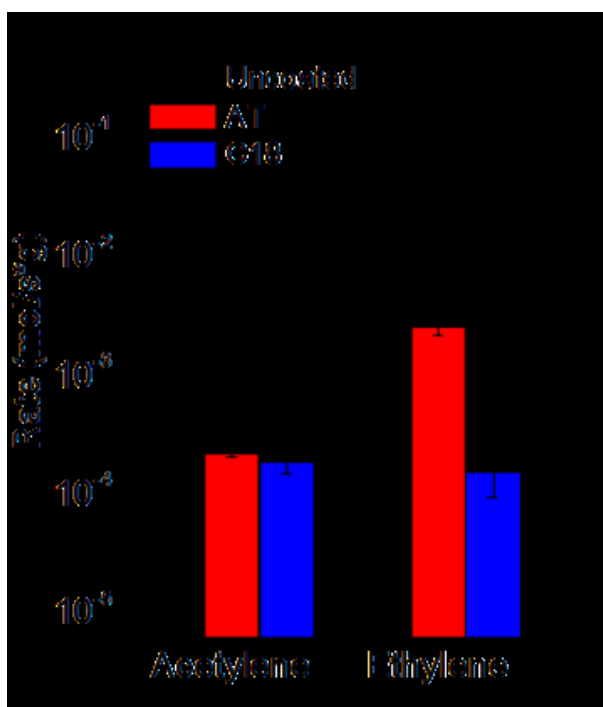


Figure 2-2. Hydrogenation rates of acetylene and ethylene on uncoated, AT, and C18 coated Pd/Al₂O₃ catalysts.

To directly probe the presence of uncontrolled crowding (i.e. coking), DRIFT spectra were recorded for modified and unmodified samples before and after a one-hour exposure to reaction conditions for acetylene and ethylene hydrogenation. These spectra are shown in Figure 2-3. The spectra before and after acetylene hydrogenation demonstrate clearly that a surface coke layer was acquired during the reaction whereas there was no evidence for this for samples exposed to ethylene reaction conditions. As confirmed by the identical reaction rates on modified and unmodified surfaces for acetylene hydrogenation, SAMs do not affect the reactivity of the reaction when significant coking occurs. However, for reactions where coking is not significant, SAMs can be used to systematically control surface crowding to examine how the modified surface affects reactivity.

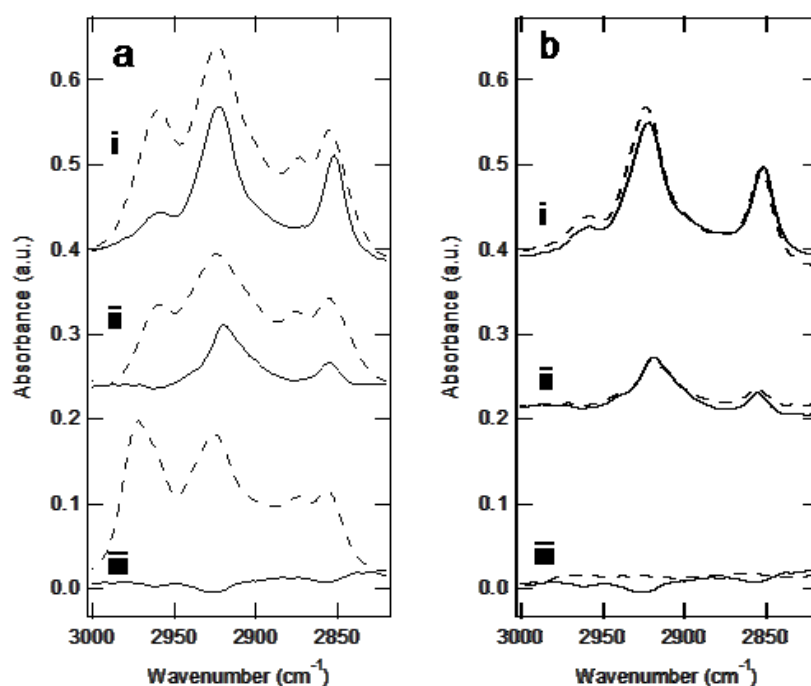


Figure 2-3. DRIFT spectra for samples before and after (a) acetylene and (b) ethylene hydrogenation on (i) C18 (ii) AT (iii) and unmodified catalysts. Solid and dashed lines are shown for samples before and after 1 hour of hydrocarbon exposure, respectively.

Effect of Crowding on Surface Reactivity

An illustration of the unit cells for C18 and AT monolayers on fcc(111) surfaces is shown in Figure 2-4.

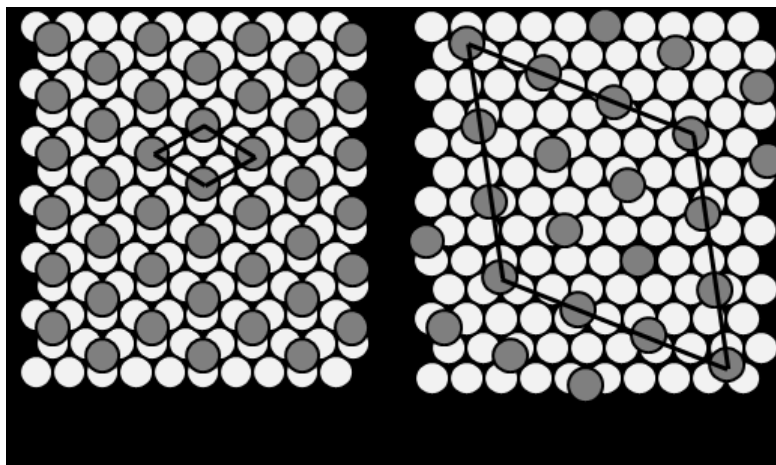


Figure 2-4. Unit cells for (a) C18 and (b) AT monolayers on fcc(111) surfaces.

From a simple geometric perspective, the sulfur on the more-dense C18 monolayer covers $\sim 1.8X$ more Pd surface area than AT surfaces assuming a sulfur radius of ~ 180 pm. However, hydrogenation rates for ethylene on AT surfaces were found to be a factor of ~ 17 faster than on C18-modified catalysts (Figure 2-2). The apparent difference between measured rates and available space suggests that sulfur attachment density alone is not sufficient to explain the higher rate on AT-coated catalysts. We suggest two hypotheses that could potentially explain this difference: (1) the ethylene adsorption strength is reduced in the presence of a more dense layer of sulfur, and/or (2) specific, more highly reactive sites are more accessible on the AT-coated catalyst. The presence of sulfur has been shown to reduce the adsorption strength of a number of species including carbon monoxide and ethylene^{23,24}. This effect has been suggested to be coverage dependent, so it is possible that the more densely-packed C18 monolayers could reduce the adsorption strength of reactants more significantly than AT monolayers leading to

lower activity on these surfaces. An alternative explanation involves the different types of sites exposed on C18 vs. AT surfaces. Specifically, the theoretical packing geometry of a C18 monolayer does not readily expose atop sites except presumably at defects. Atop sites are thought to be the preferred reaction site in ethylene hydrogenation where pi-bound species preferentially adsorb and react²⁵⁻²⁷, which may be responsible for enhanced activity.

To gain further insight into the competing hypotheses of adsorption strength and site accessibility, CO DRIFT spectroscopy was performed on uncoated, AT-, and C18-coated surfaces. Samples were exposed to increasing amounts of CO ranging from 0.15 to 300 torr and spectra were taken after 10 minutes to allow for samples to come to equilibrium. Results are shown in Figure 2-5. Figure 2-5.a illustrates how the spectrum developed as a function of increasing CO coverage on the uncoated surface. These results were similar to previous observations on palladium surfaces and catalysts^{28,29}. At low CO coverage, two major features were apparent at 2065 and 1951 cm^{-1} . The weak feature at 2065 cm^{-1} was indicative of CO bound to atop sites. The more prominent feature at 1951 cm^{-1} has been attributed to a combination of bonding in bridging and three-fold hollow sites. Upon increasing CO pressure, the peak initially at 2065 cm^{-1} was found to shift to 2090 cm^{-1} consistent with increasing dipole coupling interactions³⁰. In addition, at pressures above ~1.2 torr, there appeared to be two distinct features suggesting linear adsorption to two types of atop sites. Similarly, two features became apparent upon increasing CO pressure for the peak initially at 1951 cm^{-1} . At saturation, three major bands were discernible at 1938, 1990, and 2090 cm^{-1} . The peaks at 2090 and 1938 cm^{-1} were attributed to CO bound on atop and bridging/hollow sites, respectively. The peak at 1990 cm^{-1} was indicative of CO adsorbed on (100) facets and bridge-bonded to particle edges and steps.

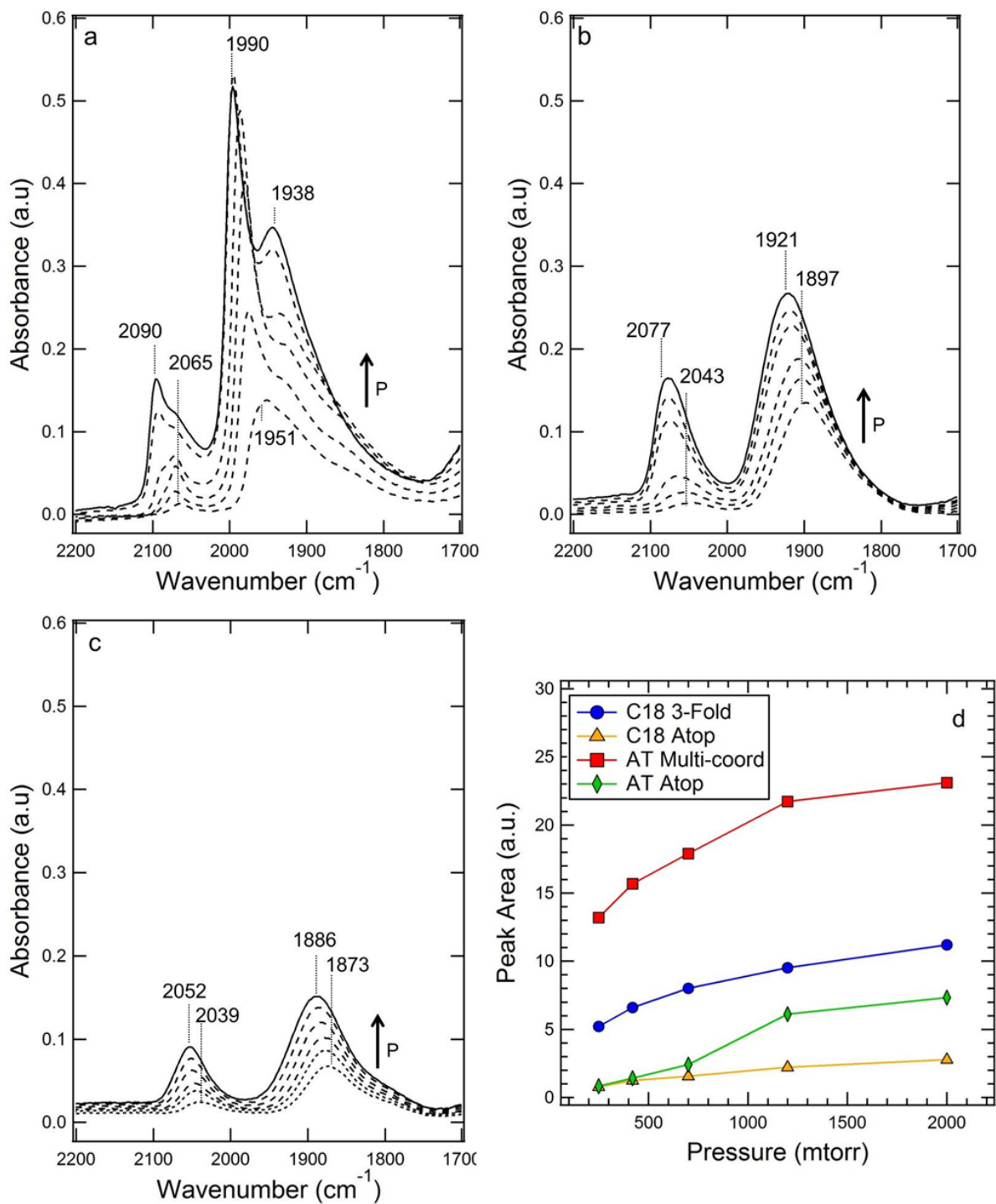


Figure 2-5. CO DRIFTS on (a) unmodified (b) AT modified, and (c) C18 modified Pd/Al₂O₃ catalysts. The series of spectra were obtained at constant temperature (298 K) with CO pressure increasing from 0.15 to 300 torr (solid black line). (d) Integrated peak areas for multi-coordinated and linear bound species for AT and C18 surfaces.

The thiol modified surfaces exhibited two major features. For the AT-coated sample, the peak initially at 1897 cm^{-1} is indicative of CO adsorbed in three-fold hollow sites. With increasing pressure, this peak was observed to shift to 1921 cm^{-1} which is consistent with CO dipole coupling and increasing occupation of bridge-bound sites²⁸. The peak initially measured at 2043 cm^{-1} was found to shift to 2077 cm^{-1} with increasing pressure and is attributed to linear bound CO experiencing a similar increase in dipole interactions. Two similar features were observed for the C18-coated sample. The peak initially at 1873 cm^{-1} (three-fold hollow) was found to shift to 1886 cm^{-1} while the peak at 2039 cm^{-1} (linear) was found to shift to 2052 cm^{-1} with increasing pressure. The proposed peak assignments for each catalyst are given in Table 2-1.

Catalyst	Vibrational Frequency (cm^{-1})	Assignment
Uncoated	1938	μ 3 hollow-bonded and μ 2 bridge-bonded CO on (111) planes
	1990	CO adsorbed on (100) facets and bridge-bonded to particle edge and steps.
	2065	CO linearly bound to steps or defects
	2090	CO linearly bound on (111) planes
AT	1921	μ 3 hollow-bonded and μ 2 bridge-bonded CO on (111) planes
	2043	CO linearly bound to steps or defects
	2077	CO linearly bound on (111) planes
C18	1886	μ 3 hollow-bonded on (111) planes
	2052	CO linearly bound to steps or defects

Table 2-1. CO frequency assignments for uncoated, C18-modified, and AT-modified catalysts.

Generally speaking, the peak areas for the AT-modified catalyst features were significantly larger than were observed for the C18-modified surface. This indicated that more CO was able to adsorb on AT-coated surfaces. The shifts for the multi-coordinated and linear bound features for the AT-modified catalyst were found to be 32cm^{-1} and 24cm^{-1} , respectively. The shifts for these same features were found to be 13cm^{-1} and 13cm^{-1} on the C18 surface. The greater shift for the AT surface is likely related to a greater amount of dipole coupling interactions that occur on these less-densely precovered surfaces. For the C18 sample, increasing the pressure of CO increased the total amount adsorbed on the surface, but the reduced peak shifting suggested there are fewer interactions of neighboring CO molecules than is seen on the AT-coated surfaces.

In addition to the greater amount of total CO adsorbed on the uncoated surface, as evidenced by the larger total peak areas, in general the unmodified surface exhibited a greater heterogeneity of sites available for CO adsorption. Specifically, the feature found at 1990cm^{-1} was not observed for either of the coated surfaces suggesting that CO is not significantly bridge-bonding to (100) facets and step sites on thiol coated surfaces.

Adsorption Strength

To probe the effect of monolayer density on adsorption strength, an adsorption coefficient ratio was extracted from the AT and C18 isotherms for the multi-coordinated species. As a first approximation, data were fit using a Langmuir isotherm adsorption model. This model is used only to gain a general sense of the differences in CO adsorption strength since there are assumptions of the model that are not likely satisfied here including: (1) no interactions between adsorbate molecules and (2) site equivalency. The Langmuir equation is expressed as:

$$\Gamma = \Gamma_{max} \frac{Kc}{1+Kc} \quad (1)$$

where K is the Langmuir adsorption constant, c is the gaseous partial pressure, Γ is the amount adsorbed, and Γ_{max} is the maximum amount adsorbed as c increases. Γ was estimated from integrated peak areas for the multi-coordinated species (Figure 2-5.d). The Langmuir equation was linearized using the Eadie-Hofstee form where:

$$\Gamma = \Gamma_{max} - \frac{\Gamma}{Kc} \quad (2)$$

Thus a plot of Γ vs. Γ/c yields a slope of $-1/K$ and an intercept Γ_{max} . The heterogeneity of the uncoated surface complicates this type of simple analysis because of the additional types of adsorption sites that are accessible at higher CO pressure. For this reason, this analysis was used only to estimate differences between C18 and AT surfaces which demonstrate similar, Langmuir-type adsorption behavior. The linearized plots for the AT and C18 surfaces are shown in Figure 2-6.

From these data, an adsorption coefficient ratio $\frac{K_{AT}}{K_{C18}} = K_{Rel}$ was determined from the slopes and found to be $K_{Rel} = 1.58 \pm 0.19$. The general expression for the adsorption coefficient can be described in terms of the enthalpic and entropic contributions by the following relationship:

$$K = A e^{\frac{-U_{ads}}{RT}} \quad (3)$$

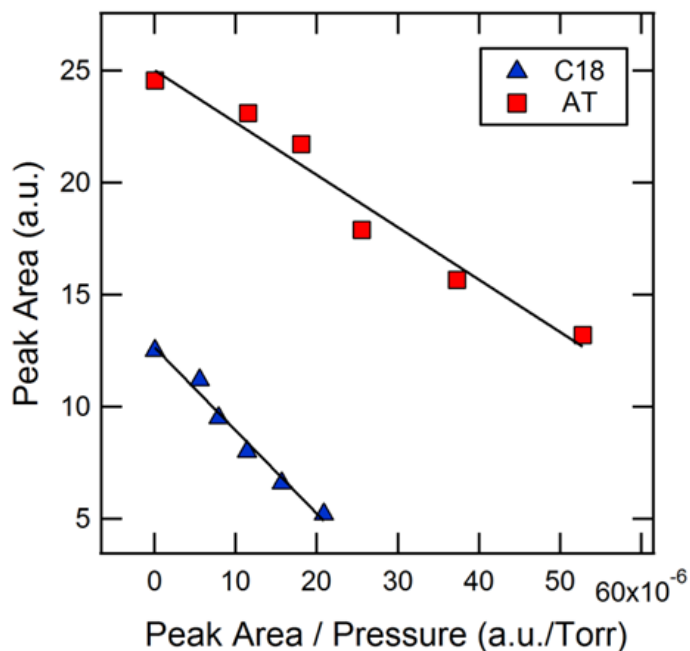


Figure 2-6. Linearized Langmuir isotherms for AT and C18 surfaces.

where U_{ads} is the adsorption energy, A is the exponential prefactor, R is the ideal gas constant, and T is the temperature. Assuming entropic losses (and thus A factors) were similar upon adsorption for both thiol-modified surfaces, this expression can be solved from the above adsorption coefficients to determine an approximate difference in adsorption energy on the two modified surfaces. From this method, the difference in adsorption energy was estimated to be $\sim(1.1 \pm 0.3)$ kJ/mol, such that adsorption on the AT-modified catalyst was slightly more exothermic. It is likely that entropic losses are in fact greater for adsorption on the C18 catalyst than on the AT catalyst. However, a greater loss in entropy on the C18 catalyst would subsequently require a greater adsorption energy in order for the binding constant, K , to remain unchanged. This would result in a smaller estimated difference in adsorption energy between the

C18 and AT catalysts. The estimated value of (1.1 ± 0.3) kJ/mol for the difference in adsorption energy thus represents the upper-limit estimation for this calculation.

This small difference in energy between CO adsorption on the AT and C18 surfaces may be rationalized by considering both CO-CO and CO-S adsorbate interactions on the surface. The adsorption energy of carbon monoxide on clean Pd surfaces ($\sim 125 - 200$ kJ/mole) tends to decrease with increasing CO coverage³¹⁻³³. Similarly, the presence of sulfur has been shown to decrease the adsorption strength of CO³⁴. This combined effect was investigated by Kiskinova and Yates²³ who demonstrated that the effect of sulfur on the activation energy for CO desorption on Pt(111) is of the same order of magnitude as that experienced by CO in denser CO overlayers on a sulfur-free surface. Specifically, the desorption energy of CO at $\theta_{\text{CO}} \sim 0.4$ was found to be the same as the desorption energy of CO on a precovered sulfur surface ($\theta_{\text{S}} \sim 0.25$) for CO coverage of $\theta_{\text{CO}} < 0.11$. Consequently, while the higher sulfur coverage on the C18 surface ($\theta_{\text{S}} \sim 0.33$) reduces CO adsorption strength, it is likely that on the less dense AT surface, ($\theta_{\text{S}} \sim 0.18$) the greater CO coverage has a similar effect on adsorption strength. This may explain why differences in adsorption energy are not more dramatic in the presence of higher sulfur coverage on the C18 surface.

The initial adsorption strength of ethylene and CO on Pd surfaces are similar ($\sim 130 - 185$ kJ/mole for strongly-bound ethylidyne), and both also decrease with coverage due to adsorbate interactions^{24,35}. We therefore hypothesize that the effect of surface crowding on adsorption energy would be related for CO and ethylene. The minor difference in adsorption energy between the two modified surfaces suggests that differences in adsorption energy alone do not likely account for the dramatic differences observed in reactivity between C18 and AT surfaces. Given the differences between the binding of CO and ethylene to the metal surface, a role for

differences in ethylene adsorption energy cannot be ruled out. However, previous surface science investigations of SAM-coated Pd(111) surfaces have shown that SAMs have a similar influence on olefin adsorption as other coadsorbates, suggesting that thiols do not have a strong, highly specific electronic effect on ethylene adsorption⁶.

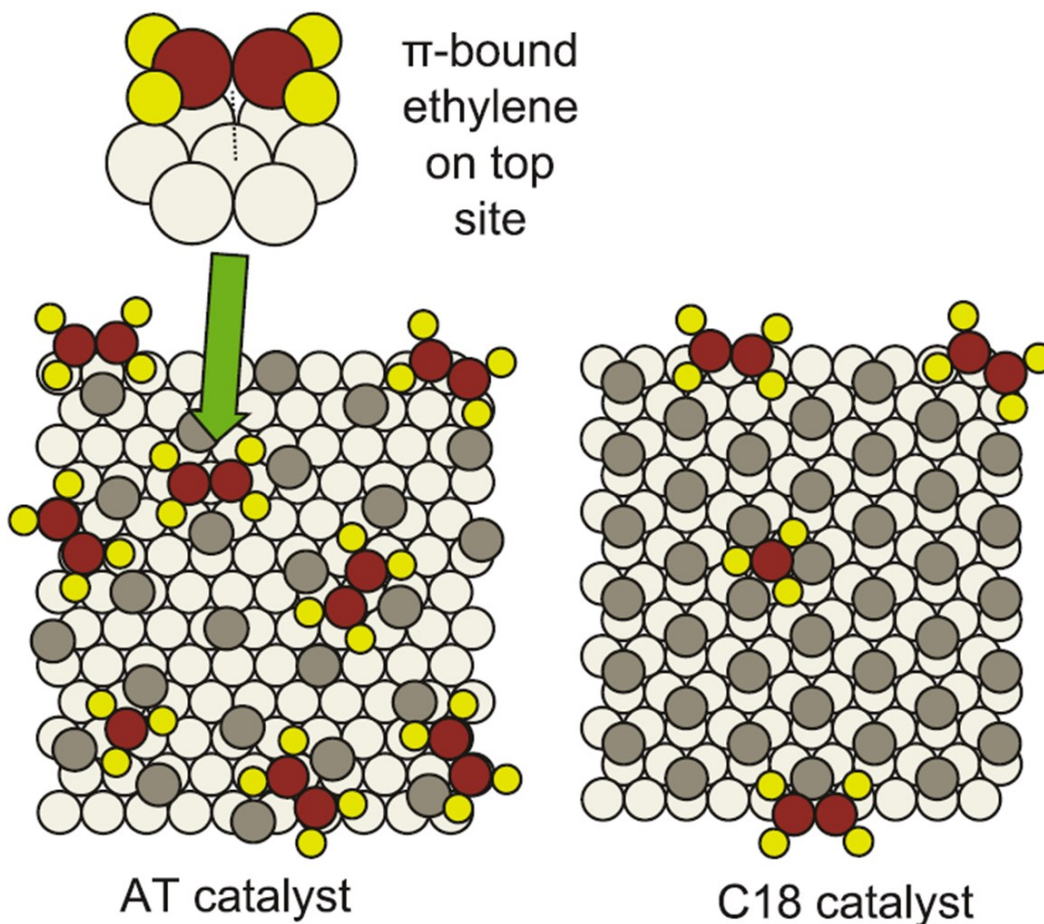
Site Accessibility

Close inspection of the DRIFT spectra revealed adsorption to two distinct types of atop sites on the unmodified surface as evidenced by the peak shoulder that begins to form at pressures above 1.2 torr. It is possible that the additional higher frequency peak was due to on-top CO on the (111) terraces³⁶. Similarly at this pressure, there was a significant jump in the integrated peak area (Figure 2-5d) for this feature on the AT surface which suggested adsorption to two types of atop sites on this surface. From these observations, it is suggested that adsorption on AT-modified catalysts occurs on three-fold hollow, bridging, and two types of atop sites. In contrast, there is no evidence for a second type of atop adsorption site on the C18-modified surface. Adsorption on C18-coated surfaces is suggested to occur only on three-fold hollow sites and a single type of atop site.

There is strong evidence suggesting that there are specific types of sites required in order for a particular reaction pathway to occur for a number of reactions. While ethylene is capable of adsorbing on different sites in multiple adsorption geometries on Pd surfaces, It has been proposed that the most reactive form of ethylene is the pi-bound species on atop sites²⁵. The additional adsorption on atop sites on the AT surface is consistent with the higher activity on this surface for ethylene hydrogenation. Scheme 2-1 highlights the proposed differences in ethylene adsorption on the two thiol-modified catalysts. The more crowded C18 catalyst restricts

adsorption primarily to atop sites on edges and more compact geometries (e.g. ethynidyne adsorption within monolayer) within the monolayer. In addition to these species, the greater sulfur spacing on the AT catalyst allows the reactive pi-bound species to adsorb and react on terrace top sites.

60



Scheme 2-1. Proposed adsorption mechanism on thiol-modified surfaces. On C18 catalysts, adsorption primarily occurs in three-fold hollow and a single type of atop site at saturation coverage. On AT-coated catalysts, adsorption occurs on these same types of sites but has additional access to bridging and a second type of reactive, linear site upon increasing coverage.

Reactivity of Specific Functional Groups

The lowest energy reaction pathway on a surface is often associated with a particular type of site or ensemble of sites³⁷. Changing the accessibility of different types of sites by altering monolayer density is therefore expected to influence catalytic activity of different reactive groups to varying extents. This idea was tested by measuring and comparing the hydrogenation rates of a number of simple reactants on uncoated, C18-coated, and AT-coated surfaces. Rates on AT and C18 surfaces normalized by the uncoated rate are shown in Figure 2-7.

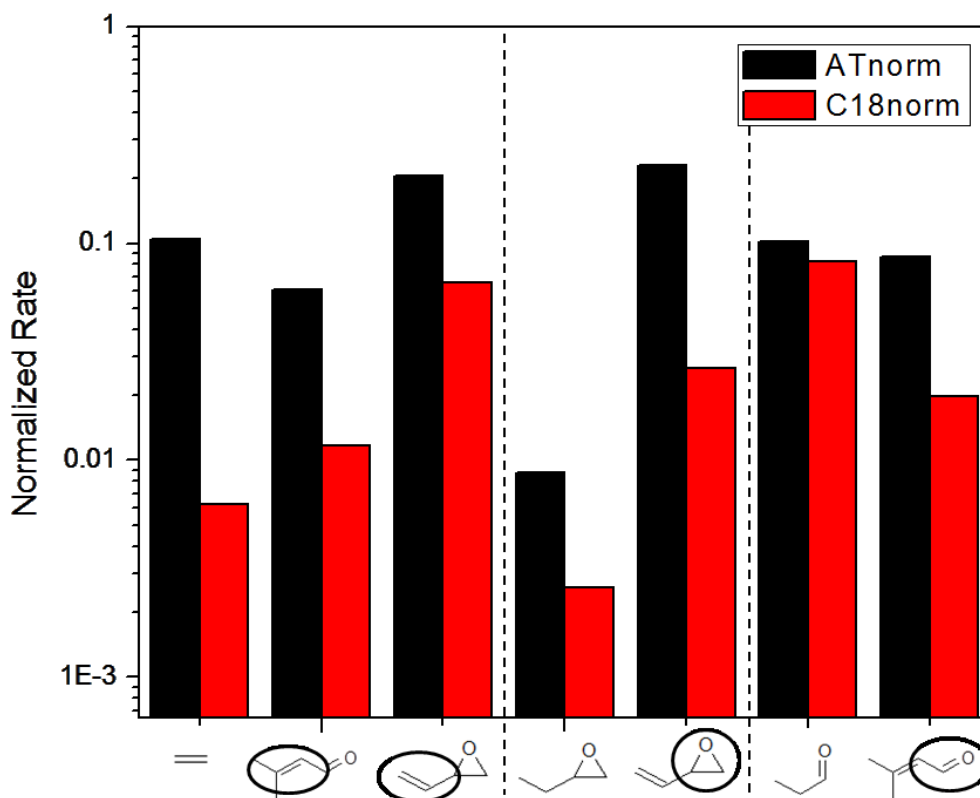


Figure 2-7. Reaction rates for mono- and bi-functional reactants on C18 and AT surfaces. Rates have been normalized to rate on unmodified surface. Circled functional groups indicate that rates are reported for the hydrogenation of the specified group.

In order to probe the effect of modifier density on the reactivity of specific functional groups, the hydrogenation rates of three mono-functional reactants were measured including ethylene, 1-epoxybutane, and propionaldehyde to represent olefin, epoxide, and aldehyde functionality, respectively. As expected, the rate of reductions on the thiol-modified surfaces were dramatically different depending on the reacting functional group. For hydrogenolysis of 1-epoxybutane to 2-butanol, the reaction rate is drastically decreased even for the AT coating. Though detailed mechanistic investigations for the ensemble size requirement of epoxide hydrogenolysis have to our knowledge not been reported, previous studies of hydrogenolysis reactions (including cyclopropane hydrogenolysis) have revealed that these reactions are highly structure sensitive³⁸⁻⁴¹ with a recent study using supported Pt catalysts reporting a required ensemble size of seven contiguous Pt atoms⁴². The dramatic reduction in rate for the AT catalyst (and further decrease for C18) in our studies is consistent with a large ensemble size requirement for this reaction.

A contrasting case is the hydrogenation of propionaldehyde, where the AT-modified catalyst and C18-modified catalyst exhibit similar reactivity. Furthermore, the reactivity is relatively high compared to the uncoated catalyst. This behavior suggests that aldehyde hydrogenation should be highly structure *insensitive*, in agreement with previous findings⁴³. In fact, many catalysts effective for hydrogenation of aldehydes involve Pt-group sites that are heavily modified by other adsorbates, promoting weak interactions between the aldehyde and site that are associated with high reactivity⁴⁴⁻⁴⁶. Thus, the extra crowding on the C18 catalyst has a minimal effect on reaction rate. An alternative hypothesis is that this reaction occurs primarily at edges/defect sites. It is likely that the number of exposed defect sites would be approximately the same for thiol-modified catalysts. Consequently, reaction rates are also

expected to be similar in cases where reactions occur primarily at defects (regardless of monolayer spacing). Overall, the significant differences in reactivity observed for these functional groups confirm that the effect of modifier density on reactivity depends strongly on the nature of the reactant, and that controlled crowding with SAMs can elucidate the active site requirements for different reactions on metal catalysts.

To determine if these effects could be generalized in terms of distinct functional group reactivity, the hydrogenation rates of the bifunctional reactants 3-methyl-2-butenal (prenal) and 1-epoxy-3-butene (EpB) were measured on the same surfaces. The hydrogenation rates of the functional constituents of these two molecules were compared to the reactivity of their monofunctional counterparts (Figure 2-7) to determine if there was a general agreement in reactivity. The results indicated significant differences both in overall rate reduction on the thiol-modified surfaces and in rate differences between the AT and C18 surfaces for the reactivity of each class of functional group. The most drastic difference was found between the epoxide containing reactants. For 1-epoxybutane and EpB, reductions in rate on the AT-modified catalyst were found to be a factor of ~ 100 and ~ 4 , respectively whereas differences in rate between the AT- and C18-coated surfaces for these epoxides were found to be a factor of ~ 3 and ~ 10 , respectively. It has been shown on hexanethiol-modified surfaces that the olefin constituent interacts more strongly with the surface than the epoxide on Pd(111)⁶. We then hypothesize that the presence of the olefin constituent in the EpB molecule increases the overall reactant interaction with the surface and, in turn, the rate of hydrogenation of the epoxide function, resulting in the greater epoxide hydrogenation rate of EpB compared to 1-epoxybutane. In other words, the presence of the olefin constituent in EpB has a dramatic effect on the reactivity of the epoxide functionality. It is similarly observed for the other reactants that the presence of

additional reactive groups affects the overall reactivity of the molecule ⁴⁴. From these observations, it is determined that the effects of modifier density cannot be generalized in terms of the reactivity of independent functional groups. Instead, each reactant is uniquely influenced by differences in modifier density. Nevertheless, the different ensemble requirements of different reactions may allow for surface crowding to be used as a strategy to control selectivity.

2.5 Conclusion

Here, we demonstrated the ability to systematically control surface crowding to investigate the effect on catalytic reactivity by utilizing thiol modifiers that form monolayers with varying sulfur coverage on Pd/Al₂O₃. CO DRIFT spectroscopy indicated that on the more crowded C18-coated catalysts, CO adsorbs only to three-fold hollow and a single type of atop site at saturation coverage. On AT-coated catalysts, CO initially adsorbs to these same types of sites but has additional access to bridging and a second type of linear site upon increasing coverage. Using a Langmuir formalism, a minor difference in adsorption energy (~1.1 kJ/mol) was calculated for the AT- and C18-coated surfaces. An increase in ethylene hydrogenation rate by a factor of ~17 was then understood in terms of the additional access to atop sites which have been identified as the preferred site for this reaction. The effect of modifier density on reactivity was found to be dramatically different for several mono- and bi- functional reactants. These unique effects allow the possibility to exploit this technique to control selectivity for other reactions in heterogeneous catalysis.

2.6 References

- 1 Marshall, S. T. *et al.* Controlled selectivity for palladium catalysts using self-assembled monolayers. *Nat Mater* **9**, 853-858 (2010).
- 2 Wu, B. H., Huang, H. Q., Yang, J., Zheng, N. F. & Fu, G. Selective Hydrogenation of alpha,beta-Unsaturated Aldehydes Catalyzed by Amine-Capped Platinum-Cobalt Nanocrystals. *Angew Chem Int Edit* **51**, 3440-3443 (2012).
- 3 Sadeghmoghaddam, E., Gaieb, K. & Shon, Y. S. Catalytic isomerization of allyl alcohols to carbonyl compounds using poisoned Pd nanoparticles. *Appl Catal a-Gen* **405**, 137-141 (2011).
- 4 Kim, J. H., Park, J. S., Chung, H. W., Boote, B. W. & Lee, T. R. Palladium nanoshells coated with self-assembled monolayers and their catalytic properties. *Rsc Adv* **2**, 3968-3977 (2012).
- 5 Gavia, D. J. & Shon, Y.-S. Controlling Surface Ligand Density and Core Size of Alkanethiolate-Capped Pd Nanoparticles and Their Effects on Catalysis. *Langmuir* **28**, 14502-14508 (2012).
- 6 Marshall, S. T., Schwartz, D. K. & Medlin, J. W. Adsorption of Oxygenates on Alkanethiol-Functionalized Pd(111) Surfaces: Mechanistic Insights into the Role of Self-Assembled Monolayers on Catalysis. *Langmuir* **27**, 6731-6737 (2011).
- 7 Ashcroft, A. T., Cheetham, A. K., Green, M. L. H. & Vernon, P. D. F. Partial Oxidation of Methane to Synthesis Gas-Using Carbon-Dioxide. *Nature* **352**, 225-226 (1991).
- 8 Barbier, J., Corro, G., Zhang, Y., Bournonville, J. P. & Franck, J. P. Coke Formation on Platinum-Alumina Catalyst of Wide Varying Dispersion. *Appl Catal* **13**, 245-255 (1985).
- 9 Duprez, D. *et al.* Deactivation of Steam-Reforming Model Catalysts by Coke Formation .1. Kinetics of the Formation of Filamentous Carbon in the Hydrogenolysis of Cyclopentane on Ni/Al₂O₃ Catalysts. *J. Catal.* **124**, 324-335 (1990).
- 10 Demicheli, M. C., Duprez, D., Barbier, J., Ferretti, O. A. & Ponzi, E. N. Deactivation of Steam-Reforming Model Catalysts by Coke Formation .2. Promotion with Potassium and Effect of Water. *J. Catal.* **145**, 437-449 (1994).
- 11 Barias, O. A., Holmen, A. & Blekkan, E. A. Propane dehydrogenation over supported Pt and Pt-Sn catalysts: Catalyst preparation, characterization, and activity measurements. *J. Catal.* **158**, 1-12 (1996).

- 12 Cooper, B. H. & Donnis, B. B. L. Aromatic saturation of distillates: An overview. *Appl Catal a-Gen* **137**, 203-223 (1996).
- 13 Chiu, M. E., Watson, D. J., Kyriakou, G., Tikhov, M. S. & Lambert, R. M. Tilt the molecule and change the chemistry: Mechanism of S-promoted chemoselective catalytic hydrogenation of crotonaldehyde on Cu(111). *Angew Chem Int Edit* **45**, 7530-7534 (2006).
- 14 Kritzinger, J. A. The role of sulfur in commercial iron-based Fischer-Tropsch catalysis with focus on C-2-product selectivity and yield. *Catal. Today* **71**, 307-318 (2002).
- 15 Schwartz, D. K. Mechanisms and kinetics of self-assembled monolayer formation. *Annu Rev Phys Chem* **52**, 107-137 (2001).
- 16 Camillone, N., Chidsey, C. E. D., Liu, G. Y., Putvinski, T. M. & Scoles, G. Surface-Structure and Thermal Motion of Normal-Alkane Thiols Self-Assembled on Au(111) Studied by Low-Energy Helium Diffraction. *J Chem Phys* **94**, 8493-8502 (1991).
- 17 Schonemberger, C., Jorritsma, J., Sondaghuethorst, J. A. M. & Fokkink, L. G. J. Domain-Structure of Self-Assembled Alkanethiol Monolayers on Gold. *J Phys Chem-Us* **99**, 3259-3271 (1995).
- 18 Love, J. C. *et al.* Formation and structure of self-assembled monolayers of alkanethiolates on palladium. *J Am Chem Soc* **125**, 2597-2609 (2003).
- 19 Dameron, A. A., Charles, L. F. & Weiss, P. S. Structures and displacement of 1-adamantanethiol self-assembled monolayers on Au{111}. *J Am Chem Soc* **127**, 8697-8704 (2005).
- 20 Saavedra, H. M. *et al.* 1-adamantanethiolate monolayer displacement kinetics follow a universal form. *J Am Chem Soc* **129**, 10741-10746 (2007).
- 21 Albers, P., Pietsch, J. & Parker, S. F. Poisoning and deactivation of palladium catalysts. *J Mol Catal a-Chem* **173**, 275-286 (2001).
- 22 Wood, J., Alldrick, M. J., Winterbottom, J. M., Stitt, E. H. & Bailey, S. Diffuse reflectance infrared Fourier transform spectroscopy (DRIFTS) study of ethyne hydrogenation on Pd/Al₂O₃. *Catal. Today* **128**, 52-62 (2007).
- 23 Kiskinova, M., Szabo, A. & Yates, J. T. Co Adsorption on Pt(111) Modified with Sulfur. *J Chem Phys* **89**, 7599-7608 (1988).
- 24 Gravil, P. A. & Toulhoat, H. Ethylene, sulphur, and chlorine coadsorption on Pd(111): a theoretical study of poisoning and promotion. *Surf Sci* **430**, 192-198 (1999).

- 25 Cremer, P. S., Su, X. C., Shen, Y. R. & Somorjai, G. A. Ethylene hydrogenation on Pt(111) monitored in situ at high pressures using sum frequency generation. *J Am Chem Soc* **118**, 2942-2949 (1996).
- 26 Neurock, M., Pallassana, V. & van Santen, R. A. The importance of transient states at higher coverages in catalytic reactions. *J Am Chem Soc* **122**, 1150-1153 (2000).
- 27 Burkholder, L., Stacchiola, D. & Tysse, W. T. Kinetic and reactive properties of ethylene on clean and hydrogen-covered Pd(111). *Surface Review and Letters* **10**, 909-916 (2003).
- 28 Mojet, B. L., Ebbesen, S. D. & Lefferts, L. Light at the interface: the potential of attenuated total reflection infrared spectroscopy for understanding heterogeneous catalysis in water. *Chem Soc Rev* **39**, 4643-4655 (2010).
- 29 Lear, T. *et al.* The application of infrared spectroscopy to probe the surface morphology of alumina-supported palladium catalysts. *J Chem Phys* **123** (2005).
- 30 Hammaker, R. M., Francis, S. A. & Eischens, R. P. Infrared Study of Intermolecular Interactions for Carbon Monoxide Chemisorbed on Platinum. *Spectrochim Acta* **21**, 1295-& (1965).
- 31 Flores-Camacho, J. M. *et al.* Adsorption energetics of CO on supported Pd nanoparticles as a function of particle size by single crystal microcalorimetry. *Phys Chem Chem Phys* **13**, 16800-16810 (2011).
- 32 Yeo, Y. Y., Vattuone, L. & King, D. A. Calorimetric investigation of NO and CO adsorption on Pd{100} and the influence of preadsorbed carbon. *J Chem Phys* **106**, 1990-1996 (1997).
- 33 Conrad, H., Ertl, G., Koch, J. & Latta, E. E. Adsorption of Co on Pd Single-Crystal Surfaces. *Surf Sci* **43**, 462-480 (1974).
- 34 Gan, L. Y. & Zhao, Y. J. Charge effect in S enhanced CO adsorption: A theoretical study of CO on Au, Ag, Cu, and Pd (111) surfaces coadsorbed with S, O, Cl, and Na. *J Chem Phys* **133** (2010).
- 35 Li, M. S. & Shen, J. Y. Microcalorimetric studies of O₂ and C₂H₄ adsorption on Pd/SiO₂ catalysts modified by Cu and Ag. *Thermochim Acta* **379**, 45-50 (2001).
- 36 Unterhalt, H., Galletto, P., Morkel, M., Rupprechter, G. & Freund, H. J. Sum frequency generation study of CO adsorption on palladium model catalysts. *Phys Status Solidi A* **188**, 1495-1503 (2001).
- 37 Marshall, S. T. & Medlin, J. W. Surface-level mechanistic studies of adsorbate-adsorbate interactions in heterogeneous catalysis by metals. *Surf. Sci. Rep.* **66**, 173-184 (2011).

- 38 Brands, D. S., U-A-Sai, G., Poels, E. K. & Blik, A. Sulfur deactivation of fatty ester hydrogenolysis catalysts. *J Catal* **186**, 169-180 (1999).
- 39 Passos, F. B., Aranda, D. A. G. & Schmal, M. Characterization and catalytic activity of bimetallic Pt-In/Al₂O₃ and Pt-Sn/Al₂O₃ catalysts. *J Catal* **178**, 478-488 (1998).
- 40 Passos, F. B., Schmal, M. & Vannice, M. A. Effect of In and Sn on the adsorption behavior and hydrogenolysis activity of Pt/Al₂O₃ catalysts. *J Catal* **160**, 106-117 (1996).
- 41 Figoli, N. S., Largentiere, P. C., Arcoya, A. & Seoane, X. L. Modification of the Properties and Sulfur Resistance of a Pd/SiO₂ Catalyst by La Addition. *J Catal* **155**, 95-105 (1995).
- 42 Zhang, J. Z., Tsai, Y. T., Sangkaewwattana, K. L. & Goodwin, J. G. Structure sensitivity of cyclopropane hydrogenolysis on carbon-supported platinum. *J Catal* **280**, 89-95 (2011).
- 43 Marinelli, T. B. L. W. & Ponec, V. A Study on the Selectivity in Acrolein Hydrogenation on Platinum Catalysts - a Model for Hydrogenation of Alpha,Beta-Unsaturated Aldehydes. *J Catal* **156**, 51-59 (1995).
- 44 Medlin, J. W. Understanding and Controlling Reactivity of Unsaturated Oxygenates and Polyols on Metal Catalysts. *Acs Catal* **1**, 1284-1297 (2011).
- 45 Loffreda, D., Delbecq, F., Vigne, F. & Sautet, P. Chemo-regioselectivity in heterogeneous catalysis: Competitive routes for C=O and C=C hydrogenations from a theoretical approach. *J Am Chem Soc* **128**, 1316-1323 (2006).
- 46 van Druten, G. M. R. & Ponec, V. Hydrogenation of carbonylic compounds Part I: Competitive hydrogenation of propanal and acetone over noble metal catalysts. *Appl Catal a-Gen* **191**, 153-162 (2000).

CHAPTER 3

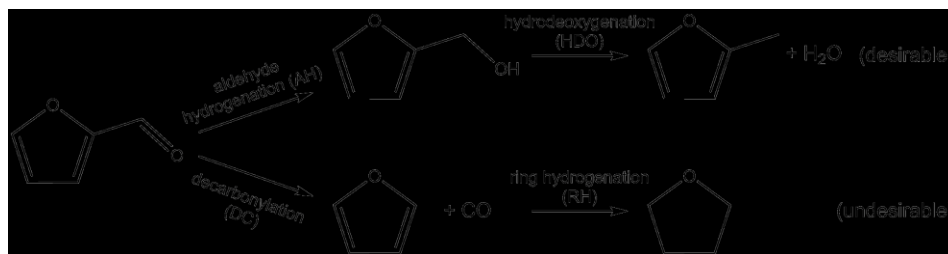
Directing reaction pathways by catalyst active-site selection using self-assembled monolayers

3.1 Abstract

One key route for controlling reaction selectivity in heterogeneous catalysis is to prepare catalysts that exhibit only specific types of sites required for desired product formation. Here we show that alkanethiolate self-assembled monolayers with varying surface densities can be used to tune selectivity to desired hydrogenation and hydrodeoxygenation products during the reaction of furfural on supported palladium catalysts. Vibrational spectroscopy studies demonstrate that the selectivity improvement is achieved by controlling the availability of specific sites for the hydrogenation of furfural on supported palladium catalysts through the selection of an appropriate alkanethiolate. Increasing self-assembled monolayer density by controlling the steric bulk of the organic tail ligand restricts adsorption on terrace sites and dramatically increases selectivity to desired products furfuryl alcohol and methylfuran. This technique of active-site selection simultaneously serves both to enhance selectivity and provide insight into the reaction mechanism.

3.2 Introduction

Furfurals are important platform chemicals produced from biomass feedstocks by dehydration of simple sugars^{1,2} and serve as important model compounds for multifunctional molecules. These highly reactive molecules represent a classic example of the challenge of *selectivity* in heterogeneous catalysis, since they interact with catalytic surfaces through all of their functional groups, resulting in a diverse range of products. In particular, on noble metal catalysts under hydrogenation conditions, the aromatic furan ring has a tendency to adsorb strongly on the surface, resulting in decarbonylation (DC) and ring hydrogenation (RH) to produce furan and tetrahydrofuran as the dominant reaction products. Conversely, reaction steps such as aldehyde hydrogenation (AH) and hydrodeoxygenation (HDO) necessary for conversion of furfuryl oxygenates to desirable fuels (furfuryl alcohol and methylfuran) do not occur as readily.³⁻⁸ Scheme 3-1 depicts the major reaction pathways for furfural hydrogenation.



Scheme 3-1. Reaction pathways for furfural hydrogenation.

A number of techniques have been used to control reaction selectivity through the use of surface modifiers. Carbon monoxide is well known as a surface poison that can reduce surface ensemble size to control selectivity^{9,10} but must continuously be added to the system at reaction temperatures, and the coverage/packing cannot be readily controlled. Organic modifiers such as thiophene¹¹ have been added to enhance selectivity, but creating a consistent surface remains a

challenge due to inconsistencies arising from different preparation techniques. Even in studies where the same modifier and preparation techniques were used, dramatic differences have been reported¹² presumably due to subtle differences in the final modifier state. While these approaches may improve catalytic performance in specific cases, it is important to develop a technique to systematically and reproducibly control the catalyst near-surface environment.

Self-assembled monolayers (SAMs) have recently been utilized as modifiers to control reactivity in heterogeneous catalysis.¹³⁻¹⁸ SAMs are attractive modifiers because they form ordered overlayers, and their chemistry (and thus their effect on surface reactivity) can be tuned by changing the molecular structure of the organic “tail” function. As demonstrated in Chapter 2, altering the surface density of alkanethiolate SAM modifiers by altering the steric bulk of the tail function dramatically affected reactivity for several reactants by controlling the availability of different active sites on supported Pd/Al₂O₃ catalysts.¹⁹ However, the manipulation of SAM sterics for controlling reaction selectivity has not previously been demonstrated. Here we report the ability of controlled modifier density to direct furfural hydrogenation along a desired reaction pathway using SAMs formed from octadecanethiol (C18), which forms a dense ($\sqrt{3}\times\sqrt{3}$)R30 adsorption geometry with a nearest neighbor distance of ~ 4.7 Å on Pd fcc(111) surfaces,²⁰ or 1-adamantanethiol (AT), which forms a sparse (7 \times 7) unit cell structure²¹ with a nearest neighbor distance of ~ 6.4 Å, to coat supported Pd/Al₂O₃ catalysts. Measurements of furfural hydrogenation kinetics were performed in conjunction with infrared spectroscopy to provide insight into the principles of *active-site selection* for the production of the valuable products methylfuran and furfural alcohol, as opposed to the less desirable furan and tetrahydrofuran.

3.3 Experimental Methods

5 wt% and 1 wt% Pd/Al₂O₃ catalysts, 1-octadecanethiol (98%), 1-adamantanethiol (95%), furfural (99%), and 200-proof HPLC-grade ethanol were purchased from Sigma Aldrich. Catalysts were used as-received for uncoated reactions. Ultra-high purity H₂ and He were obtained from Airgas.

AT and C18 SAMs were deposited on the catalysts by dissolving the thiol in 40 mL ethanol at a concentration of 4.25 mmol/L. The surface area of the less disperse 5 wt% Pd/Al₂O₃ (D = 0.266) was approximately 2.7 times that of the more disperse 1 wt% Pd/Al₂O₃ (D = 0.414) per mass of supported catalyst as determined by TEM. TEM images and particle size distributions for 5 and 1 wt% Pd/Al₂O₃ catalysts are shown in Figure 3-1. Thus, 250 mg of 1 wt% Pd/Al₂O₃ or 100 mg of 5 wt% Pd/Al₂O₃ was added to the solution to expose a similar surface area of Pd to the thiol solution. The catalysts were allowed to settle for at least 12 h. The supernatant was decanted, and 40 mL ethanol was added to wash off any excess thiol that had not adsorbed. The catalysts were allowed to settle for an additional 2 h, and then the supernatant was decanted. The catalysts were allowed to dry in air before use.

The sulfur content was analyzed using ICP-AES. The results demonstrated that there was 2.1x the amount of sulfur present on the C18 catalysts than on the AT catalysts, which is approximately the amount expected from differences in coverage on single crystal surfaces (~1.8x more molecules for the C18 surface^{20,21}). No sulfur adsorption was found on pure Al₂O₃. In addition, an approximate thiolate concentration was inferred from the hydrocarbon stretching region of the freshly modified catalysts. With 18 carbons for C18 and 10 for AT, the total hydrocarbon peak area was nominally expected to be ~3.3x greater for the C18 catalyst, taking into account the 1.8x difference in coverage. Actual peaks had ~3.7x greater areas, indicating a

more densely packed monolayer for the C18 than AT. While the overall packing density of the C18 SAM was higher, defects were almost certainly present. Overall, the C18 and AT modified catalysts exhibited features associated with an ordered monolayer where the asymmetric methylene stretches were observed at 2923 cm^{-1} and 2915 cm^{-1} for each catalyst coating, respectively. This is compared to fcc(111) surfaces where these peaks were observed at 2918 cm^{-1} and 2911 cm^{-1} , respectively.^{20,28}

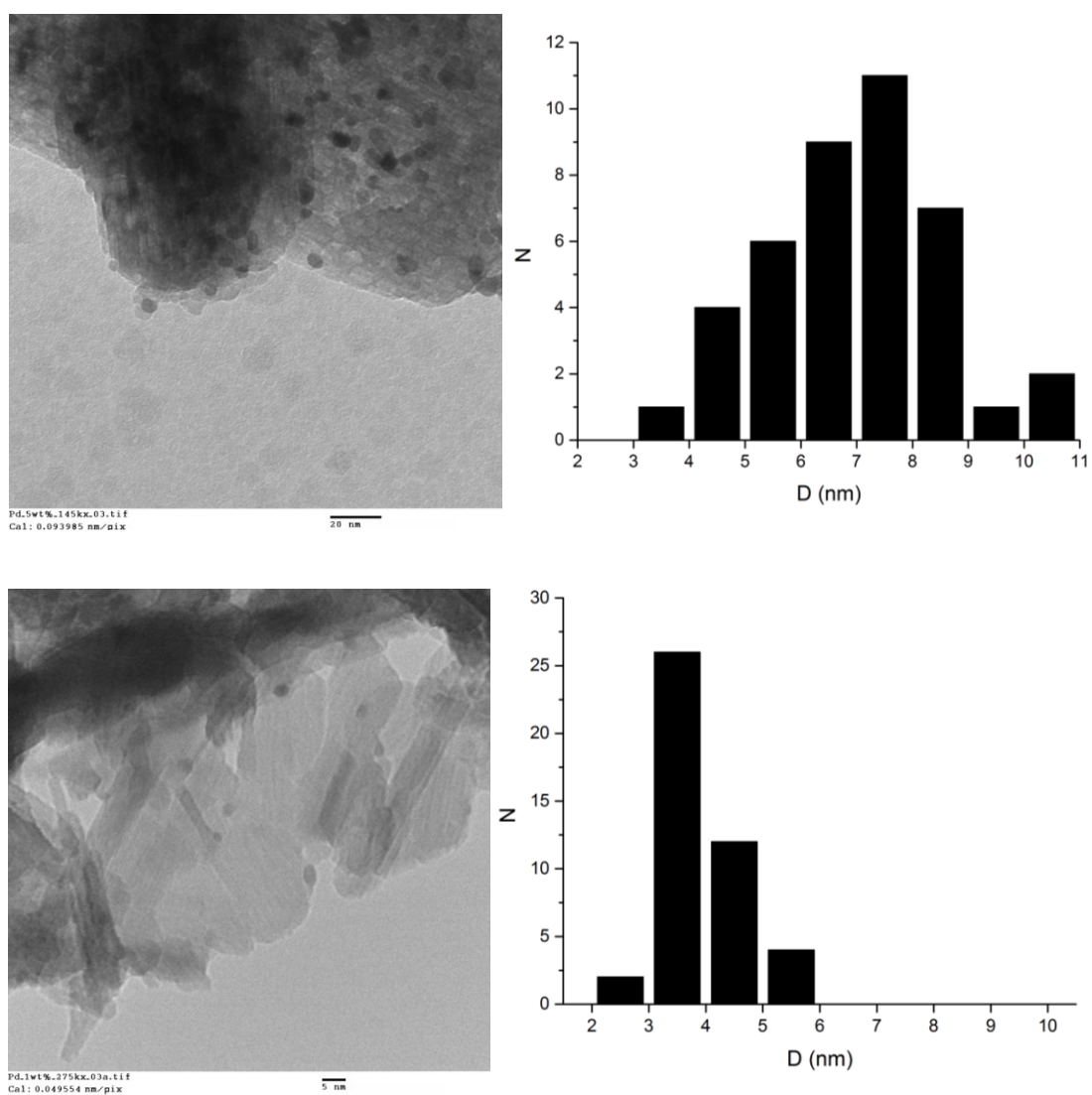


Figure 3-1. Representative TEM image and particle size distribution for 5 wt% (top) and 1 wt% (bottom) Pd/Al₂O₃.

Hydrogenations were conducted in a tubular packed bed flow reactor at 190 °C and atmospheric pressure. Helium was bubbled through furfural (Sigma Aldrich) to achieve furfural mole fraction of $y_{\text{furfural}} = 0.016$ and mixed with H₂ at a 25:1 molar ratio of H₂ to furfural. The amount of catalyst used was varied systematically to achieve a conversion of 13±1.8% in all cases. Each reaction was run for at least 200 minutes; selectivity and conversion at the end of this period are reported here. Additional reactions were performed varying temperature and conversion to demonstrate the sequential nature of the reaction; as conversion increased, more methylfuran was produced relative to furfuryl alcohol, and vice versa for decreased conversion, indicating that reaction selectivity could be tuned using conversion. This will be discussed in further detail in the results section.

Selectivity and conversion as a function of time on stream revealed that over the course of the reaction, the uncoated catalyst experiences continuously decreasing activity. Conversely, the C18 coated catalyst exhibited constant conversion, showing that the SAMs are mostly stable under reaction conditions. Representative kinetic plots showing selectivity and conversion as a function of time on stream for these two catalysts are shown in Figure 3-2. Additional reactions were performed using the uncoated and C18-coated 5 wt% Pd/Al₂O₃, allowing the reaction to proceed for at least 15 hours to further examine the stability of selectivity, conversion on the uncoated and C18-coated catalyst are shown in Figure 3-3. Comparison of reaction selectivity at 4 and 15 hours shows no significant increase in the selectivity to furan for the C18-coated catalyst, but a drop in conversion from 12% to 5%. DRIFT spectra before and after 15 hours of reaction reveal a 3 cm⁻¹ and 5 cm⁻¹ shift in the peak positions for asymmetric and symmetric methylene stretching, respectively. These data indicated some disordering of the monolayer, possibly due to the generation of gauche defects²⁰. Importantly, the SAM was still present on the

surface under reaction conditions at the time that selectivity and rates are reported. For stable operation over longer reaction times, it may be desirable to pursue approaches such as post-assembly cross-linking of SAMs.³⁷

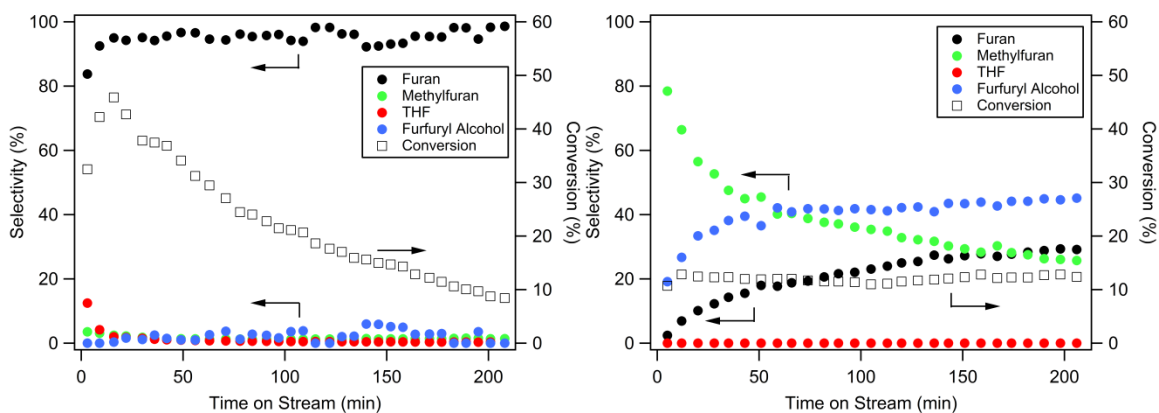


Figure 3-2. Representative kinetic plots of conversion and selectivity as a function of time on stream for uncoated 5 wt% Pd/Al₂O₃ (left), and C18-coated 5 wt% Pd/Al₂O₃ (right). Uncoated catalysts deactivate quickly; on the other hand, the SAM coating stabilizes conversion.

For gas phase reactions, the gas mixture passed over the catalyst and the reactor effluent was analysed using an Agilent Technologies 7890A gas chromatograph equipped with a 30m x 0.320mm Agilent HP-5 capillary column and flame ionization detector (split ratio = 25:1, column flow rate = 2 mL/min, oven temperature = 50°C). Turnover frequencies for individual products were calculated by dividing the product flow rates by the number of surface sites on unmodified catalyst, based on the size of the metal particles and mass of catalyst used.

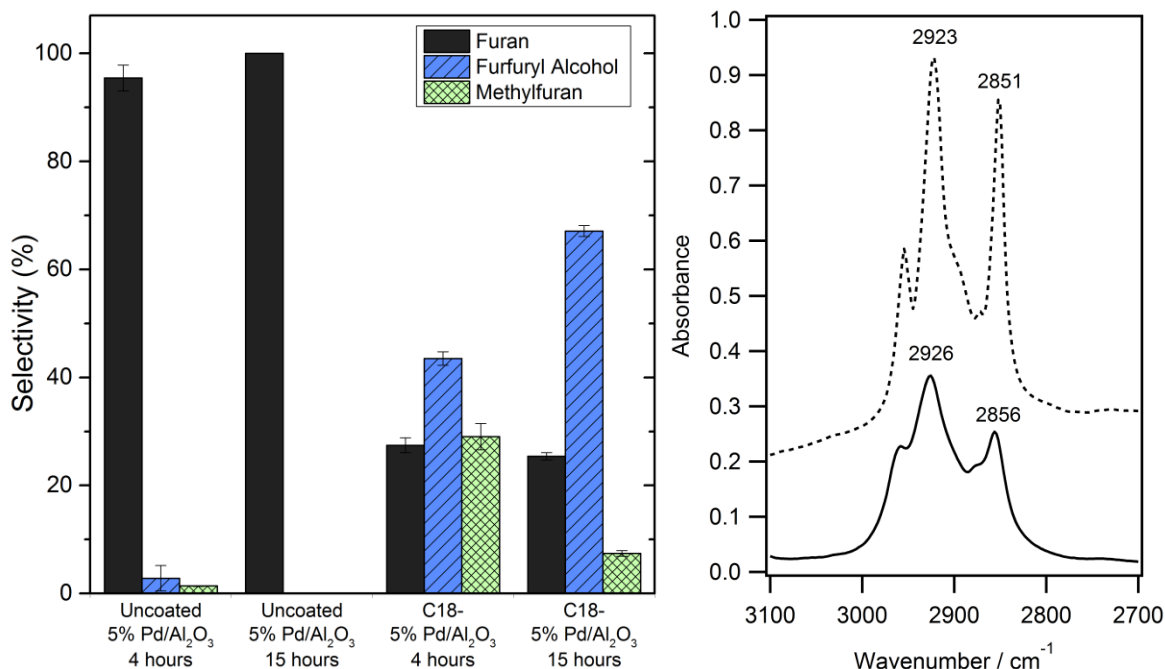


Figure 3-3. Left: Selectivity to furan does not significantly increase for the C18-coated 5 wt% Pd/Al₂O₃ catalyst, indicating that the SAM layer is still intact. Furfural conversion for the uncoated catalyst at 4 hours and 15 hours are 12.0% and 0.5%, respectively. Furfural conversion for the C18-coated catalyst at 4 hours and 15 hours are 12.2% and 4.9%, respectively. Right: DRIFT spectra for the methylene stretching region on the C18-coated 5 wt% Pd/Al₂O₃ catalyst, before (dashed) and after (solid) 15 hours under reaction conditions.

FTIR analysis was performed using a Thermo Scientific Nicolet 6700 FT-IR with a closed cell attachment (Harrick) for Diffuse Reflectance Infrared Fourier Transform Spectroscopy (DRIFTS). Fifty scans at 4 cm⁻¹ resolution were used for each spectrum. The quality of all coated samples was characterized in the C-H stretching region (2,800 – 3,000 cm⁻¹) to confirm monolayer formation prior to catalytic testing. For CO DRIFT experiments, catalyst samples were placed in a gastight cell that was evacuated to achieve an initial baseline pressure of <0.10 Torr. The 1% catalysts were determined to have ~2.7x fewer active sites per gram of supported catalyst (as determined by TEM imaging) which resulted in an overall weaker signal

intensity in the DRIFT spectra. In addition, the signal was further weakened because a reduced sample mass was loaded into the sample cup due to the lower density of the alumina support for the 1% Pd/Al₂O₃ catalyst. Differences in the apparent density of the alumina support were determined to be ~3x. TEM images confirmed a more porous Al₂O₃ support morphology for the 1% catalysts (Figure 3-1). This resulted in a weaker signal on the 1% catalyst than on the 5% catalyst (~8x).

3.4 Results and discussion

Catalytic Reactions

Gas phase hydrogenation of furfural was conducted over 5 wt% and 1 wt% Pd/Al₂O₃ catalysts in a tubular packed bed flow reactor at atmospheric pressure. TEM was used to determine the average size of the supported Pd particles, 6 nm and 3 nm (Figure 3-1), for the 5 wt% and 1 wt% catalysts, respectively.

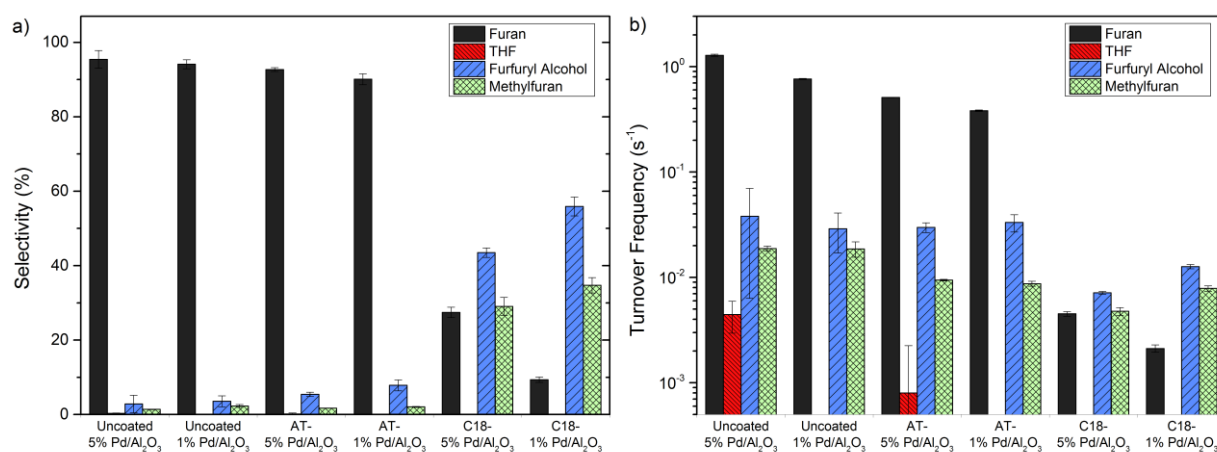


Figure 3-4. Gas phase hydrogenation of furfural. a) Product selectivity for furfural hydrogenation over uncoated and alkanethiolate SAM coated Pd/Al₂O₃ catalysts. b) Rate of production normalized by number of surface sites on the uncoated catalyst. Hydrogenations were carried out continuously at 190°C at a 25:1 molar ratio of H₂ to furfural. Selectivity and rate are

reported at $(13 \pm 1.8)\%$ conversion of furfural fed. Error bars indicate s.d. of 12 repeated measurements of product concentration.

As shown in Figure 3-4, using uncoated Pd catalysts, the dominant product was furan, and the rate of decarbonylation (DC) was about two orders of magnitude higher than that of aldehyde hydrogenation (AH) and hydrodeoxygenation (HDO). Accordingly, the selectivity towards the desirable products, furfuryl alcohol and methylfuran, was negligible using the uncoated Pd catalyst. When the catalysts were modified with the sparsely packed AT SAM, there was a minor enhancement in selectivity towards the desired products, though selectivity to furan was still high. Notably, the densely coated C18-catalysts exhibited a dramatic improvement in selectivity towards the desired products. In particular, the C18-coated 1 wt% Pd/Al₂O₃ catalyst exhibited over 55% selectivity to furfuryl alcohol and 35% selectivity to methylfuran. Because methylfuran is produced in a series reaction from furfuryl alcohol, its selectivity can be improved to >70% even on the C18-coated 5% Pd/Al₂O₃ catalyst at higher conversion. A summary of these results are shown together in Table 3-1.

Catalyst	T (°C)	WHSV	Conversion	Selectivity			
				Furan	THF	FA	Methylfuran
C18-1%	190	2.1×10^2	15%	9.4%	0.0%	55.9%	34.7%
C18-1%	150	2.1×10^2	6%	9.4%	0.0%	77.9%	12.7%
C18-5%	190	1.2×10^2	8%	24.9%	0.0%	60.2%	15.0%
C18-5%	190	9.8×10^1	12%	27.5%	0.0%	43.5%	29.1%
C18-5%	190	2.0×10^1	57%	21.1%	2.3%	15.5%	61.0%
C18-5%	190	1.1×10^1	86%	22.1%	2.6%	2.5%	72.7%

Table 3-1. Selectivity to furfuryl alcohol enhanced at lower temperature and smaller conversion; selectivity to methylfuran enhanced at higher conversion. WHSV is reported in units of (mg furfural fed) (mg Pd)⁻¹ h⁻¹.

Importantly, while the overall rate of reaction was decreased by the SAM coatings, as expected, this decrease was nearly completely attributed to the undesirable decarbonylation pathway (see Figure 3-4b). As the SAM packing became increasingly dense, the rate of decarbonylation decreased by three orders of magnitude. However, the rates of aldehyde hydrogenation and hydrodeoxygenation were nearly unaffected. Thus, the increase in selectivity to the desired products was not due to an increase in the rate of the desired reaction, but rather due to inhibition of the undesired reaction.

We demonstrated in Chapter 2 that adsorption on catalyst terrace sites was reduced systematically with increasing thiol SAM density, whereas adsorption on step edges and defects was mostly unaffected.¹⁹ We therefore hypothesized that the reduction in the rate of decarbonylation on the thiol-modified catalysts was a direct effect of limiting access to terrace sites. Supporting this notion, single crystal studies of benzyl alcohol and benzaldehyde (functionally similar to furfural) on Pd(111) have shown that decarbonylation to produce benzene is dominant when the molecules can adopt a flat-lying conformation.²² In addition, DFT calculations show that the furan ring in furfural preferentially adsorbs in a three-fold hollow site for flat-lying structures.^{7,8,23} Thus, we expect that decarbonylation and ring hydrogenation occur primarily on three-fold terrace sites where a large contiguous ensemble of sites is available. In the case of furfural, the high selectivity to furan on both the uncoated and AT-modified catalysts suggested that the ensemble requirement for decarbonylation was satisfied on these catalysts, but not on the C18-modified catalyst. Since the rates of furfural alcohol and methylfuran production were unaffected on the coated catalysts, we hypothesize that these products were formed primarily at step edge and defect sites.

Identification of Adsorption Sites by Infrared Spectroscopy

To directly test the availability of specific adsorption sites, diffuse reflectance Fourier transform infrared spectroscopy (DRIFTS) was performed under variable pressures of carbon monoxide; in these experiments, peak positions are readily attributed to CO binding in three-fold, bridging, and top sites.²⁴ We previously found that on unmodified 5 wt% catalyst, increasing thiol density restricted adsorption on terrace sites (Figure 3-5a adapted from ref. 15). On the more crowded C18-coated catalysts, CO adsorbed only on three-fold hollow (1885 cm^{-1}) and top sites at step edges and defects (2051 cm^{-1}). On AT-coated catalysts, CO had additional access to adsorption on terrace bridging (1919 cm^{-1}) and an additional type of linear (2077 cm^{-1}) sites on terraces.

The C18-modified 1 wt% particles inhibited furan production more than the same coating on the 5 wt% catalysts (Figure 3-4). Thus, if production of furan requires an ensemble of terrace sites, we would expect to see limited terrace CO adsorption on C18-modified 1 wt% catalysts. Figure 3-5b shows the DRIFT spectra for the modified and unmodified 1 wt% catalysts. The major peak features at 1905 cm^{-1} and 1863 cm^{-1} on the uncoated and AT catalysts, respectively, were attributed to CO binding primarily on three-fold terrace sites. The smaller peak area for this feature on the AT catalyst indicated reduced adsorption at terraces. On the C18 catalyst, this feature was essentially non-existent, supporting the hypothesis that the crowded monolayer on these smaller particles limited the availability of terrace sites. In contrast, the feature at 2018 cm^{-1} was attributed to linear adsorption primarily at steps and edges. This feature was also present on the uncoated 1% catalyst at low pressures but was obscured at higher pressure by species adsorbed linearly on terrace sites. Low CO pressure spectra are shown in Figure 3-6. The peaks above 2100 cm^{-1} were due to gas phase CO, indicating that the catalysts were saturated with CO.

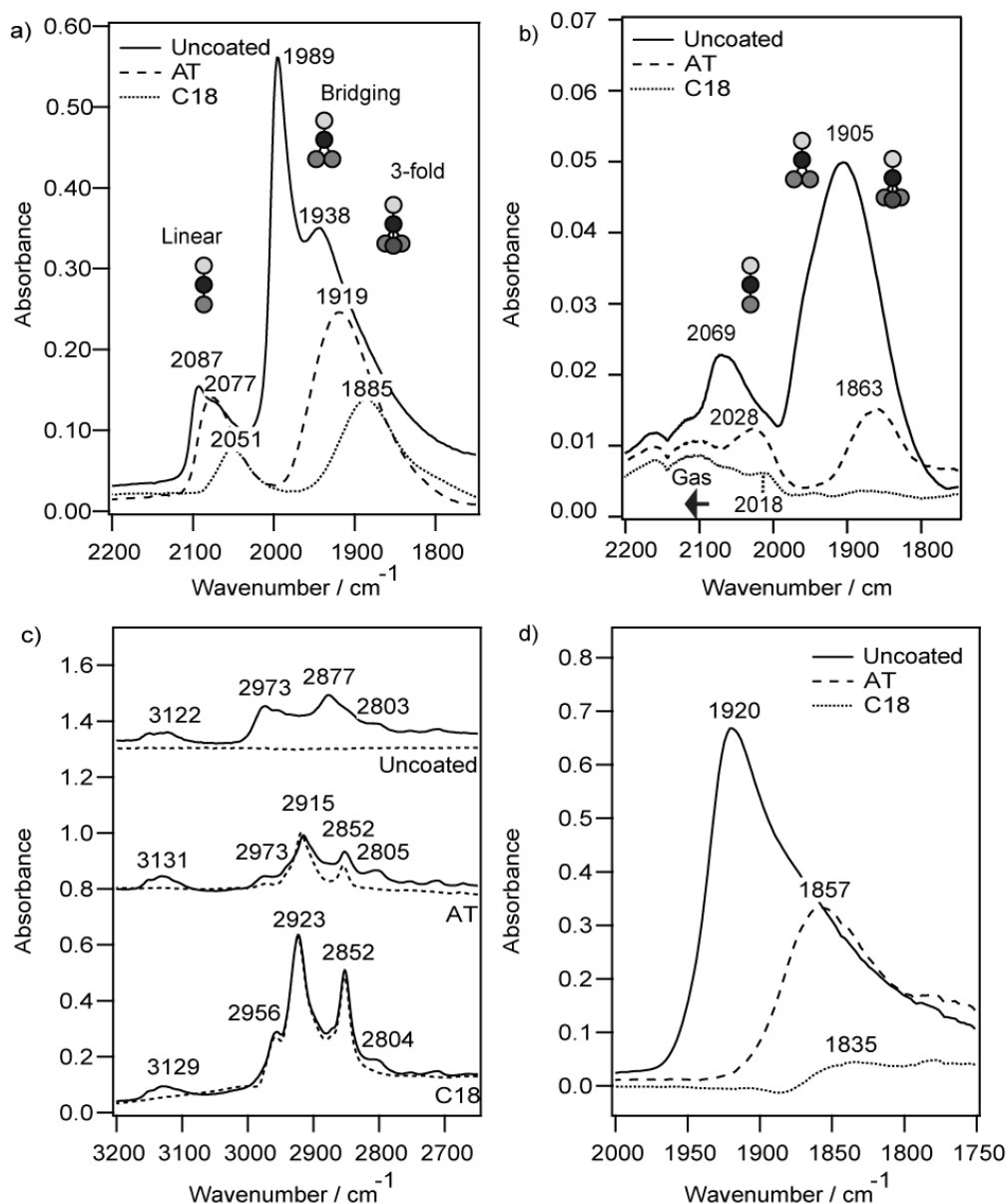


Figure 3-5. DRIFT spectra for uncoated and SAM coated catalysts. CO stretch region for uncoated and alkanethiolate SAM coated a) 5 wt% (adapted from ref. 15) and b) 1 wt% Pd/Al₂O₃ catalysts. For linear adsorption on top sites, the lower wavenumber features are associated with adsorption at steps and edges whereas higher wavenumber features are indicative of adsorption on terrace sites.²⁵ DRIFT spectra for samples after furfural exposure. c) Hydrocarbon stretching region for uncoated, AT, and C18 catalysts. Dashed and solid lines are shown for samples before and after exposure, respectively. d) CO production on the uncoated, AT, and C18 catalysts after exposure to furfural.

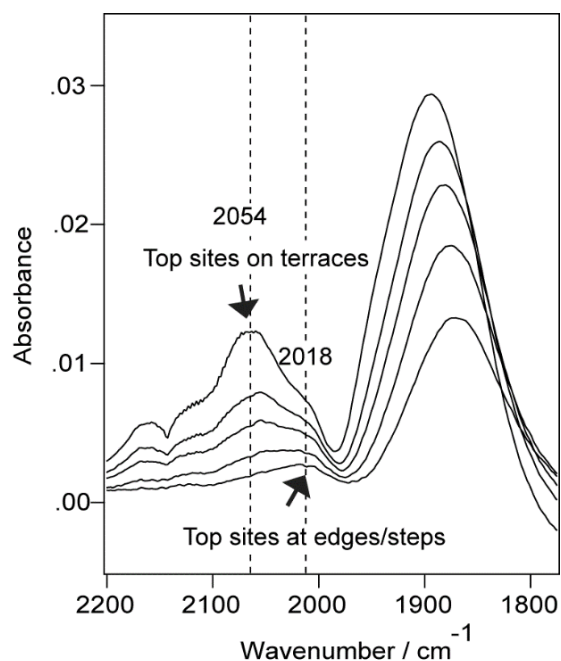


Figure 3-6. CO DRIFTS for unmodified 1% Pd/Al₂O₃ showing the evolution of peaks associated with CO binding in three-fold and linear configurations.

Discussion

Since the rates of production of furfuryl alcohol and methylfuran were nearly the same on all the catalysts and the availability of step and edge sites was mostly unaffected by the thiol modifiers, we suggest that the production of these species occur preferentially at these sites, whereas furan production likely requires terrace sites. The dearth of three-fold hollow sites on the 1 wt% catalyst was presumably responsible for the absence of the THF product, since ring hydrogenation requires a large number of contiguous surface sites^{26,27} allowing the ring to lie flat. The proposed adsorption mechanism is depicted in Figure 3-7.

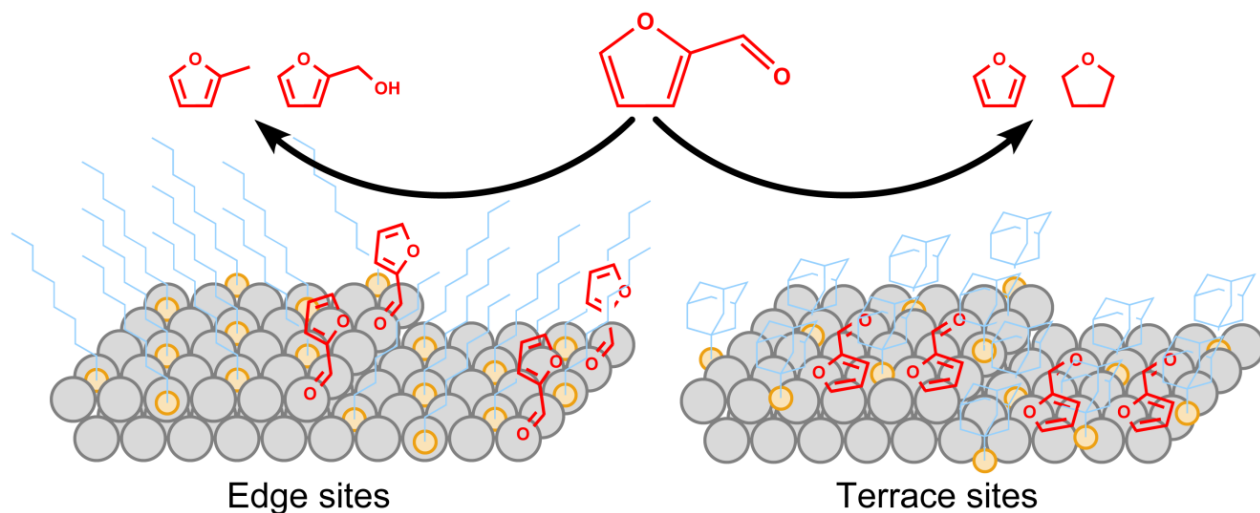


Figure 3-7. Proposed schematic depicting *active-site selection* using self-assembled monolayers of octadecanethiol and adamantanethiol. On C18-modified surfaces, furfural binds upright on step edges and defects while on AT-modified surfaces, furfural can lie flat on a terrace.

In-situ DRIFT spectroscopy during exposure to furfural on modified and unmodified catalysts provided further evidence for reduced decarbonylation and decomposition on the more crowded surfaces. C18, AT, and unmodified 5 wt% Pd/Al₂O₃ were each exposed to ~60 (mg furfural fed)/(mg Pd × h) for 20 minutes using He carrier gas. Spectra were collected after removing the gas phase furfural, but still under flow of He (see Figure 3-5c). The dashed spectra show the catalyst before exposure to furfural for the uncoated, AT, and C18 catalysts. Before exposure, both the C18 and AT modified catalysts exhibited spectral features associated with an ordered monolayer, where the asymmetric methylene stretches were observed at 2923 cm⁻¹ and 2915 cm⁻¹ for C18 and AT, respectively. This is compared to fcc(111) surfaces where these peaks were observed at 2918 cm⁻¹ and 2911 cm⁻¹, respectively.^{20,28} In the case of C18, these positions are intermediate between crystalline (2918 cm⁻¹) and liquid-like (2928 cm⁻¹)²⁹ features

for C18. The appearance of the broad C-H stretching peaks between $\sim 2800\text{-}3000\text{ cm}^{-1}$ on the uncoated catalyst indicated the production of decomposition intermediates bound to the catalyst. Single crystal and DFT studies of furanic species on Pd(111) have attributed stretches in this range to a combination of CH and CH₂ containing fragments from adsorption of the furan ring and decomposition to surface hydrocarbon species.^{7,30,31} The appearance of CH₂ stretches, not present in the parent furfural molecule, may be due to reaction of the adsorbed furan ring with surface hydrogen atoms produced from decomposition of neighbouring adsorbates. On the AT catalyst, the amount of furfural decomposition was significantly reduced; however, peaks at 2852 cm^{-1} and 2973 cm^{-1} , similarly attributed to CH and CH₂ stretches, indicated some adsorption of the furan ring, consistent with the production of both furan and THF on this catalyst. On the C18 catalyst, there was essentially no production of decomposition products on the catalyst after furfural exposure. The appearance of the broad peak around $\sim 3130\text{ cm}^{-1}$ and the peak at $\sim 2805\text{ cm}^{-1}$, present on all of the catalysts after furfural exposure, indicated the presence of the symmetric and asymmetric C-H stretches of the unsaturated furan ring and the aldehyde constituent, respectively. These stretches are also present in the spectrum of liquid-like furfural,³² suggesting the presence of physisorbed or weakly chemisorbed furfural on all catalyst surfaces.

Spectra obtained after exposure to furfural also provided direct information about the extent of decarbonylation (Figure 3-5d) in the form of the presence of bound CO. The uncoated catalyst showed significant CO binding in both three-fold and bridging sites (peak at 1920 cm^{-1}). CO production on the AT-modified catalyst occurred primarily on three-fold sites and was reduced with respect to the uncoated catalyst. Minimal CO production occurred on the C18 catalyst, with a small amount formed at three-fold hollow sites, likely in defects in the SAM. Adsorption to these sites can be seen in the results of CO DRIFTS experiments on C18 modified

5 wt% Pd Al₂O₃, but not the C18-modified 1 wt% Pd/Al₂O₃, consistent with the decreased rate of production of furan on the C18 modified 1 wt%. These results again support the kinetic data, demonstrating that decarbonylation is inhibited by increasing modifier crowding on the catalyst terraces.

3.5 Conclusions

Here, we have shown that alkanethiolate self-assembled monolayer modified Pd catalysts increase the selectivity of furfural hydrogenation to furfuryl alcohol and methylfuran by limiting the availability of particular surface sites. By using a less dense SAM, such as one created by adamantanethiol, a portion of the three-fold terrace sites can be blocked, and the rate of decarbonylation and ring hydrogenation decreased. Using a dense SAM, such as one created by octadecanethiol, access to the three-fold sites can be severely limited, drastically reducing the rate of decarbonylation leading to selectivity enhancement for aldehyde hydrogenation and hydrodeoxygenation. Thus, *active-site selection* using SAM modifiers in catalysis can potentially serve as an alternative (or complement) to recent efforts³³⁻³⁶ aimed at modifying shape, and thus surface site distribution, of supported metal nanoparticles to control selectivity.

3.6 References

- 1 Serrano-Ruiz, J. C., West, R. M. & Dumesic, J. A. Catalytic conversion of renewable biomass resources to fuels and chemicals. *Annu. Rev. Chem. Biomol. Eng.* **1**, 79-100 (2010).
- 2 Werpy, T. & Petersen, G. "Top Value Added Chemicals from Biomass: Volume 1 – Results of Screening for Potential Candidates from Sugars and Synthesis Gas." U.S. Department of Energy (2004).
- 3 Sitthisa, S. & Resasco, D. E. Hydrodeoxygenation of furfural over supported metal catalysts: A comparative study of Cu, Pd and Ni. *Catal. Lett.* **141**, 784-791 (2011).

- 4 Sitthisa, S. *et al.* Conversion of furfural and 2-methylpentanal on Pd/SiO₂ and PdCu/SiO₂ catalysts. *J. Catal.* **280**, 17-27 (2011).
- 5 Sitthisa, S., An, W. & Resasco, D. E. Selective conversion of furfural to methylfuran over silica-supported NiFe bimetallic catalysts. *J. Catal.* **284**, 90-101 (2011).
- 6 Zhang, W., Zhu, Y., Niu, S. & Li, Y. A study of furfural decarbonylation on K-doped Pd/Al₂O₃ catalysts. *J. Mol. Catal. A: Chem.* **335**, 71-81 (2011).
- 7 Pang, S. H. & Medlin, J. W. Adsorption and reaction of furfural and furfuryl alcohol on Pd(111): Unique reaction pathways for multifunctional reagents. *ACS Catal.* **1**, 1272-1283 (2011).
- 8 Vorotnikov, V., Mpourmpakis, G. & Vlachos, D. G. DFT study of furfural conversion to furan, furfuryl alcohol, and 2-methylfuran on Pd(111). *ACS Catal.* **2**, 2496-2504 (2012).
- 9 McGown, W. T., Kemball, C., Whan, D. A. & Scurrall, M. S. Hydrogenation of acetylene in excess ethylene on an alumina supported palladium catalyst in a static system. *J. Chem. Soc., Faraday Trans.* **73**, 632-647 (1977).
- 10 Monnier, J. R., Medlin, J. W. and Kuo, Y.-J. Selective isomerization of 2,5-dihydrofuran to 2,3-dihydrofuran using CO-modified, supported Pd catalysts. *Appl. Catal., A* **194-195**, 463-474 (2000).
- 11 Hutchings, G. J., King, F., Okoye, I. P., Padley, M. B. and Rochester, C. H. Selectivity enhancement in the hydrogenation of α , β -unsaturated aldehydes and ketones using thiophene-modified catalysts. *J. Catal.* **148**, 453-463 (1994).
- 12 Marinelli, T. B. L. W. & Ponc, V. A Study on the selectivity in acrolein hydrogenation on platinum catalysts: A model for hydrogenations of α,β -unsaturated aldehydes. *J. Catal.* **156**, 51-59 (1995).
- 13 Marshall, S. T. *et al.* Controlled selectivity for palladium catalysts using self-assembled monolayers. *Nat. Mater.* **9**, 853-858 (2010).
- 14 Sadeghmoghaddam, E., Gaïeb, K. & Shon, Y.-S. Catalytic isomerization of allyl alcohols to carbonyl compounds using poisoned Pd nanoparticles. *Appl. Catal., A* **405**, 137-141 (2011).
- 15 Makosch, M. *et al.* Organic thiol modified Pt/TiO₂ catalysts to control chemoselective hydrogenation of substituted nitroarenes. *ACS Catal.* **2**, 2079-2081 (2012).
- 16 Wu, B., Huang, H., Yang, J., Zheng, N. & Fu, G. Selective hydrogenation of α,β -unsaturated aldehydes catalyzed by amine-capped platinum-cobalt nanocrystals. *Angew. Chem., Int. Ed.* **51**, 3440-3443 (2012).

- 17 Kim, J.-H., Park, J.-S., Chung, H.-W., Boote, B. W. & Lee, T. R. Palladium nanoshells coated with self-assembled monolayers and their catalytic properties. *RSC Adv.* **2**, 3968-3977 (2012).
- 18 Gavia, D. J. & Shon, Y.-S. Controlling surface ligand density and core size of alkanethiolate capped Pd nanoparticles and their effects on catalysis. *Langmuir* **28**, 14502-14508 (2012).
- 19 Schoenbaum, C. A., Schwartz, D. K. & Medlin, J. W. Controlling surface crowding on a Pd catalyst with thiolate self-assembled monolayers. *J. Catal.* (2013).
- 20 Love, J. C. et al. Formation and structure of self-assembled monolayers of alkanethiolates on palladium. *J. Am. Chem. Soc.* **125**, 2597-2609 (2003).
- 21 Dameron, A. A., Charles, L. F. & Weiss, P. S. Structures and displacement of 1-adamantanethiol self-assembled monolayers on Au(111). *J. Am. Chem. Soc.* **127**, 8697-8704 (2005).
- 22 Pang, S. H., Román, A. M. & Medlin, J.W. Adsorption orientation-induced selectivity control of reactions of benzyl alcohol on Pd(111). *J. Phys. Chem. C* **116**, 13654-13660 (2012).
- 23 Bradley, M. K., Robinson, J. & Woodruff, D. P. The structure and bonding of furan on Pd(111). *Surf. Sci.* **604**, 920-925 (2010).
- 24 Lear, T. et al. The application of infrared spectroscopy to probe the surface morphology of alumina-supported palladium catalysts. *J. Chem. Phys.* **123**, 174706 (2005).
- 25 Brandt, R. K., Sorbello, R. S., & Greenler, R. G. Site-specific, coupled-harmonic-oscillator model of carbon monoxide adsorbed on extended, single-crystal surfaces and on small crystals of platinum. *Surf. Sci.* **271**, 605-615 (1992).
- 26 Morin, C., Simon, D. & Sautet, P. Intermediates in the hydrogenation of benzene to cyclohexene on Pt(111) and Pd(111): A comparison from DFT calculations. *Surf. Sci.* **600**, 1339-1350 (2006).
- 27 Kliewer, C. J. et al. Furan hydrogenation over Pt(111) and Pt(100) single-crystal surfaces and Pt nanoparticles from 1 to 7 nm: A kinetic and sum frequency generation vibrational spectroscopy study. *J. Am. Chem. Soc.* **132**, 13088-13095 (2010).
- 28 Saavedra, H. M., Barbu, C. M., Dameron, A. A., Mullen, T. J., Crespi, V. H. & Weiss, P. S., 1-adamantanethiolate monolayer displacement kinetics follow a universal form. *J. Am. Chem. Soc.* **129**, 10741-10746 (2007).

- 29 Hostetler, M. J., Stokes, J. J. & Murray, R. W. Infrared spectroscopy of three-dimensional self-assembled monolayers: N-alkanethiolate monolayers on gold cluster compounds. *Langmuir* **12**, 3604-3612 (1996).
- 30 Horiuchi, C. M. & Medlin, J. W. Adsorption and reactivity of 2,3-dihydrofuran and 2,5-dihydrofuran on Pd(111): Influence of the C=C position on the reactivity of cyclic ethers. *Langmuir* **26**, 13320-13332 (2010).
- 31 Xu, Y. Decomposition of furan on Pd(111). *Top. Catal.* **55**, 290-299 (2012).
- 32 Allen, G. & Bernstein, H. J. Internal rotation: VIII. The infrared and raman spectra of furfural. *Can. J. Chem.* **33**, 1055-1061 (1955).
- 33 Bhattacharjee, S., Dotzauer, D. M. & Bruening, M. L. Selectivity as a function of nanoparticle size in the catalytic hydrogenation of unsaturated alcohols. *J. Am. Chem. Soc.* **131**, 3601-3610 (2009).
- 34 Crespo-Quesada, M., Yarulin, A., Jin, M., Xia, Y. & Kiwi-Minsker, L. Structure sensitivity of alkynol hydrogenation on shape- and size-controlled palladium nanocrystals: Which sites are most active and selective? *J. Am. Chem. Soc.* **133**, 12787-12794 (2011).
- 35 An, K. & Somorjai, G. A. Size and shape control of metal nanoparticles for reaction selectivity in catalysis. *ChemCatChem* **4**, 1512-1524 (2012).
- 36 Chen, G. et al. Kinetically controlled synthesis of nickel tetrahedron nanocrystals for high performance catalytic hydrogenation. *RSC Adv.* **3**, 5314-5317 (2013).
- 37 Batchelder, D. N., Evans, S. D., Freeman, T. L., Haussling, L., Ringsdorf, H., Wolf, H. Self-assembled monolayers containing polydiacetylenes. *J. Amer. Chem. Soc.* **116**, 1050-1053 (1994).

CHAPTER 4

Effects of thiol modifiers on the kinetics of furfural hydrogenation over Pd catalysts

4.1 Abstract

Thiolate self-assembled monolayers (SAMs) were used to block specific active sites on Pd/Al₂O₃ during the hydrogenation of furfural to elucidate site requirements for each process involved in this complex reaction network. Reactions were performed on uncoated, 1-octadecanethiol (C18) coated and benzene-1,2-dithiol (BDT) coated catalysts. Selectivity among key reaction pathways was sensitive to the SAM modifier, with increasing sulfur density strongly suppressing furfural decarbonylation, less strongly suppressing furfural hydrogenation, and minimally affecting furfuryl alcohol hydrodeoxygenation to methylfuran. Diffuse reflectance infrared Fourier transform spectroscopy with CO was used to characterize site availability on the catalysts. The presence of a C18 modifier restricted the availability of Pd terrace sites while accessibility to Pd edges and steps was practically unaffected with respect to the uncoated catalyst. The BDT modifier further restricted terrace accessibility but additionally restricted adsorption at particle edges and steps. Comparison between reaction rates and site availability suggested that decarbonylation occurred primarily on terrace sites while hydrodeoxygenation occurred on particle steps and edges. Aldehyde hydrogenation, and its reverse process of alcohol

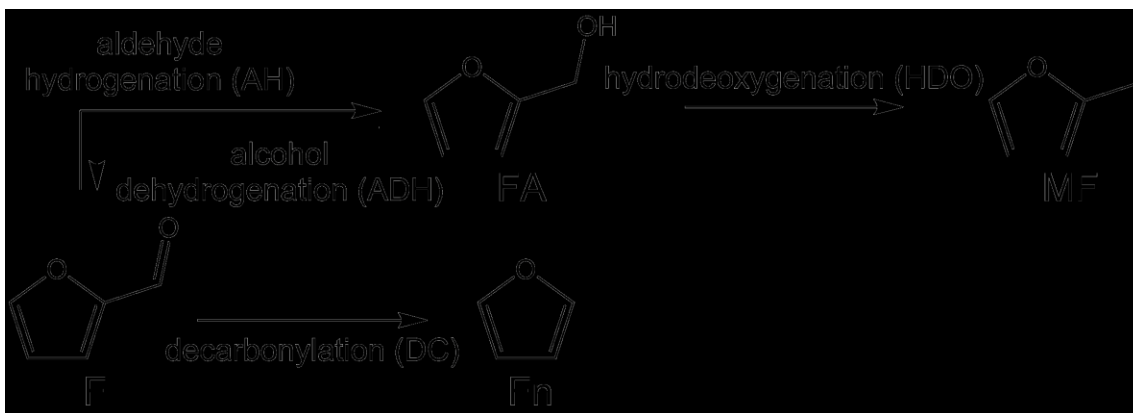
dehydrogenation, was found to occur on both terrace or edge sites, with the dominant pathway dependent on surface coverage as determined by reaction conditions. The results of a detailed kinetic study indicate that in addition to changing the availability of specific sites, thiol monolayers can strongly affect reaction energetics, and decrease the coverage of strongly adsorbed furfural-derived intermediates under reaction conditions. Ambient pressure x-ray photoelectron spectroscopy experiments indicated that the metal-sulfur bonds were not changed appreciably under reaction conditions. The results of this work show that HDO is not appreciably affected even with drastic decreases in the density of available sites as measured by CO adsorption, providing opportunities to design isolated catalyst sites for selective reaction.

4.2 Introduction

Self-assembled monolayers (SAM) of organic thiolates have been used as surface modifiers to influence the reactivity of heterogeneous catalysts.¹ They are attractive for use as surface modifiers because they form ordered overlayers of predictable density according to the functionality of the tail group utilized. SAMs have recently attracted attention because their presence on catalyst surfaces can dramatically influence the reaction selectivity for molecules with multiple functional groups.² In some cases, this reaction selectivity change has been ascribed to the presence of the SAM preventing a particular, often multi-coordinated, adsorption conformation of the reactant, thus increasing selectivity. For example, Wu et al. recently demonstrated that an amine capping layer on Pt₃Co nanocatalysts prevented α,β -unsaturated aldehydes from lying flat on the surface, inhibiting direct contact of the C=C bonds with the catalyst and resulting in a dramatic improvement to the corresponding alcohol.³

There is strong evidence suggesting that specific types of sites or groups of sites may be required in order for a particular pathway to occur.⁴ Traditionally, the relationship between reactivity and site requirements has been probed using particle size.⁵ Smaller particles are expected to have a higher fraction of particle edge sites than larger particles. Therefore, if the formation rate of a particular product is found to increase with decreasing particle size, it is likely that this pathway occurs preferentially at edge sites. Conversely, when the opposite trend is observed, the reaction likely requires a site or group of sites located on the particle terraces. While particle-size experiments provide information about reaction pathways, it can be difficult to synthesize and characterize particles with specific and systematic size variation. Small discrepancies in conditions can result in significant changes in resulting particle morphology.⁶ An alternative approach for discerning the locations of individual reaction steps is to selectively block specific types of sites, e.g. with SAMs. This approach is particularly useful for complex reaction systems in which a number of simultaneous processes may be occurring. By understanding the type of surface environments required for particular reaction pathways, we can improve our ability to design more selective catalysts.

As discussed in the previous chapter, furfural is an important probe molecule for understanding key reactions of biomass derivatives for synthesis of chemicals and fuels.^{7,8} On Pd catalysts, furfural (F) binds strongly through its aromatic ring, resulting primarily in decarbonylation (DC) to produce furan (Fn). Steps such as aldehyde hydrogenation (AH) and hydrodeoxygenation (HDO), which are desirable for conversion of aldehydes to fuels such as methylfuran (MF), do not occur readily. Additionally, the aldehyde hydrogenation pathway is reversible, and furfuryl alcohol (FA) can undergo alcohol dehydrogenation (ADH) to form furfural on the surface. Scheme 4-1 depicts the reaction pathways described here.



Scheme 4-1. Furfural hydrogenation pathways over Pd.

In Chapter 2, we demonstrated that the density of the modifier can be controlled to systematically reduce the number of contiguous sites on particle terraces, while leaving accessibility to edges and steps largely unaffected, to improve selectivity toward hydrogenation and hydrodeoxygenation products during furfural hydrogenation.⁹ While desirable reaction pathways were generally found to be associated with reactions at particle edge sites, the individual reaction processes were not treated independently to obtain mechanistic information about the formation of intermediate products. More generally, there have been few detailed kinetic studies of the hydrogenation of furfural on late transition metal catalysts. A recent density functional theory study has illustrated some of the reaction pathways on Pd(111) in vacuum,¹⁰ but corroboration with experimental kinetic measurements can provide key additional insights at the elementary step level for these complex reaction networks.

Here we report a systematic kinetic analysis of the hydrogenation pathways of furfural over Pd catalysts. Our aim was to understand the effects on reaction mechanism of modification by either 1-octadecanethiol (C18), which forms a $(\sqrt{3}\times\sqrt{3})R30$ structure on the Pd(111) surface,¹¹

or benzene-1,2-dithiol (BDT) which has been shown on Pt(111) to form a $p(2 \times 2)$ structure in the thiol,¹² to investigate the influence of a high density of metal-sulfur bonds (up to 0.50 fractional coverage of sulfur). A Langmuir-Hinshelwood model was developed to help elucidate the effect of increasing SAM density on reaction mechanisms.

4.3 Experimental methods

Thiol-coated catalysts were prepared by immersing 5 wt% Pd/Al₂O₃ (SigmaAldrich Lot no. MKBH9857V) in a 5 mM ethanolic solution of 1-octadecanethiol (C18, 98%, SigmaAldrich) or benzene-1,2-dithiol (BDT, 96%, SigmaAldrich) for at least 12 hours. The supernatant was decanted and the catalysts were rinsed in ethanol to remove any physisorbed thiol. The catalysts were allowed to settle, the rinsing solution was decanted, and the catalysts were dried in air overnight before use.

FTIR analysis was performed using a Thermo Scientific Nicolet 6700 FT-IR with a closed cell attachment (Harrick) for Diffuse reflectance infrared Fourier transform spectroscopy (DRIFTS). To determine information about the structure and integrity of monolayer formation, spectra were collected in the hydrocarbon stretching region for the C18- and BDT-modified catalysts. These spectra are shown together in Figure 4-1. For the C18 catalyst, the position of the asymmetric methylene stretch at $\sim 2922 \text{ cm}^{-1}$ indicated an ordered monolayer. For the BDT catalyst, the absorption feature at $\sim 3050 \text{ cm}^{-1}$ was attributed to the C-H ring stretch of the phenyl moiety. For CO DRIFT experiments, catalyst samples were first exposed to reaction conditions for two hours at mole fractions $y_{\text{H}_2} = 0.250$ and $y_{\text{furfural}} = 0.010$ and a reaction temperature of 190°C. Samples were then placed in a gas tight cell that was evacuated to achieve a baseline

pressure of 0.15 torr. CO was then introduced into the cell to a pressure of 2.00 torr at which point spectra were collected. 100 scans at 4 cm^{-1} resolution were used for each spectrum.

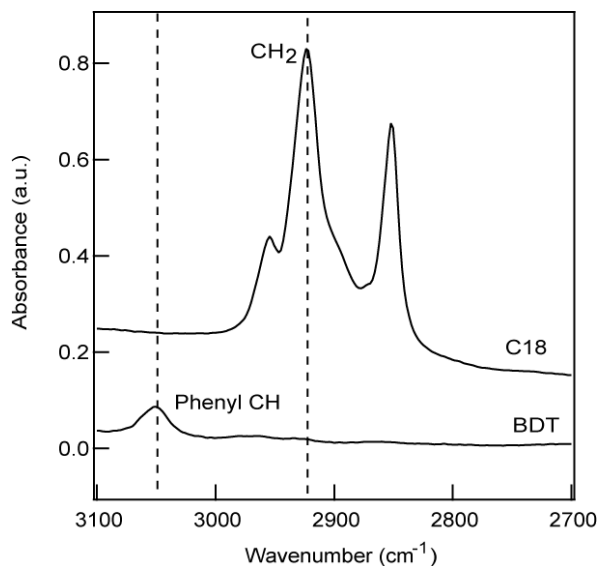


Figure 4-1. Infrared spectra of the hydrocarbon stretching region for C18 and BDT monolayers on 5 wt% Pd/Al₂O₃ catalysts. The feature found at 2923 cm^{-1} for the C18 catalyst was attributed to a CH₂ methylene stretch. The feature at 3050 cm^{-1} for BDT was attributed to a CH stretch of the phenyl moiety.

Active metal surface area measurement was performed on a Micromeritics ChemiSorb 2720. Approximately 100 mg of as-purchased Pd catalyst was reduced in 20 sccm H₂ at 200°C for three hours, then purged in 20 sccm Ar at 200°C for 20 hours without exposure to air. CO pulse chemisorption was performed at 50°C using 1 mL injections of 20% CO (balance Ar). Injections were performed until there was no change in the amount of CO detected, indicating that none was adsorbing. Using this technique, the active metal surface area was calculated to be approximately $3.8\text{ m}^2/\text{g}$ catalyst (17% dispersion), corresponding to an average Pd particle size of 8.3 nm.

The types of sulfur present on the catalysts were characterized using (near) ambient pressure x-ray photoelectron spectroscopy (AP-XPS). Thin films of Pd were prepared by thermal evaporation onto a Si wafer using a CVC 3-boat thermal evaporator. A bonding layer of 1.5 nm Cr was used, onto which 200 nm of Pd was deposited at a rate of 0.7 nm/s. Thiol coatings were prepared in a similar manner to the supported catalyst, using a 1 mM ethanolic solution of thiol. After rinsing in ethanol, the thin films were removed from the solution and excess solution was wicked away and finally dried in air.

AP-XPS experiments were performed at Brookhaven National Laboratory at the National Synchrotron Light Source, beamline X1A1. This system has been described in detail elsewhere.¹³ In brief, a differentially pumped hemispherical analyzer (Specs Phoibos 150 NAP) was positioned at 70° with respect to the incident x-ray beam and 20° to the surface normal. The sample was positioned 0.5 mm from the aperture to ensure that the local surface pressure was not affected by differential pumping. The temperature was measured with a type K thermocouple spot-welded to a Ta backplate located between the heater and crystal. All spectra intensities were normalized with respect to the NSLS ring current. Pd 3d and S 2p spectra were collected at a photon energy of 562 eV. In situ spectra were taken by exposing the sample to 0.1 torr furfural and 0.5 torr H₂ while the sample was heated to 190 °C. Post reaction spectra were taken under vacuum after exposure of the thin film to reaction conditions for over two hours.

XPS analysis and peak deconvolution were performed in OriginLab 9.0. Baseline subtractions were performed using the Shirley method.¹⁴ Peaks were fit using a pseudo-Voigt function composed of the sum of 70% Gaussian and 30% Lorentzian. The S 2p_{3/2}/2p_{1/2} peak area ratio was fixed at 2:1 and the peaks were fit with a doublet separation of 1.19 ± 0.02 eV. Spectra for BDT- and C18-coated Pd thin films were obtained on separate trips to BNL. Thus, peaks on

the BDT surface were fit with Gaussian and Lorentzian fwhm at 1.63 ± 0.04 eV and peaks on the C18 surface were fit with fwhm at 1.38 ± 0.03 eV; intensities were not directly comparable between catalysts.

Hydrogenation reactions were performed in a tubular packed bed flow reactor at atmospheric pressure and constant total gas flow rate. Helium was bubbled through furfural or furfuryl alcohol which was immersed in a water bath to control the temperature. The saturated helium was mixed with H₂ and diluent He before being passed through the catalyst bed. All gases were obtained at ultra-high purity from Airgas. The temperature of the water bath was varied to change the gas phase concentration of furfural/furfuryl alcohol, and the flow rates of H₂ and diluent He were varied to change the concentration of H₂. The amount of catalyst used in each experiment was varied systematically to achieve a conversion of <10% in all cases. All data are reported after at least two hours on stream.

The gas mixture passed through the catalyst bed and the reactor effluent was analyzed using an Agilent Technologies 7890A gas chromatograph with a 30 m × 0.320 mm Agilent HP-5 (5% phenyl)-methylpolysiloxane capillary column and flame ionization detector (split ratio = 25:1, column flow rate = 2 mL min⁻¹, oven temperature = 40°C). Turnover frequencies used to perform reaction order and activation energy analyses were calculated by dividing the product flow rates by the number of surface sites on the unmodified catalyst, based on measurement of active metal surface area from CO chemisorption and mass of catalyst used.

Apparent activation energy studies were performed using the mole fractions $y_{\text{H}_2} = 0.400$ and $y_{\text{furfural}} = 0.010$ or $y_{\text{furfuryl alcohol}} = 0.001$ at reactor temperatures ranging from 160°C to 190°C. Apparent reaction order studies were performed at a reactor temperature of 190°C. For reaction orders in furfural and furfuryl alcohol, the hydrogen mole fraction was held constant at $y_{\text{H}_2} =$

0.400. For reaction order in hydrogen, the furfural and furfuryl alcohol mole fractions were held constant at $y_{\text{furfural}} = 0.010$ and $y_{\text{furfuryl alcohol}} = 0.001$, respectively. Analysis of these experiments assumed that the rate of each reaction could be expressed in a power law form:

$$\text{rate} = k \times y_{\text{F}}^{\alpha} \times y_{\text{H}_2}^{\beta}$$

where y_{F} represents the mole fraction in the gas phase of either furfural or furfuryl alcohol. The activation energies and reaction orders were determined by performing linear regression analysis with inverse variance weighting of the data points. The errors reported are the standard errors in the slopes of the Arrhenius or power law plot. For all catalysts, we ensured that external mass transport was not a limiting factor by varying the weight hourly space velocity.

4.4 Results and discussion

Uncoated Catalyst Characterization

The uncoated catalyst was characterized using a combination of CO chemisorption and CO DRIFTS. The chemisorption uptake of 75 m^2/g of metal was consistent with an average Pd particle size of 8.3 nm. The CO DRIFT spectrum for the uncoated catalyst after reduction is shown in Figure 4-2. The catalyst used in this study had features attributable to CO bound in atop ($\sim 2040\text{-}2080 \text{ cm}^{-1}$), bridge ($\sim 1980 \text{ cm}^{-1}$), and hollow sites ($\sim 1850\text{-}1940 \text{ cm}^{-1}$). Note that the measured average Pd particle size for the catalyst used in these studies was larger than that for catalysts used in our previous work ($\sim 6 \text{ nm}$). This resulted in a significant reduction of CO bound to bridge sites on particle edges and steps for the larger particles used in this study.

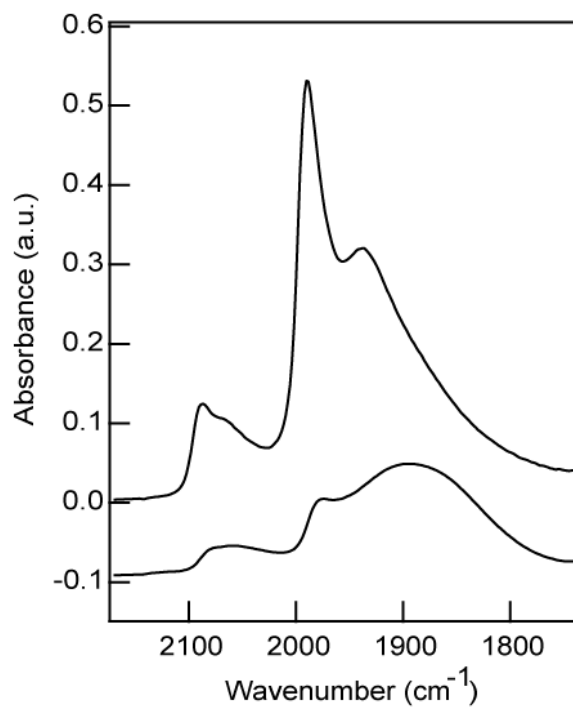


Figure 4-2. Infrared spectra of bound CO (2,000 mTorr exposure) on (top) 5 wt% Pd/Al₂O₃ particles used in previous study compared to (bottom) new 5 wt% Pd/Al₂O₃ particles used in this study.

X-Ray Photoelectron Spectroscopy

Near ambient-pressure XPS was used to characterize the state of sulfur on the surface both before and during exposure to reaction conditions. Analysis of sulfur species (Figure 4-3) indicated three types of sulfur on the surface, with 2p_{3/2} binding energies of 161.99 ± 0.06, 162.90 ± 0.04 and 163.75 ± 0.04 eV, which have previously been assigned to sulfur bound as thiolate, thiol, and disulfide, respectively.^{15,16}

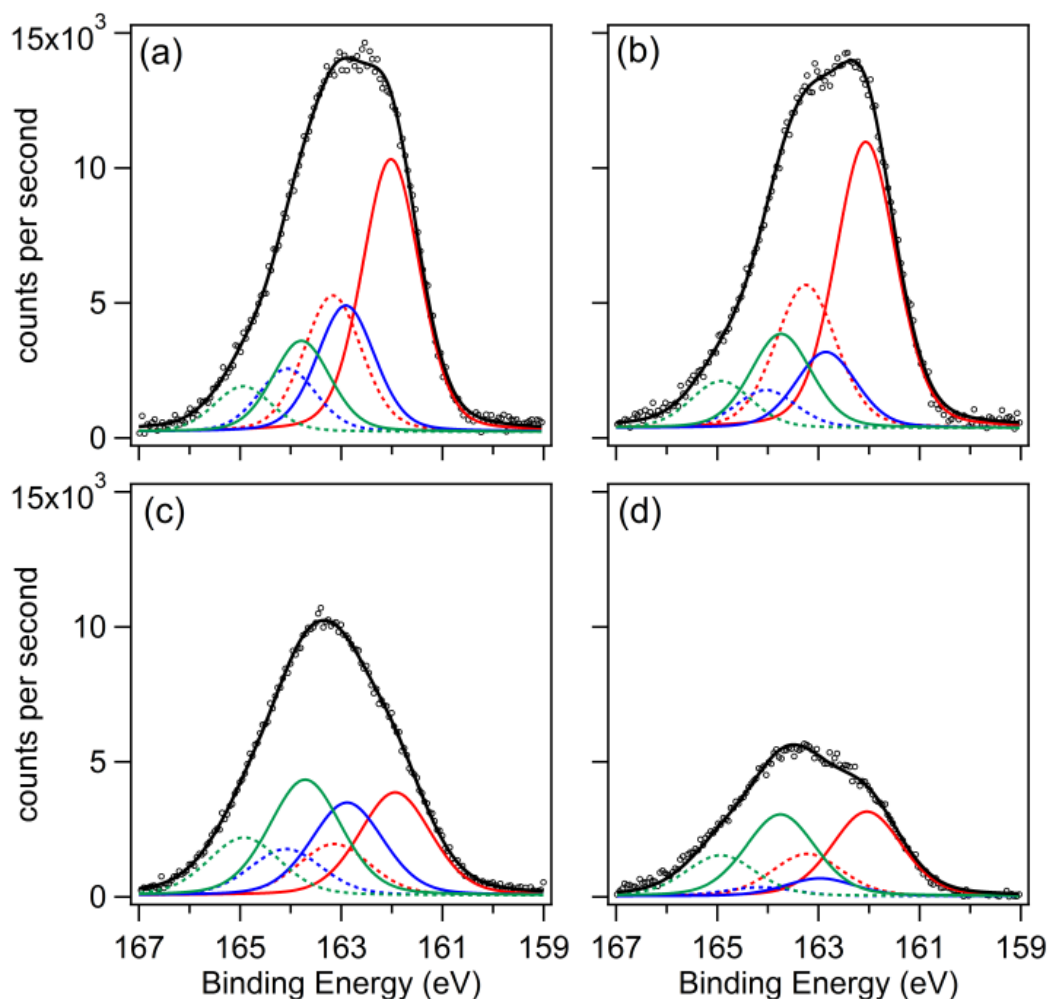


Figure 4-3. X-ray photoelectron spectra (open circles) in the S 2p region taken in situ under reaction conditions for: (a), (b) the C18-coated catalyst and (c), (d) the BDT-coated catalyst. Spectra (a) and (c) were taken upon introduction of gases and heating to 190°C. Spectra (b) and (d) were obtained after exposure to reaction conditions for two hours. S 2p_{3/2}/2p_{1/2} doublet separation = 1.19 ± 0.02 eV (solid/dashed colored lines).

The peak associated with weakly adsorbed thiol at 162.90 eV decreased in intensity over the course of the reaction, suggesting that physisorbed thiol precursor molecules were gradually removed. In contrast, the peaks associated with more strongly bound sulfur, thiolate and disulfide, did not change in intensity. This suggested that the metal-sulfur bonds on the surfaces

of the catalysts did not change appreciably over the course of the reaction, despite the presence of hydrogen.

Comparison of sulfur coverage on C18 and BDT catalysts after two hours under reaction conditions was achieved by normalization based on the Pd signal. The attenuation in electron flux due to the organic layer has been studied previously for electron kinetic energies in the range 500-1500 eV.¹⁷ Under the assumption that the linear relation is still valid at 400 eV (the approximate measured kinetic energy of the detected S 2p electrons) the signal was attenuated to approximately 29% and 78% of the electron flux from the uncoated catalyst for the catalysts with C18 and BDT monolayers, respectively. The S 2p_{3/2} signals were normalized against the Pd 3d_{5/2} signal, taking into account the inelastic mean free path of the approximately 227 eV electrons in Pd and the signal attenuation due to the organic layer. From in situ XPS data, we calculated that the BDT-coated surface had approximately 50% more sulfur than the C18-coated surface, in agreement with the theoretically-expected value of 50% based on the nominal surface structure of the two thiols on single crystal surfaces.

Selectivity over Thiol-Modified Catalysts

Gas-phase hydrogenation of furfural or furfuryl alcohol was conducted in a tubular packed bed flow reactor at 190°C on 5 wt% Pd/Al₂O₃ that was either left uncoated or was coated with a self-assembled monolayer of 1-octadecanethiol (C18) or benzene-1,2-dithiol (BDT). The Pd surface area of the uncoated catalyst was used for all turnover frequency calculations. Because a large fraction of Pd sites are occupied by thiol modifiers on the coated catalysts, this results in an under-reporting of the “true” turnover frequency, as discussed in more detail below.

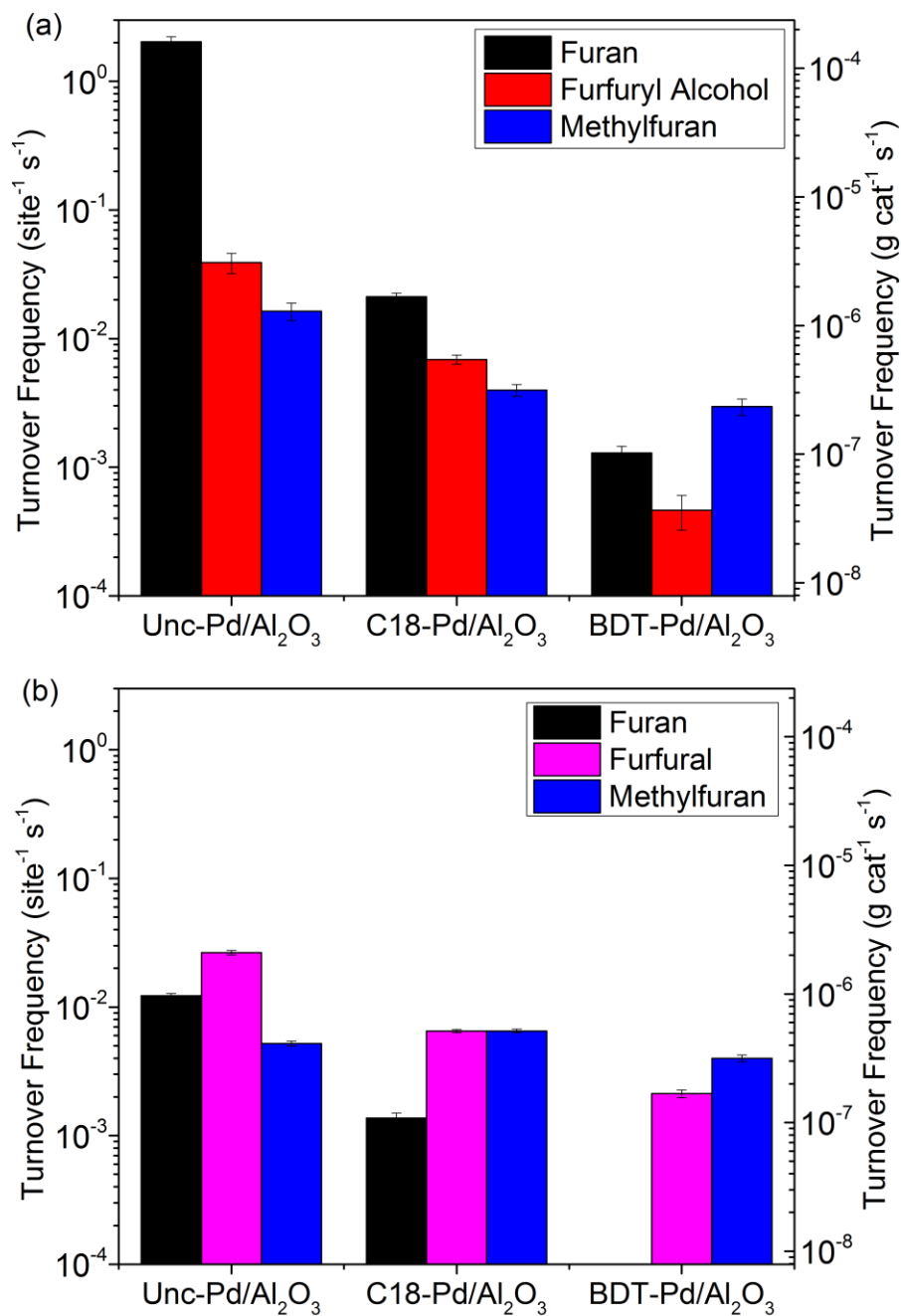


Figure 4-4. Turnover frequencies for various products from (a) furfural hydrogenation ($y_F = 0.010$ and $y_{H_2} = 0.250$) and (b) furfuryl alcohol hydrogenation ($y_{FA} = 0.001$ and $y_{H_2} = 0.300$) over uncoated, C18-coated and BDT-coated 5 wt% Pd/Al₂O₃. Turnover frequencies are reported per surface Pd atom (site⁻¹ s⁻¹) where the number of surface atoms was determined from the clean, uncoated catalyst. Selectivity and rate are reported under 10% conversion of reactant fed. Error bars indicate the standard deviation of five repeated measurements of product concentration over the course of an hour.

Figure 4-4a reports the turnover frequency obtained at $8 \pm 1\%$ conversion of furfural. Using uncoated Pd catalysts, the dominant product was furan ($>95\%$ selectivity), and the rate of decarbonylation (DC) was about two orders of magnitude greater than those of aldehyde hydrogenation (AH) and hydrodeoxygenation (HDO). C18-coated catalysts exhibited a modest increase in selectivity to the desired AH/HDO products, and reached a combined selectivity of about 34%. As shown in Figure 4-4(a), this selectivity enhancement was achieved through a large decrease in the rate of decarbonylation, and a more modest decrease in the rate of hydrogenation. BDT-coated catalysts, with more sulfur on the surface, continued this trend, reaching a combined AH/HDO selectivity of over 70%. Accordingly, the rate of DC was reduced by three orders of magnitude from the uncoated case, whereas the rate of hydrogenation was only reduced by one order of magnitude. These selectivity and rate observations may be partially explained by a site-blocking mechanism. The availability of active sites was systematically reduced through the use of C18¹¹ and BDT¹² SAMs which form monolayers with approximate sulfur coverages of 0.33 and 0.50, respectively. The selectivity trends obtained here for the C18-coated catalyst were consistent with those we previously reported, but the quantitative effect of the coating on rates and selectivities was slightly different.⁹ Note that the previous results were reported at a different conversion (13%), feed mole fractions ($y_{\text{H}_2} = 0.400$ and $y_{\text{furfural}} = 0.016$), and for a more highly dispersed Pd catalyst.

Figure 4-4b reports the rate obtained at $3 \pm 1\%$ conversion of furfuryl alcohol. The mole fraction of furfuryl alcohol was chosen to reflect the amount of furfuryl alcohol produced in the experiments performed from furfural in Figure 4-4a. Increasing the thiol coverage caused an increase in the selectivity of methylfuran from 12% on the uncoated catalyst to 65% on the BDT-coated catalyst. The combined rates for furfural and furan production were reduced by about a

factor of 20 with the BDT modifier. Remarkably, even in the presence of large amounts of sulfur on the surface, the rate of production of methylfuran on the C18-coated catalyst was unaffected and only reduced by a factor of two on the BDT-coated catalyst. Thus, while the rate of furfural decarbonylation decreased by between two and three orders of magnitude for the C18- and BDT-coated catalysts, the rate of furfuryl alcohol hydrodeoxygenation was practically unaffected.

CO DRIFTS on Post-Reaction Catalysts

To directly test the availability of specific adsorption sites on the modified and unmodified catalysts after exposure to reaction conditions, diffuse reflectance Fourier transform infrared spectroscopy (DRIFTS) was performed using carbon monoxide as a probe molecule. In these experiments, peak positions were readily attributed to CO binding in three-fold, bridging, and top sites.¹⁸ DRIFT spectra during a saturating exposure of CO on the uncoated, C18, and BDT catalysts are shown in Figure 4-5.

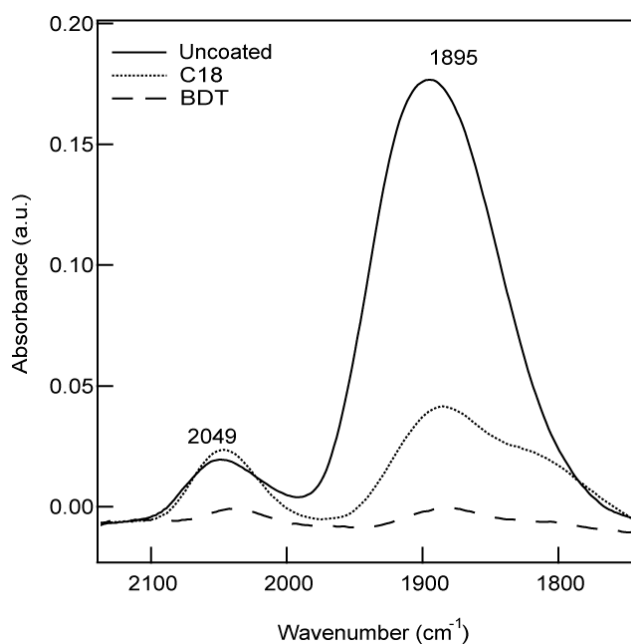


Figure 4-5. CO stretching region for uncoated, C18- and BDT-modified 5 wt% Pd/Al₂O₃ after exposure to reaction conditions for two hours.

Previous attempts to elucidate site information on catalysts used CO adsorption before catalysts were exposed to reaction conditions. Since carbonaceous deposits formed during reaction may alter the types of sites available, the experimental results in Figure 4-5 were collected after reaction to characterize sites available under reaction conditions. With increasing thiol density, the availability of sites on particle terraces ($\sim 1895 \text{ cm}^{-1}$) was systematically reduced. Accessibility to particle edges and steps ($\sim 2050 \text{ cm}^{-1}$) was essentially unchanged between the uncoated and C18 catalyst but was significantly reduced on the BDT catalyst.

By comparing the available sites on these catalysts with the differential rates of each reaction, we elucidated the types of sites required for each particular reaction pathway shown in Scheme 4-1. The rates of DC and AH from reaction of furfural and the rates ADH and HDO from the reaction of furfuryl alcohol are shown together in Figure 4-6.

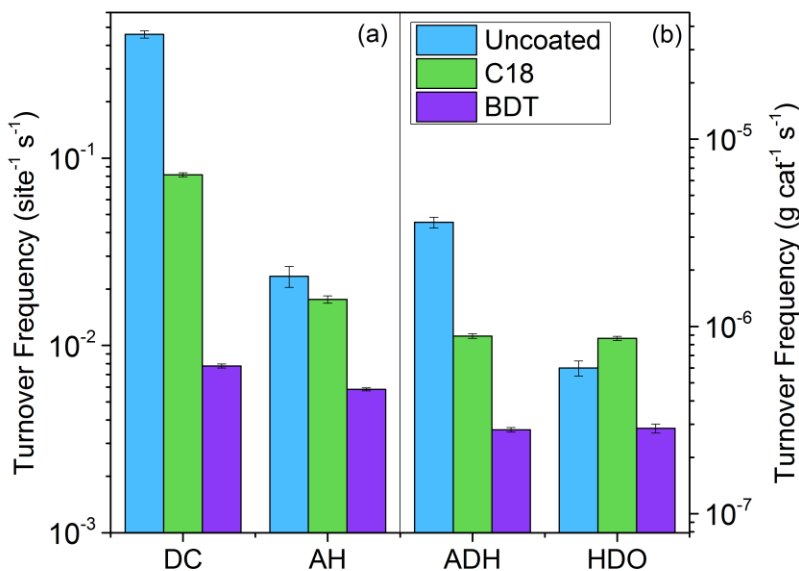


Figure 4-6. Differential rates of (a) decarbonylation and aldehyde hydrogenation of furfural and (b) alcohol dehydrogenation and hydrodeoxygenation of furfuryl alcohol. For the furfural reactions, the mole fractions of furfural and hydrogen were $y_F = 0.010$ and $y_{H_2} = 0.400$, respectively. For the furfuryl alcohol reactions, the mole fractions of furfuryl alcohol and hydrogen were $y_{FA} = 0.001$ and $y_{H_2} = 0.400$, respectively.

Combining results from the reactivity data and CO DRIFTS, a number of general conclusions were reached about the types of sites on which particular reactions occurred. First, because addition of the C18 and the BDT modifiers successively reduced the number of terrace sites available, a systematic reduction in rate may be attributed to a reaction occurring on terrace sites. Additionally, a reaction that has larger site requirements will be affected more strongly by this site reduction. This appeared to be the case for the DC and ADH processes; upon addition of the BDT modifier, the rate of DC was reduced by a factor of ~60 and the rate of ADH was reduced by a factor of ~15. This suggested that the number of contiguous active sites required for the DC process was greater than that necessary for ADH. This hypothesis is consistent with surface science studies of aromatic aldehydes that demonstrated that DC is the dominant process when the molecules can lie flat on the surface.¹⁹ We then hypothesized that ADH occurred from two different structures on the surface – a flat lying structure that occupied a large number of surface sites and that is restricted by the addition of thiol modifiers, and an upright structure that occupied fewer sites. Further support for this hypothesis will be discussed in detail below.

The second general conclusion concerns reactions that occur primarily on edges and steps. Because the accessibility to these sites appeared nearly unchanged upon addition of the C18 modifier but was affected by the BDT modifier, cases where reaction rates mimicked this trend were assumed to occur on particle steps and edges. This was the case for the AH and HDO processes. In particular, surface science studies have demonstrated that HDO reactions occur from upright structures that do not require large numbers of contiguous surface atoms.¹⁹

We now focus our attention on ADH and AH. According to the principle of microscopic reversibility, ADH and AH should occur with the same, but reversed, mechanism, since they are

reverse processes of each other. Therefore, we would assume that the dependence of these rates on catalyst modification would be the same. This is apparently inconsistent with the data shown in Figure 4-6 since the rate of ADH was reduced by the C18 modifier (and reduced further by the BDT modifier), suggesting that it occurred from flat-lying structures, while AH was reduced only by the BDT modifier, suggesting that it occurred from upright structures. We explain this discrepancy by noting that the coverage of reactant in these experiments was likely different due to the order of magnitude reduction in mole fraction necessary in order for FA to mimic the amount of FA produced in the experiments performed in generating Figure 4-4a. Previous surface science work has suggested that adsorbate coverage variations may lead to variations in rates since major shifts in TPD peak position are observed with increasing adsorbate coverage.²⁰ This coverage effect will be investigated more closely in the discussion of reaction order studies below.

Apparent Activation Energy

In order to probe how site blocking may influence these reaction processes, apparent activation energies for each reaction process were measured and compared to DFT-calculated values on a Pd(111) surface at 1/16 monolayer coverage by Vlachos, et al.¹⁰ Reactions were carried out at temperatures ranging from 160°C to 190°C. The results are summarized in Table 4-1. In general, the apparent activation energies reported in Table 4-1 may be due to a combination of processes, making exact determination of the limiting process difficult. It is also important to note that all of the calculated barriers were performed with adsorbates in a flat-lying configuration on Pd(111). With these caveats in mind, we can make several observations based on measured values.

Catalyst	DC E _a (kJ/mol)	AH E _a (kJ/mol)	ADH E _a (kJ/mol)	HDO E _a (kJ/mol)
5% Pd/Al ₂ O ₃	80 ± 20	50 ± 10	14 ± 7	28 ± 8
C18-5% Pd/Al ₂ O ₃	60 ± 10	13 ± 4	50 ± 20	85 ± 8
BDT-5% Pd/Al ₂ O ₃	70 ± 10	12 ± 5	40 ± 10	82 ± 8
Pd(111) ¹⁰	91.7	77.2	49.2	82.0

Table 4-1. Apparent activation energies for processes involved in Scheme 4-1. DC and AH activation energies were determined using furfural as the reactant; ADH and HDO activation energies were determined using furfuryl alcohol as the reactant. The error reported is the standard error of the slope of the Arrhenius plot using a weighted linear regression. Calculated Pd(111) activation barriers were taken from ref. 10.

First, Table 4-1 shows that the thiol-coated catalysts have very similar activation barriers for all reaction processes, despite the difference in sulfur coverage. We hypothesize that this similarity is related to the fact that the most abundant surface species for both SAM-coated catalysts is the thiol rather than furfural-derived intermediates, and both thiol-coated catalysts present a relatively dense organic layer at the surface. Further support for this hypothesis is provided by the reaction order studies discussed below. In general, the apparent activation energies for the uncoated catalyst differ substantially, consistent with a much different active site environment.

A possible exception to this difference is for the decarbonylation reaction, which exhibits similar apparent barriers for all catalysts, as well as for the prior DFT studies on Pd(111). The apparently similar kinetics among catalysts, as well as the agreement with DFT calculations, are consistent with a mechanism in which DC requires a relatively large ensemble of sites to proceed through a flat-lying furfural intermediate. In this flat-lying conformation, the aldehyde and furan species inherently occupy nearest neighbor sites and will undergo decarbonylation. Therefore, while increasing thiolate coverage reduces the overall fraction of contiguous sites large enough

to permit adsorption of a flat-lying intermediate, once adsorbed in this conformation furfural will undergo decarbonylation via the same mechanism.

Furfural, Furfuryl Alcohol and Hydrogen Reaction Order

Reaction order studies were carried out to investigate how site-blocking from the SAM modifier affects adsorbate coverage. The results are summarized for furfural and furfuryl alcohol as reactants in Table 4-2.

Catalyst	Furfural R.O.		Hydrogen R.O.		Furfuryl Alcohol R.O.		Hydrogen R.O.	
	DC	AH	DC	AH	ADH	HDO	ADH	HDO
5% Pd/Al ₂ O ₃	0.3(2)	0.5(2)	-0.5(3)	0.3(4)	1.1(1)	1.0(2)	-0.03(7)	0.10(5)
C18-5% Pd/Al ₂ O ₃	0.85(6)	0.80(1)	-0.36(9)	0.54(8)	1.12(2)	0.96(8)	0.32(6)	0.24(7)
BDT-5% Pd/Al ₂ O ₃	0.7(2)	0.79(2)	-0.3(2)	0.76(6)	0.9(2)	0.90(6)	0.2(1)	0.32(6)

Table 4-2. Reaction orders for processes depicted in Scheme 4-1. Reaction order experiments for DC and AH were performed with furfural; experiments for ADH and HDO were performed with furfuryl alcohol. The numbers in parentheses represent the uncertainty in the least significant digit. The uncertainty is the standard error of the slope of the power law plot using a weighted linear regression.

In general, a reaction order near unity indicates that the adsorbate has low coverage on the surface, and thus in this range, the rate increases monotonically with increasing partial pressure of the corresponding gas phase molecule. Negative reaction orders indicate that the reaction process is hindered by presence of that adsorbate. This could be because this reactant is acting as a site blocker for other adsorbates as would be the case in a competitive adsorption model.

In examining Table 4-2 for reactions involving furfural (DC and AH), several trends become apparent. The reaction order for furfural in DC and AH increased with addition of the SAM modifiers. This suggested that the coverage of furfural was lower on the thiol-coated catalysts, consistent with a site-blocking effect of the SAMs. The reaction order for hydrogen in DC was negative in all cases, consistent with the fact that hydrogen was not involved in the DC process. Hydrogen may have acted as a site blocker for furfural in this case, reducing the coverage of furfural on the surface. Additionally, the hydrogen reaction order for AH increased on the thiol-coated catalysts, indicating that hydrogen coverage was also reduced when the SAMs were present, similar to furfural.

The reaction order for furfuryl alcohol in ADH and HDO, Table 4-2, was near unity on both the uncoated and thiol-coated catalysts. This is consistent with the fact that the concentration of furfuryl alcohol in these reactions was an order of magnitude smaller than furfural to mimic the low concentration of furfuryl alcohol produced under the furfural hydrogenation reaction conditions, and so the surface coverage of furfuryl alcohol was likely small on all catalysts. Correspondingly, the reaction order for hydrogen in HDO was near zero in all cases, indicating that additional hydrogen did not significantly assist the reaction rate because there was enough surface hydrogen available. The hydrogen reaction order increased slightly on the thiol-coated catalysts, consistent with the idea that coverage of all species was reduced by the presence of the SAM.

The reaction order in hydrogen for the ADH reaction presents an interesting trend. One would expect, since the reaction requires no stoichiometric hydrogen, that the reaction order would be negative in all cases since hydrogen would act as a site blocker. However, the reaction order actually switched from near zero to slightly positive on the thiol-coated catalysts. This

could be due to the effect of hydrogen lowering the concentration of strongly bound flat-lying intermediates on the surface, and would be consistent with the hypothesis that the rate of ADH is larger when the adsorbate is upright. Alternatively, Vlachos, et al. have identified a reaction pathway for ADH that involves dehydrogenation of furfuryl alcohol to the acyl species before addition of a single hydrogen atom to form the aldehyde.¹⁰ Though they identified an overall activation barrier of 106.1 kJ/mol, it is possible that this pathway becomes important on the thiol-coated catalysts and thus the ADH reaction could be assisted by the presence of hydrogen.

Discussion

From the results presented here, the following interpretations were made regarding the effect of thiolate modifiers on the furfural reaction network.

1) The decarbonylation reaction mechanism appeared to be similar on modified and unmodified catalysts. From comparisons between reactivity and site availability, the rate of DC was systematically reduced with increasing coverage, consistent with the hypothesis that furfural needed a larger ensemble of contiguous active sites to bind in the multi-coordinated adsorption geometry required for DC. Apparent activation energies were found to be the same for this process on all catalysts tested, and reaction order studies confirmed that increasing thiolate coverage serves to reduce coverage of furfural on the surface. This reduced coverage could be due to either a change in the binding affinity of the adsorbates when there are SAMs on the surface, or could be attributed more simply to a site blocking effect from the sulfur. If the former hypothesis were true, we would expect to see differences in the rate limiting mechanism between the C18 and BDT coated catalysts due to an increased amount of sulfur. We cannot definitively rule out a change in the binding affinity without direct measurement of adsorption equilibrium

constants. However, the apparent activation energy data indicated that the energy barriers on the C18 and BDT coated catalysts were the same, suggesting that the reduction in adsorbate coverage was predominantly due to a site blocking effect rather than a change in the binding affinity of the furanic species on the available sites.

2) Comparison between site availability and reactivity provided insight with respect to the sites required for the remaining processes: aldehyde hydrogenation/alcohol dehydrogenation and hydrodeoxygenation. Previous surface science studies show that high coverage of these aromatic oxygenates can cause the flat-lying and upright structures to coexist,¹⁹ suggesting that AH and ADH reactions could proceed through either type of intermediate. Under furfuryl alcohol hydrogenation conditions, the application of thiol coatings decreased the ADH rate by a much smaller factor than the DC rate, consistent with the participation of intermediates with reduced site requirements in ADH. Under furfural hydrogenation conditions where surface crowding is more severe, the addition of thiols has even less of an effect on the AH rate. Hypothetically this is due to a low coverage of more flat-lying AH/ADH intermediates even on the uncoated catalyst. As discussed above, comparison between reactivity and site availability suggests that HDO occurred primarily on particle edges and steps from an upright structure of furfuryl alcohol. Even in the presence of high sulfur coverage, the production of methylfuran was unaffected the presence of the C18-modifier and modestly reduced by the BDT-modifier. Thus, whereas DC preferentially occurs on terraces and HDO on step edges, AH/ADH has intermediate site requirements and the dominant pathway may be dictated by reaction conditions.

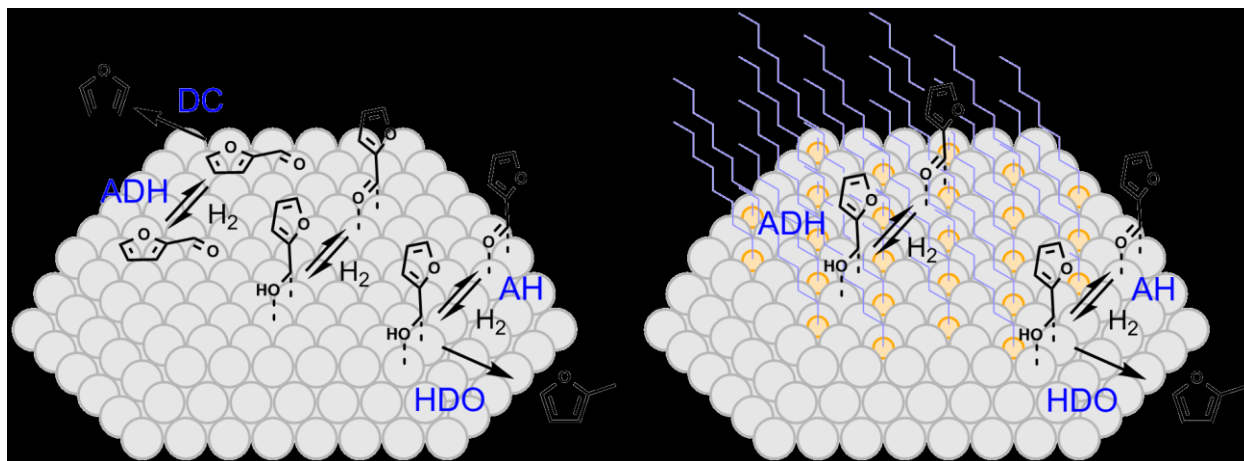
While reactivity/structure relationships suggest that AH and ADH occurred on both terrace and edge sites and that HDO occurred primarily on particle edges, comparison between apparent activation energies on the coated and uncoated catalysts provided evidence that the

presence of the modifiers affected the rate limiting mechanisms for these processes. This effect may be, in part, related to the role of hydrogen since the presence of sulfur has been shown to alter both hydrogen adsorption and diffusion on single crystal surfaces.^{22,23}

3) The mechanism by which the modifiers improved selectivity toward the hydrogenation pathways was the same for the thiol-coated catalysts. In other words, the improved selectivity behavior observed using the denser BDT-modified catalyst was fundamentally the same as C18 catalyst, but the higher sulfur coverage essentially made this coating more effective for restricting the undesired DC process. Apparent activation energies were found to be statistically identical for all reaction processes between the BDT and C18 catalysts. This similarity likely results from the fact that both SAMs serve to isolate Pd sites, creating a more uniform reaction environment than on the uncoated surface.

In order to quantitatively determine the effect of thiol coverage on the specific kinetic properties for this reaction network (e.g. inherent rate constants and adsorption equilibrium constants), we developed a Langmuir-Hinshelwood kinetic model that was fit to reaction data. Two significant challenges were encountered during this treatment: 1) because rate constants and adsorption equilibrium constants appeared as paired products in these expressions, they could not be solved for independently, and 2) large uncertainties in estimations for vacant site availability have a significant effect on resulting kinetic parameter values. The detailed treatment is included Appendix A. A primary conclusion from the modeling results is that the dense BDT coating is associated with elementary step reaction rates that are far higher than would be predicted on the basis of CO chemisorption. This result is reflected in the data reported above, where (for example) a relatively high rate for HDO is achieved (Figure 4-4), even though site availability is drastically reduced compared to the uncoated and C18 coated catalysts.

Scheme 4-2 summarizes the reactions that occurred on uncoated and thiol-coated Pd catalysts based on site availability, apparent activation energies, and reaction orders. On the uncoated catalyst, furfural and furfuryl alcohol adsorbed in either a flat-lying or an upright conformation. These two adsorbates hydrogenated/dehydrogenated in both configurations. However, decarbonylation required that adsorbates adopt the flat-lying conformation while hydrodeoxygenation occurred from an upright conformation. On the thiol-coated catalysts, the adsorbates tended to adopt the upright conformation, leading to drastically decreased rate of decarbonylation. This kind of orientation-selectivity effect for decarbonylation and hydrodeoxygenation has also been seen in surface science studies.¹⁹



Scheme 4-2. Proposed reaction pathways for furfural and furfuryl alcohol on uncoated and thiol-coated catalysts. On uncoated catalysts, the reactants adsorbed in a flat-lying conformation on terraces or in an upright conformation on both terraces and edges; reactants were restricted to the upright conformation on both terraces and edges when the thiol coating was present.

4.5 Conclusions

Here, we report results for a comprehensive kinetic investigation on the effect of increasing SAM-modifier concentration during furfural hydrogenation on uncoated, 1-octadecanethiol, and benzene-1,2-dithiol coated Pd/Al₂O₃ heterogeneous catalysts. Addition of

C18 and BDT surface modifiers systematically increased the hydrogenation selectivity of furfural to furfuryl alcohol and methylfuran. Ambient-pressure XPS experiments demonstrated that the metal-sulfur bonds were not appreciably changed over the course of the reaction, implying that the thiolate monolayer was stable under reaction conditions. Decarbonylation was found to occur on particle terrace sites via the same apparent mechanism on both coated and uncoated catalysts. Aldehyde hydrogenation and the reverse process alcohol dehydrogenation occurred on particle terraces and steps via reaction of both flat-lying and upright furfural, with reaction from the upright structure being more important. Hydrodeoxygenation occurred primarily at particle edges and steps likely from an upright conformation of furfuryl alcohol. The rate of this reaction was hardly decreased by increasing sulfur coverage. The mechanism by which the BDT- and C18-modifiers enhance selectivity toward hydrogenation products was thus the same; improved selectivity with the BDT modifier was attributed to the higher sulfur coverage which was more effective for restricting the undesired decarbonylation process. Increasing thiol density on the surface resulted in a decrease in adsorbate coverage, as evidenced by reduction in available sites in CO DRIFTS and increase in reaction order with SAM modification. Thus, SAM modification can serve the role of isolating certain types of surface sites; intriguingly, the isolated sites are highly active for hydrodeoxygenation, while being much less reactive toward undesired decarbonylation.

4.6 References

- 1 Schoenbaum, C. A., Schwartz, D. K. & Medlin, J. W. Controlling the Surface Environment of Heterogeneous Catalysts using Self-Assembled Monolayers. *Acc. Chem. Res.* **47**, 1438-1445, (2014).

- 2 Kahsar, K. R., Schwartz, D. K. & Medlin, J. W. Selective Hydrogenation of Polyunsaturated Fatty Acids Using Alkanethiol Self-Assembled Monolayer-Coated Pd/Al₂O₃ Catalysts. *ACS Catal.* **3**, 2041-2044 (2013).
- 3 Wu, B., Huang, H., Yang, J., Zheng, N. & Fu, G. Selective Hydrogenation of alpha,beta-Unsaturated Aldehydes Catalyzed by Amine-Capped Platinum-Cobalt Nanocrystals. *Angew. Chem. Int. Ed.* **51**, 3440–3443 (2012).
- 4 Nørskov, J. K., Bligaard, T., Hvolbæk, B., Abild-Pedersen, F., Chorkendorff, I. & Christensen, C. H. The nature of the active site in heterogeneous metal catalysis. *Chem. Soc. Rev.* **37**, 2163-2171 (2008).
- 5 Bond, G. C. Small particles of the platinum metals *Platinum Met. Rev.* **19**, 126-134 (1975).
- 6 Zhang, H., Jin, M., Xiong, Y., Lim, B & Xia, Y. Catalysing sustainable fuel and chemical synthesis. *Acc. Chem. Res.* **46**, 1783-1794 (2013).
- 7 Serrano-Ruiz, J. C., West, R. M. & Dumesic, J. A. Catalytic conversion of renewable biomass resources to fuels and chemicals. *Annu. Rev. Chem. Biomol. Eng.* **1**, 79-100 (2010).
- 8 Sitthisa, S. & Resasco, D. E. *Catal. Lett.* Hydrodeoxygenation of furfural over supported metal catalysts: A comparative study of Cu, Pd and Ni. *Catal. Lett.* **141**, 784-791 (2011).
- 9 Pang, S. H., Schoenbaum, C. A., Schwartz, D. K. & Medlin, J. W. Directing reaction pathways by catalyst active-site selection using self-assembled monolayers. *Nat. Commun.* **4**, 2448 (2013).
- 10 Vorotnikov, V. & Mpourmpakis, G.; Vlachos, D. G. DFT study of furfural conversion to furan, furfuryl alcohol, and 2-methylfuran on Pd(111). *ACS Catal.* **2**, 2496-2504 (2012).
- 11 Love, J. C. et al. Formation and structure of self-assembled monolayers of alkanethiolates on palladium. *J. Am. Chem. Soc.* **125**, 2597-2609 (2003).
- 12 Yang, Y.-C., Lee, Y.-L., Yang, L.-Y. O. & Yau, S.-L. In situ scanning tunneling microscopy of 1,6-hexanedithiol, 1,9-nonanedithiol, 1,2-benzenedithiol, and 1,3-benzenedithiol adsorbed on Pt(111) electrodes. *Langmuir* **22**, 5189-5195 (2006).

- 13 Tenney, S. A., Lu, D., He, F., Levy, N., Perera, U. G. E., Starr, D. E., Müller, K., Bluhm, H. & Sutter, P. submitted for publication.
- 14 Shirley, D. High-resolution X-ray photoemission spectrum of the valence bands of gold. *Phys. Rev. B* **5**, 4709-4714 (1972).
- 15 Bain, C. D., Biebuyck, H. A. & Whitesides, G. M. Comparison of self-assembled monolayers on gold: coadsorption of thiols and disulfides. *Langmuir* **5**, 723-727 (1989).
- 16 Castner, D. G., Hinds, K. & Grainger, D. W. X-ray photoelectron spectroscopy sulfur 2p study of organic thiol and disulfide binding interactions with gold surfaces. *Langmuir* **12**, 5083-5086 (1996).
- 17 Laibinis, P. E., Bain, C. D. & Whitesides, G. M. Attenuation of photoelectrons in monolayers of n-alkanethiols adsorbed on copper, silver, and gold. *J. Phys. Chem.* **95**, 7017-7021 (1991).
- 18 Schoenbaum, C. A., Schwartz, D. K. & Medlin, J. W. Controlling surface crowding on a Pd catalyst with thiolate self-assembled monolayers. *J. Catal.* **303**, 92-99 (2013).
- 19 Pang, S. H., Román, A. M. & Medlin, J. W. Adsorption orientation-induced selectivity control of reactions of benzyl alcohol on Pd(111). *J. Phys. Chem. C* **116**, 13654-13660 (2012).
- 20 Pang, S. H. & Medlin, J. W. Adsorption and Reaction of Furfural and Furfuryl Alcohol on Pd(111): Unique Reaction Pathways for Multifunctional Reagents. *ACS Catal.* **1**, 1272-1283 (2011).
- 21 Michel, C. & Auneau, F.; Delbecq, F.; Sautet, P. C-H versus O-H bond dissociation for alcohols on a Rh(111) surface: a strong assistance from hydrogen bonded neighbors. *ACS Catal.* **1**, 1430-1440 (2011).
- 22 Gravil, P. A. & Toulhoat, H. Hydrogen, sulphur and chlorine coadsorption on Pd(111): a theoretical study of poisoning and promotion. *Surf. Sci.* **430**, 176-191 (1999).
- 23 Wilke, S. & Scheffler, M. Poisoning of Pd(100) for the dissociation of H₂: a theoretical study of co-adsorption of hydrogen and sulfur. *Surf. Sci.* **329**, L605-L610 (1995).

CHAPTER 5

Summary and future directions

5.1 Summary

The work performed for this thesis has demonstrated that self-assembled monolayers are a convenient and versatile approach for tailoring the types of exposed active sites on metal particles for applications in heterogeneous catalysis. The following points have been demonstrated for alkanethiolate-modified palladium catalysts.

1) The structure of the tail moiety could be tuned to control the types of active sites that were exposed on particle surfaces¹. By varying the steric bulkiness of the tail moiety, the density of the monolayer and, consequently, the number of contiguous active sites on particle terraces could be controlled. Increasing thiolate density restricted the ability for reactants occupy a large number of adjacent active sites on the particle surface. Active sites at particle edges could either be left exposed by using a simple alkanethiol modifier like 1-octadecanethiol (C18) or could be restricted by using a dithiol like 1,2-benzene dithiol (BDT) with significantly higher sulfur coverage. This modification technique offered a viable alternative to the more traditional (but synthetically-intensive) approach of changing particle size in order to probe structure/reactivity relationships.

2) Catalyst performance could be directed by selectively exposing specific active sites. This effect was apparent even for small reactant molecules with limited functionality like

ethylene, epoxybutane, and propionaldehyde; the effect of site availability on reactivity depended strongly on molecule structure indicating important differences in the site requirements for conversion of these molecules. For molecules containing a higher degree of functionality, this approach could be used to control selectivity when conversion of particular functional groups had different site requirements. This was demonstrated for the conversion of furfural which could either decarbonylate to produce furan and CO or could undergo a series of hydrogenation reactions to produce furfuryl alcohol and methylfuran². Increasing thiolate density served to restrict the decarbonylation pathway resulting in a dramatic improvement in selectivity toward the hydrogenation pathway from ~5% (unmodified) to > 90% (C18-modified).

3) Performing careful kinetic studies provided key insight into the effects of catalyst modification on the energetics and reactivity of furfural. Comparison between site availability and reactivity suggested that decarbonylation occurred primarily on terrace sites, while hydrodeoxygenation occurred primarily on particle steps and edges. Aldehyde hydrogenation, and its reverse process of alcohol dehydrogenation, was found to occur on both terrace and edge sites, with the dominant pathway dependent on surface coverage. Measurements of apparent activation energies and reaction orders indicated that in addition to changing the availability of specific sites, thiol monolayers strongly affected reaction energetics, and decreased the coverage of strongly adsorbed furfural-derived intermediates under reaction conditions. This careful and comprehensive kinetic treatment helped to elucidate both the major and more subtle effects due to the presence of the modifiers on this complex reaction system.

5.2 Future directions

Particle-size studies

As mentioned in Chapter 1, the more traditional approach for determining relationships between structure and reactivity involves systematically changing particle size. For cubo-octahedral shaped particles greater than ~ 10 nm in diameter, only a minor fraction of the surface atoms reside at particle edges and steps³. However, as the size of the particle decreases below this size, the fraction of sites located at corners and edges becomes significant. Figure 5-1 illustrates the relative distribution of the adsorption sites for an idealized cubo-octahedron Pd particle as a function of particle diameter from reference 3.

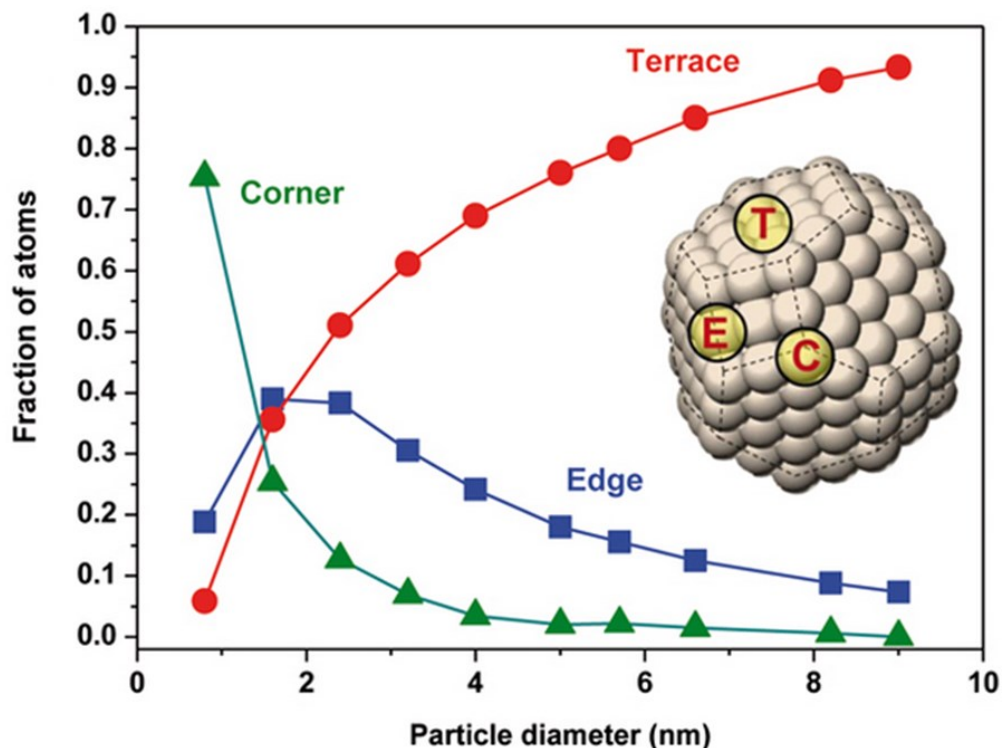


Figure 5-1. The relative distribution of the adsorption sites for an idealized cubo-octahedron Pd particle as a function of particle diameter. Figure adapted from reference 3.

While particle size and shape can be difficult to control since subtle changes in preparation conditions can result in materials with widely varying properties, careful characterization including particle imaging, CO chemisorption, and CO DRIFT spectroscopy can be performed to thoroughly characterize synthesized particles. Having a range of particle sizes would aid in the pursuit to more quantitatively describe particle structure/reactivity relationships. While we present strong evidence that the presence of the SAM serves primarily to block specific active sites, these findings should be corroborated with reactions performed on particles with well characterized size and, if possible, structure.

Determining ensemble size requirements

In addition to particle size experiments, it would be beneficial to develop a comprehensive approach aimed at quantitatively determining ensemble size requirements for the adsorption of reactant molecules. We have demonstrated that on a densely packed C18-modified catalyst, the flat-lying conformation of furfural was inhibited as evidenced by the reduction of nearly three orders of magnitude in decarbonylation rate as compared to the uncoated catalyst. Conversely, similar decarbonylation reactivity between AT-modified and the unmodified catalyst suggested that the spacing between adjacent AT molecules was sufficient to allow adsorption of the flat-lying species. This result suggests that the spacing of the monolayer could potentially be used to determine ensemble requirements for particular adsorption geometries.

Willey et al. has investigated the formation of SAMs formed from increasingly bulky diamondoid thiolates which are shown together in Figure 5-2⁴. Monolayers formed with these kinds of thiolates would be expected to have only minor, incremental differences in spacing on the metal and would be optimal for determining ensemble requirements where a sudden change

in reactivity with decreasing thiolate density would indicate at which spacing the ensemble requirement was no longer met. While the work discussed in this thesis demonstrated the potential for this approach, this extension could potentially allow for a more quantitative description of the site requirements necessary for different reaction pathways.

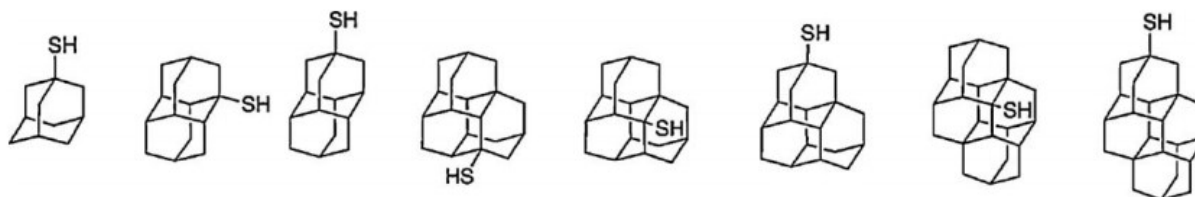


Figure 5-2. Additional caged modifiers that could potentially be used to control modifier density. Image adapted from reference 4.

Investigating adsorbate orientation on modified and unmodified Pd

It would be advantageous to relate ensemble size requirements with particular adsorption geometries; this relationship could potentially be probed using polarization modulation reflection adsorption infrared spectroscopy (PM-RAIRS). This infrared spectroscopy technique is generally used to study the air-liquid or air-solid interface and has the advantage that it is surface sensitive and can potentially provide structural/organization information about adsorbates on flat, reflective surfaces like palladium.

One of the unique features of this technique involves the use of polarized radiation which is described by specifying the orientation of the wave's electric field. One component of radiation is polarized parallel with respect to the plane of incidence and is referred to as p-polarized radiation. The other is polarized perpendicular to the plane of incidence, and is actually parallel to the surface, and so is called s-polarized radiation. The phase change of

radiation reflected from a metal depends both upon the angle of incidence and the state of polarization. At virtually all angles of incidence, s- polarized radiation undergoes a phase change of $\sim 180^\circ$. Thus, the electric field vectors, which are in opposite directions at the surface, approximately sum to zero yielding no net electric field. At grazing incidence, p- polarized radiation undergoes a phase shift of about 90° which leads to a nonzero electric field component at the surface oriented along the surface normal. The maximum absorption for p-polarized radiation occurs when theta is $\sim 88^\circ$, and therefore RAIRS is generally conducted near or at this angle. This design has the consequence that 1) only the parallel component of the incident radiation will be absorbed, and 2) the dipole transition moment of the surface species must have a component that is perpendicular to the substrate in order to absorb incident radiation. These features aid in the ability to probe adsorbate orientation on the surface. A schematic of this technique is shown in Figure 5-3⁵.

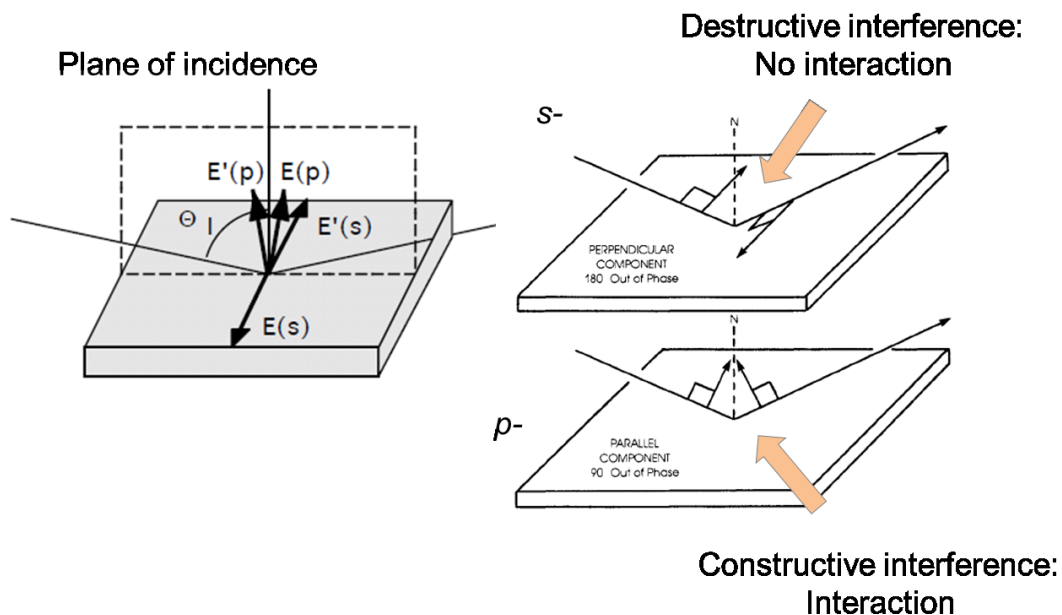


Figure 5-3. Schematic of RAIRS setup. S- polarized radiation is oriented perpendicular to the plane of incidence whereas p- polarized radiation is oriented parallel to this plane. Figure adapted from reference 5.

With the current experimental setup (Thermo Fisher Scientific tabletop optical module (TOM) mainframe equipped with a liquid N₂ cooled MCT-detector), general characterization of monolayer composition can easily be obtained. However, in order to determine information about adsorbates from the gas phase, an enclosed gas-tight dosing cell is required. A prototype for this cell was designed and built and is shown in Figure 5-4.

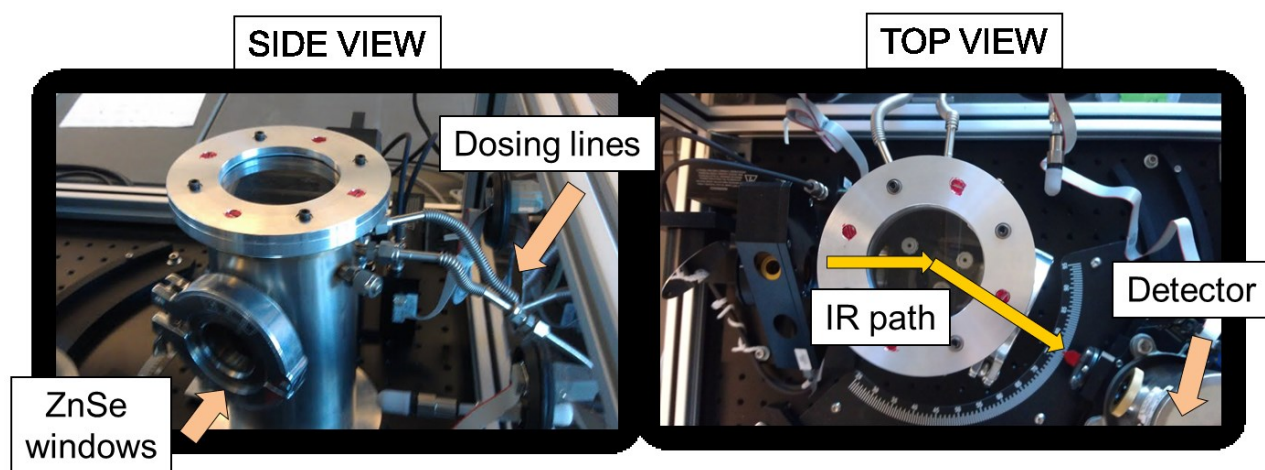


Figure 5-4. Dosing system built for RAIRS.

In its current state, this setup allows gases to be dosed into the system and is compatible with the existing IR equipment. Further optimization is required, however, in order to observe the low coverage of adsorbates (in some cases sub-monolayer) actually bound to the surfaces. With the addition of this equipment, insight into adsorbate orientation and concentration could potentially be probed on different modified catalyst surfaces.

5.3 References

- 1 Schoenbaum, C. A., Schwartz, D. K. & Medlin, J. W. Controlling surface crowding on a Pd catalyst with thiolate self-assembled monolayers. *J Catal* **303**, 92-99 (2013).
- 2 Pang, S. H., Schoenbaum, C. A., Schwartz, D. K. & Medlin, J. W. Directing reaction pathways by catalyst active-site selection using self- assembled monolayers. *Nat Commun* **4** (2013).
- 3 Piumetti, M., Freyria, F. S. & Bonelli, B. Catalytically active sites and their complexity: a micro-review. *Chim Oggi* **31**, 55-58 (2013).
- 4 Willey, T. M. *et al.* Near-edge X-ray absorption fine structure spectroscopy of diamondoid thiol monolayers on gold. *J Am Chem Soc* **130**, 10536-10544 (2008).
- 5 Golden, W. G., Ferraro & Basile, L. J. in *Fourier Transform Infrared Spectroscopy* Vol. 4 315–344 (Academic Press, New York, 1985).

BIBLIOGRAPHY

Abbott, N. L., Gorman, C. B. & Whitesides, G. M. Active control of wetting using applied electrical potentials and self-assembled monolayers. *Langmuir* **11**, 16-18 (1995).

Albers, P., Pietsch, J. & Parker, S. F. Poisoning and deactivation of palladium catalysts. *J Mol Catal a-Chem* **173**, 275-286 (2001).

Allen, G. & Bernstein, H. J. Internal rotation: VIII. The infrared and raman spectra of furfural. *Can. J. Chem.* **33**, 1055-1061 (1955).

An, K. & Somorjai, G. A. Size and shape control of metal nanoparticles for reaction selectivity in catalysis. *ChemCatChem* **4**, 1512-1524 (2012).

Anderson, R. B., Karn, F. S. & Shultz, J. F. Factors in Sulfur Poisoning of Iron Catalysts in Fischer-Tropsch Synthesis. *J Catal* **4**, 56-& (1965).

Ashcroft, A. T., Cheetham, A. K., Green, M. L. H. & Vernon, P. D. F. Partial Oxidation of Methane to Synthesis Gas-Using Carbon-Dioxide. *Nature* **352**, 225-226 (1991).

Bain, C. D., Biebuyck, H. A. & Whitesides, G. M. Comparison of self-assembled monolayers on gold: coadsorption of thiols and disulfides. *Langmuir* **5**, 723-727 (1989).

Barbier, J., Corro, G., Zhang, Y., Bournonville, J. P. & Franck, J. P. Coke Formation on Platinum-Alumina Catalyst of Wide Varying Dispersion. *Appl Catal* **13**, 245-255 (1985).

Barias, O. A., Holmen, A. & Blekkan, E. A. Propane dehydrogenation over supported Pt and Pt-Sn catalysts: Catalyst preparation, characterization, and activity measurements. *J. Catal.* **158**, 1-12 (1996).

Batchelder, D. N., Evans, S. D., Freeman, T. L., Haussling, L., Ringsdorf, H., Wolf, H. Self-assembled monolayers containing polydiacetylenes. *J. Amer. Chem. Soc.* **116**, 1050-1053 (1994).

Berner, S. *et al.* Activity boost of a biomimetic oxidation catalyst by immobilization onto a gold surface. *J. Catal.* **244**, 86-91 (2006).

Bhattacharjee, S., Dotzauer, D. M. & Bruening, M. L. Selectivity as a function of nanoparticle size in the catalytic hydrogenation of unsaturated alcohols. *J. Am. Chem. Soc.* **131**, 3601-3610 (2009).

Bond, G. C. *Metal-Catalysed Reactions of Hydrocarbons*. (Springer Science+Business Media, Inc., 2005).

- Bond, G. C. Small Particles of the Platinum Metals. *Platinum Metals Review* **19**, 126-134 (1975).
- Bradley, M. K., Robinson, J. & Woodruff, D. P. The structure and bonding of furan on Pd(111). *Surf. Sci.* **604**, 920-925 (2010).
- Brands, D. S., U-A-Sai, G., Poels, E. K. & Blik, A. Sulfur deactivation of fatty ester hydrogenolysis catalysts. *J Catal* **186**, 169-180 (1999).
- Brandt, R. K., Sorbello, R. S., & Greenler, R. G. Site-specific, coupled-harmonic-oscillator model of carbon monoxide adsorbed on extended, single-crystal surfaces and on small crystals of platinum. *Surf. Sci.* **271**, 605-615 (1992).
- Burke, M. L. & Madix, R. J. Hydrogen on Pd(100)-S - the Effect of Sulfur on Precursor Mediated Adsorption and Desorption. *Surf Sci* **237**, 1-19 (1990).
- Burkholder, L., Stacchiola, D. & Tysse, W. T. Kinetic and reactive properties of ethylene on clean and hydrogen-covered Pd(111). *Surface Review and Letters* **10**, 909-916 (2003).
- Camillone, N., Chidsey, C. E. D., Liu, G. & Scoles, G. Substrate Dependence of the Surface-Structure and Chain Packing of Docosyl Mercaptan Self-Assembled on the (111), (110), and (100) Faces of Single-Crystal Gold. *J Chem Phys* **98**, 4234-4245 (1993).
- Camillone, N., Chidsey, C. E. D., Liu, G. Y., Putvinski, T. M. & Scoles, G. Surface-Structure and Thermal Motion of Normal-Alkane Thiols Self-Assembled on Au(111) Studied by Low-Energy Helium Diffraction. *J Chem Phys* **94**, 8493-8502 (1991).
- Campbell, C. T. & Paffett, M. T. The Role of Chlorine Promoters in Catalytic Ethylene Epoxidation over the Ag(110) Surface. *Appl Surf Sci* **19**, 28-42 (1984).
- Campbell, C. T. Chlorine Promoters in Selective Ethylene Epoxidation over Ag(111) - a Comparison with Ag(110). *J Catal* **99**, 28-38 (1986).
- Cargnello, M. *et al.* A Versatile Approach to the Synthesis of Functionalized Thiol-Protected Palladium Nanoparticles. *Chem. Mat.* **23**, 3961-3969 (2011).
- Castner, D. G., Hinds, K. & Grainger, D. W. X-ray photoelectron spectroscopy sulfur 2p study of organic thiol and disulfide binding interactions with gold surfaces. *Langmuir* **12**, 5083-5086 (1996).
- Chen, G. *et al.* Kinetically controlled synthesis of nickel tetrahedron nanocrystals for high performance catalytic hydrogenation. *RSC Adv.* **3**, 5314-5317 (2013).
- Chiu, M. E., Watson, D. J., Kyriakou, G., Tikhov, M. S. & Lambert, R. M. Tilt the molecule and change the chemistry: Mechanism of S-promoted chemoselective catalytic hydrogenation of crotonaldehyde on Cu(111). *Angew Chem Int Edit* **45**, 7530-7534 (2006).
- Conrad, H., Ertl, G., Koch, J. & Latta, E. E. Adsorption of Co on Pd Single-Crystal Surfaces. *Surf Sci* **43**, 462-480 (1974).

- Cooper, B. H. & Donnis, B. B. L. Aromatic saturation of distillates: An overview. *Appl Catal a-Gen* **137**, 203-223 (1996).
- Cremer, P. S., Su, X. C., Shen, Y. R. & Somorjai, G. A. Ethylene hydrogenation on Pt(111) monitored in situ at high pressures using sum frequency generation. *J Am Chem Soc* **118**, 2942-2949 (1996).
- Crespo-Quesada, M., Yarulin, A., Jin, M., Xia, Y. & Kiwi-Minsker, L. Structure sensitivity of alkynol hydrogenation on shape- and size-controlled palladium nanocrystals: Which sites are most active and selective? *J. Am. Chem. Soc.* **133**, 12787-12794 (2011).
- Crooks, R. M. & Ricco, A. J. New organic materials suitable for use in chemical sensor arrays. *Acc. Chem. Res.* **31**, 219-227, (1998).
- Dameron, A. A., Charles, L. F. & Weiss, P. S. Structures and displacement of 1-adamantanethiol self-assembled monolayers on Au{111}. *J Am Chem Soc* **127**, 8697-8704 (2005).
- Demicheli, M. C., Duprez, D., Barbier, J., Ferretti, O. A. & Ponzi, E. N. Deactivation of Steam-Reforming Model Catalysts by Coke Formation .2. Promotion with Potassium and Effect of Water. *J. Catal.* **145**, 437-449 (1994).
- Dubois, L. H., Zegarski, B. R. & Nuzzo, R. G. Molecular Ordering of Organosulfur Compounds on Au(111) and Au(100) - Adsorption from Solution and in Ultrahigh-Vacuum. *J Chem Phys* **98**, 678-688 (1993).
- Duprez, D. *et al.* Deactivation of Steam-Reforming Model Catalysts by Coke Formation .1. Kinetics of the Formation of Filamentous Carbon in the Hydrogenolysis of Cyclopentane on Ni/Al₂O₃ Catalysts. *J. Catal.* **124**, 324-335 (1990).
- Ederth, T. *et al.* Resistance of galactoside-terminated alkanethiol self-assembled monolayers to marine fouling organisms. *ACS Appl. Mater. Interfaces* **3**, 3890-3901 (2011).
- Edsger, P. C. *et al.* Bottom-up organic integrated circuits. *Nature* **455**, 956-959 (2008).
- Feibelman, P. J. & Hamann, D. R. Modification of Transition-Metal Electronic-Structure by P, S, Cl, and Li Adatoms. *Surf Sci* **149**, 48-66 (1985).
- Feng, B. *et al.* Functionalized Poly(ethylene glycol)-Stabilized Water-Soluble Palladium Nanoparticles: Property/Activity Relationship for the Aerobic Alcohol Oxidation in Water. *Langmuir* **26**, 2505-2513 (2010).
- Fernandes, A. *et al.* Increased Catalytic Activity of Surface-Immobilized Palladium Complexes in the Fluorogenic Deprotection of an Alloc-Derivatized Coumarin. *Chem.-Eur. J.* **18**, 788-792 (2012).
- Figoli, N. S., Largentiere, P. C., Arcoya, A. & Seoane, X. L. Modification of the Properties and Sulfur Resistance of a Pd/SiO₂ Catalyst by La Addition. *J Catal* **155**, 95-105 (1995).

- Flores-Camacho, J. M. *et al.* Adsorption energetics of CO on supported Pd nanoparticles as a function of particle size by single crystal microcalorimetry. *Phys Chem Chem Phys* **13**, 16800-16810 (2011).
- Frank, E. R. & Hamers, R. J. Chlorine-induced restructuring of Ag(111) films observed by scanning tunneling microscopy. *J Catal* **172**, 406-413 (1997).
- Freund, H. J., Libuda, J., Baumer, M., Risse, T. & Carlsson, A. Cluster, facets, and edges: Site-dependent selective chemistry on model catalysts. *Chem Rec* **3**, 181-200 (2003).
- Gan, L. Y. & Zhao, Y. J. Charge effect in S enhanced CO adsorption: A theoretical study of CO on Au, Ag, Cu, and Pd (111) surfaces coadsorbed with S, O, Cl, and Na. *J Chem Phys* **133** (2010).
- Garcia-Mota, M. *et al.* A density functional theory study of the 'mythic' Lindlar hydrogenation catalyst. *Theor Chem Acc* **128**, 663-673 (2011).
- Gavia, D. J. & Shon, Y.-S. Controlling surface ligand density and core size of alkanethiolate capped Pd nanoparticles and their effects on catalysis. *Langmuir* **28**, 14502-14508 (2012).
- Golden, W. G., Ferraro & Basile, L. J. in *Fourier Transform Infrared Spectroscopy* Vol. 4 315–344 (Academic Press, New York, 1985)
- Gravil, P. A. & Toulhoat, H. Ethylene, sulphur, and chlorine coadsorption on Pd(111): a theoretical study of poisoning and promotion. *Surf Sci* **430**, 192-198 (1999).
- Gravil, P. A. & Toulhoat, H. Hydrogen, sulphur and chlorine coadsorption on Pd(111): a theoretical study of poisoning and promotion. *Surf Sci* **430**, 176-191 (1999).
- Gross, E. *et al.* Asymmetric Catalysis at the Mesoscale: Gold Nanoclusters Embedded in Chiral Self-Assembled Monolayer as Heterogeneous Catalyst for Asymmetric Reactions. *J. Am. Chem. Soc.* **135**, 3881-3886 (2013).
- Hammaker, R. M., Francis, S. A. & Eischens, R. P. Infrared Study of Intermolecular Interactions for Carbon Monoxide Chemisorbed on Platinum. *Spectrochim Acta* **21**, 1295-& (1965).
- Hara, K. *et al.* Self-assembled monolayers of compact phosphanes with alkanethiolate pendant groups: Remarkable reusability and substrate selectivity in Rh catalysis. *Angew. Chem.-Int. Edit.* **47**, 5627-5630 (2008).
- He, B. L., Ha, Y., Liu, H. F., Wang, K. M. & Liew, K. Y. Size control synthesis of polymer-stabilized water-soluble platinum oxide nanoparticles. *J Colloid Interf Sci* **308**, 105-111 (2007).
- Hirai, H. & Yakura, N. Protecting polymers in suspension of metal nanoparticles. *Polym Advan Technol* **12**, 724-733 (2001).

Horiuchi, C. M. & Medlin, J. W. Adsorption and reactivity of 2,3-dihydrofuran and 2,5-dihydrofuran on Pd(111): Influence of the C=C position on the reactivity of cyclic ethers. *Langmuir* **26**, 13320-13332 (2010).

Hostetler, M. J. *et al.* Alkanethiolate gold cluster molecules with core diameters from 1.5 to 5.2 nm: Core and monolayer properties as a function of core size. *Langmuir* **14**, 17-30 (1998).

Hostetler, M. J., Stokes, J. J. & Murray, R. W. Infrared spectroscopy of three-dimensional self-assembled monolayers: N-alkanethiolate monolayers on gold cluster compounds. *Langmuir* **12**, 3604-3612 (1996).

Hutchings, G. J. Promotion in heterogeneous catalysis: a topic requiring a new approach? *Catal Lett* **75**, 1-12 (2001).

Hutchings, G. J., King, F., Okoye, I. P. & Rochester, C. H. Influence of Sulfur Poisoning of Copper Alumina Catalyst on the Selective Hydrogenation of Crotonaldehyde. *Appl. Catal. A-Gen.* **83**, L7-L13 (1992).

Hutchings, G. J., King, F., Okoye, I. P., Padley, M. B. & Rochester, C. H. Selectivity Enhancement in the Hydrogenation of Alpha,Beta-Unsaturated Aldehydes and Ketones Using Thiophene-Modified Catalysts. *J. Catal.* **148**, 453-463 (1994).

Jiang, Y. *et al.* Modifying the Atomic and Electronic Structures of Gold Nanocrystals via Changing the Chain Length of n-Alkanethiol Ligands. *J. Phys. Chem. C* **116**, 24999-25003 (2012).

Joyner, R. W. & Santen, R. A. *Elementary Reaction Steps in Heterogeneous Catalysis*. (Kluwer Academic Publishers, 1993).

Kahsar, K. R., Schwartz, D. K. & Medlin, J. W. Control of Metal Catalyst Selectivity through Specific Noncovalent Molecular Interactions. *J. Am. Chem. Soc.* **136**, 520-526 (2014).

Kahsar, K. R., Schwartz, D. K. & Medlin, J. W. Liquid-and vapor-phase hydrogenation of 1-epoxy-3-butene using self-assembled monolayer coated palladium and platinum catalysts. *Appl. Catal. A-Gen.* **445**, 102-106 (2012).

Kahsar, K. R., Schwartz, D. K. & Medlin, J. W. Selective Hydrogenation of Polyunsaturated Fatty Acids Using Alkanethiol Self-Assembled Monolayer-Coated Pd/Al₂O₃ Catalysts. *ACS Catal.* **3**, 2041-2044 (2013).

Kanaoka, S. *et al.* Thermosensitive gold nanoclusters stabilized by well-defined vinyl ether star polymers: Reusable and durable catalysts for aerobic alcohol oxidation. *J Am Chem Soc* **129**, 12060-+ (2007).

Kershen, K., Celio, H., Lee, I. & White, J. M. Chlorine-modified properties of Ag(111) probed by C₂H₄, C₃H₆, C₃H₅Cl, and CO. *Langmuir* **17**, 323-328 (2001).

Kim, J.-H., Park, J.-S., Chung, H.-W., Boote, B. W. & Lee, T. R. Palladium nanoshells coated with self-assembled monolayers and their catalytic properties. *RSC Adv.* **2**, 3968-3977 (2012).

Kim, M. *et al.* Creating Favorable Geometries for Directing Organic Photoreactions in Alkanethiolate Monolayers. *Science* **331**, 1312-1315 (2011).

Kiskinova, M. & Goodman, D. W. Modification of Chemisorption Properties by Electronegative Adatoms - H₂ and Co on Chlorided, Sulfided, and Phosphided Ni(100). *Surf Sci* **108**, 64-76 (1981).

Kiskinova, M., Szabo, A. & Yates, J. T. Co Adsorption on Pt(111) Modified with Sulfur. *J Chem Phys* **89**, 7599-7608 (1988).

Kliwer, C. J. *et al.* Furan hydrogenation over Pt(111) and Pt(100) single-crystal surfaces and Pt nanoparticles from 1 to 7 nm: A kinetic and sum frequency generation vibrational spectroscopy study. *J. Am. Chem. Soc.* **132**, 13088-13095 (2010).

Kritzinger, J. A. The role of sulfur in commercial iron-based Fischer-Tropsch catalysis with focus on C₂-product selectivity and yield. *Catal. Today* **71**, 307-318 (2002).

Kwon, S. G. *et al.* Capping Ligands as Selectivity Switchers in Hydrogenation Reactions. *Nano Lett.* **12**, 5382-5388 (2012).

Laibinis, P. E., Bain, C. D. & Whitesides, G. M. Attenuation of photoelectrons in monolayers of n-alkanethiols adsorbed on copper, silver, and gold. *J. Phys. Chem.* **95**, 7017-7021 (1991).

Laibinis, P. E. *et al.* Comparison of the structures and wetting properties of self-assembled monolayers of normal-alkanethiols on the coinage metal-surfaces, Cu, Ag, Au. *J. Am. Chem. Soc.* **103**, 7152-7167 (1991).

Lear, T. *et al.* The application of infrared spectroscopy to probe the surface morphology of alumina-supported palladium catalysts. *J Chem Phys* **123** (2005).

Li, M. S. & Shen, J. Y. Microcalorimetric studies of O₂ and C₂H₄ adsorption on Pd/SiO₂ catalysts modified by Cu and Ag. *Thermochim Acta* **379**, 45-50 (2001).

Li, Y., Boone, E. & El-Sayed, M. A. Size effects of PVP-Pd nanoparticles on the catalytic Suzuki reactions in aqueous solution. *Langmuir* **18**, 4921-4925 (2002).

Li, Z. P. *et al.* Synthesis and Characterization of n-Alkylamine-Stabilized Palladium Nanoparticles for Electrochemical Oxidation of Methane. *J. Phys. Chem. C* **114**, 723-733 (2010).

Lindlar, H. *Ein Neuer Katalysator Fur Selektive Hydrierungen. *Helv Chim Acta* **35**, 446-456 (1952).

Loffreda, D., Delbecq, F., Vigne, F. & Sautet, P. Chemo-regioselectivity in heterogeneous catalysis: Competitive routes for C=O and C=C hydrogenations from a theoretical approach. *J Am Chem Soc* **128**, 1316-1323 (2006).

Love, J. C. *et al.* Formation and structure of self-assembled monolayers of alkanethiolates on palladium. *J Am Chem Soc* **125**, 2597-2609 (2003).

Love, J. C., Estroff, L. A., Kriebel, J. K., Nuzzo, R. G. & Whitesides, G. M. Self-assembled monolayers of thiolates on metals as a form of nanotechnology. *Chem. Rev.* **105**, 1103-1169 (2005).

Lu, C. H. & Chang, F. C. Polyhedral Oligomeric Silsesquioxane-Encapsulating Amorphous Palladium Nanoclusters as Catalysts for Heck Reactions. *ACS Catal.* **1**, 481-488 (2011).

Lu, F., Ruiz, J. & Astruc, D. Palladium-dodecanethiolate nanoparticles as stable and recyclable catalysts for the Suzuki-Miyaura reaction of aryl halides under ambient conditions. *Tetrahedron Lett.* **45**, 9443-9445 (2004).

Luedtke, W. D. & Landman, U. Structure and thermodynamics of self-assembled monolayers on gold nanocrystallites. *J Phys Chem B* **102**, 6566-6572 (1998).

Makosch, M. *et al.* Organic Thiol Modified Pt/TiO₂ Catalysts to Control Chemoselective Hydrogenation of Substituted Nitroarenes. *ACS Catal.* **2**, 2079-2081 (2012).

Mallat, T. & Baiker, A. Selectivity enhancement in heterogeneous catalysis induced by reaction modifiers. *Appl Catal a-Gen* **200**, 3-22 (2000).

Mallat, T., Orglmeister, E. & Baiker, A. Asymmetric catalysis at chiral metal surfaces. *Chem Rev* **107**, 4863-4890 (2007).

Marinelli, T. B. L. W. & Ponc, V. A Study on the selectivity in acrolein hydrogenation on platinum catalysts: A model for hydrogenations of α,β -unsaturated aldehydes. *J. Catal.* **156**, 51-59 (1995).

Marshall, S. T. & Medlin, J. W. Surface-level mechanistic studies of adsorbate-adsorbate interactions in heterogeneous catalysis by metals. *Surf. Sci. Rep.* **66**, 173-184 (2011).

Marshall, S. T. *et al.* Controlled selectivity for palladium catalysts using self-assembled monolayers. *Nat. Mater.* **9**, 853-858 (2010).

Marshall, S. T., Schwartz, D. K. & Medlin, J. W. Adsorption of Oxygenates on Alkanethiol-Functionalized Pd(111) Surfaces: Mechanistic Insights into the Role of Self-Assembled Monolayers on Catalysis. *Langmuir* **27**, 6731-6737 (2011).

Masel, R. I. *Chemical Kinetics and Catalysis*. 28 (John Wiley & Sons, Inc., 2001).

McEwen, A. B., Guttieri, M. J., Maier, W. F., Laine, R. M. & Shvo, Y. Metallic Palladium, the Actual Catalyst in Lindlar and Rosenmund Reductions. *J Org Chem* **48**, 4436-4438 (1983).

McGown, W. T., Kembal, C., Whan, D. A. & Scurrill, M. S. Hydrogenation of acetylene in excess ethylene on an alumina supported palladium catalyst in a static system. *J. Chem. Soc., Faraday Trans.* **73**, 632-647 (1977).

- McKenna, F. M. & Anderson, J. A. Selectivity enhancement in acetylene hydrogenation over diphenyl sulphide-modified Pd/TiO₂ catalysts. *J. Catal.* **281**, 231-240 (2011).
- Medlin, J. W. Understanding and Controlling Reactivity of Unsaturated Oxygenates and Polyols on Metal Catalysts. *Acs Catal* **1**, 1284-1297 (2011).
- Meisenheimer, R. G. & Wilson, J. N. Interaction of Oxygen and of Ethylene Dichloride with Silver Surfaces. *J Catal* **1**, 151-155 (1962).
- Michel, C. & Auneau, F.; Delbecq, F.; Sautet, P. C-H versus O-H bond dissociation for alcohols on a Rh(111) surface: a strong assistance from hydrogen bonded neighbors. *ACS Catal.* **1**, 1430-1440 (2011).
- Mojet, B. L., Ebbesen, S. D. & Lefferts, L. Light at the interface: the potential of attenuated total reflection infrared spectroscopy for understanding heterogeneous catalysis in water. *Chem Soc Rev* **39**, 4643-4655 (2010).
- Monnier, J. R., Medlin, J. W. and Kuo, Y.-J. Selective isomerization of 2,5-dihydrofuran to 2,3-dihydrofuran using CO-modified, supported Pd catalysts. *Appl. Catal., A.* **194-195**, 463-474 (2000).
- Monnier, J. R., Stavinoha, J. L. & Hartley, G. W. Effects of chlorine and chlorine dynamics during silver-catalyzed epoxidation of butadiene. *J Catal* **226**, 321-333 (2004).
- Moreno, M., Ibanez, F. J., Jasinski, J. B. & Zamborini, F. P. Hydrogen Reactivity of Palladium Nanoparticles Coated with Mixed Monolayers of Alkyl Thiols and Alkyl Amines for Sensing and Catalysis Applications. *J. Am. Chem. Soc.* **133**, 4389-4397 (2011).
- Morin, C., Simon, D. & Sautet, P. Intermediates in the hydrogenation of benzene to cyclohexene on Pt(111) and Pd(111): A comparison from DFT calculations. *Surf. Sci.* **600**, 1339-1350 (2006).
- Neurock, M., Pallassana, V. & van Santen, R. A. The importance of transient states at higher coverages in catalytic reactions. *J Am Chem Soc* **122**, 1150-1153 (2000).
- Nigra, M. M., Arslan, I. & Katz, A. Gold nanoparticle-catalyzed reduction in a model system: Quantitative determination of reactive heterogeneity of a supported nanoparticle surface. *J. Catal.* **295**, 115-121 (2012).
- Niu, Y. H. & Crooks, R. M. Dendrimer-encapsulated metal nanoparticles and their applications to catalysis. *Cr Chim* **6**, 1049-1059 (2003).
- Nørskov, J. K., Bligaard, T., Hvolbæk, B., Abild-Pedersen, F., Chorkendorff, I. & Christensen, C. H. The nature of the active site in heterogeneous metal catalysis. *Chem. Soc. Rev.* **37**, 2163-2171 (2008).
- Palczewska, W., Jablonski, A., Kaszukur, Z., Zuba, G. & Wernisch, J. Study on Lead Additives in Modified Palladium Catalysts. *J Mol Catal* **25**, 307-316 (1984).

- Paluti, C. C. & Gawalt, E. S. Immobilized aza-bis(oxazoline) copper catalysts on alkanethiol self-assembled monolayers on gold: Selectivity dependence on surface electronic environments. *J. Catal.* **275**, 149-157 (2010).
- Pang, S. H. & Medlin, J. W. Adsorption and reaction of furfural and furfuryl alcohol on Pd(111): Unique reaction pathways for multifunctional reagents. *ACS Catal.* **1**, 1272-1283 (2011).
- Pang, S. H., Román, A. M. & Medlin, J.W. Adsorption orientation-induced selectivity control of reactions of benzyl alcohol on Pd(111). *J. Phys. Chem. C* **116**, 13654-13660 (2012).
- Pang, S. H., Schoenbaum, C. A., Schwartz, D. K. & Medlin, J. W. Directing reaction pathways by catalyst active-site selection using self-assembled monolayers. *Nat. Commun.* **4**, 2448 (2013).
- Passos, F. B., Aranda, D. A. G. & Schmal, M. Characterization and catalytic activity of bimetallic Pt-In/Al₂O₃ and Pt-Sn/Al₂O₃ catalysts. *J Catal* **178**, 478-488 (1998).
- Passos, F. B., Schmal, M. & Vannice, M. A. Effect of In and Sn on the adsorption behavior and hydrogenolysis activity of Pt/Al₂O₃ catalysts. *J Catal* **160**, 106-117 (1996).
- Piumetti, M., Freyria, F. S. & Bonelli, B. Catalytically active sites and their complexity: a micro-review. *Chim Oggi* **31**, 55-58 (2013).
- Poirier, G. E. & Tarlov, M. J. The C(4x2) Superlattice of N-Alkanethiol Monolayers Self-Assembled on Au(111). *Langmuir* **10**, 2853-2856 (1994).
- Poirier, G. E. Mechanism of formation of Au vacancy islands in alkanethiol monolayers on Au(111). *Langmuir* **13**, 2019-2026 (1997).
- Ponec, V. & Bond, G. C., *Catalysis by Metals and Alloys*, Elsevier: Amsterdam (1995).
- Recognizing the best in innovation: Breakthrough Catalyst. *R&D Magazine* (2005).
- Saavedra, H. M., Barbu, C. M., Dameron, A. A., Mullen, T. J., Crespi, V. H. & Weiss, P. S., 1-adamantanethiolate monolayer displacement kinetics follow a universal form. *J. Am. Chem. Soc.* **129**, 10741-10746 (2007).
- Sadeghmoghaddam, E., Gaieb, K. & Shon, Y. S. Catalytic isomerization of allyl alcohols to carbonyl compounds using poisoned Pd nanoparticles. *Appl. Catal. A-Gen.* **405**, 137-141 (2011).
- Sadeghmoghaddam, E., Gu, H. M. & Shon, Y. S. Pd Nanoparticle-Catalyzed Isomerization vs Hydrogenation of Allyl Alcohol: Solvent-Dependent Regioselectivity. *ACS Catal.* **2**, 1838-1845 (2012).
- Sadeghmoghaddam, E., Lam, C., Choi, D. & Shon, Y. S. Synthesis and catalytic properties of alkanethiolate-capped Pd nanoparticles generated from sodium S-dodecylthiosulfate. *J Mater Chem* **21**, 307-312 (2011).

Schauermaun, S. *et al.* Catalytic activity and poisoning of specific sites on supported metal nanoparticles. *Angew Chem Int Edit* **41**, 2532-+ (2002).

Schoenbaum, C. A., Schwartz, D. K. & Medlin, J. W. Controlling surface crowding on a Pd catalyst with thiolate self-assembled monolayers. *J Catal* **303**, 92-99 (2013).

Schoenbaum, C. A., Schwartz, D. K. & Medlin, J. W. Controlling the Surface Environment of Heterogeneous Catalysts using Self-Assembled Monolayers. *Acc. Chem. Res.* **47**, 1438-1445, (2014).

Schonenberger, C., Jorritsma, J., Sondaghuethorst, J. A. M. & Fokkink, L. G. J. Domain-Structure of Self-Assembled Alkanethiol Monolayers on Gold. *J Phys Chem-US* **99**, 3259-3271 (1995).

Schwartz, D. K. Mechanisms and kinetics of self-assembled monolayer formation. *Annu Rev Phys Chem* **52**, 107-137 (2001).

Schwarz, J. A. & Kelemen, S. R. Adsorption - Desorption-Kinetics of Co from Clean and Sulfur Covered Ru(001). *Surf Sci* **87**, 510-524 (1979).

Sellers, H., Ulman, A., Shnidman, Y. & Eilers, J. E. Structure and binding of alkanethiolates on gold and silver surfaces - implications for self-assembled monolayers. *J. Am. Chem. Soc.* **115**, 9389-9401 (1993).

Serrano-Ruiz, J. C., West, R. M. & Dumesic, J. A. Catalytic conversion of renewable biomass resources to fuels and chemicals. *Annu. Rev. Chem. Biomol. Eng.* **1**, 79-100 (2010).

Shirley, D. High-resolution X-ray photoemission spectrum of the valence bands of gold. *Phys. Rev. B* **5**, 4709-4714 (1972).

Simons, K. E. *et al.* A Model for the Enantioselective Hydrogenation of Pyruvate Catalyzed by Alkaloid-Modified Platinum. *Recl Trav Chim Pay B* **113**, 465-474 (1994).

Sitthisa, S. & Resasco, D. E. Hydrodeoxygenation of furfural over supported metal catalysts: A comparative study of Cu, Pd and Ni. *Catal. Lett.* **141**, 784-791 (2011).

Sitthisa, S. *et al.* Conversion of furfural and 2-methylpentanal on Pd/SiO₂ and PdCu/SiO₂ catalysts. *J. Catal.* **280**, 17-27 (2011).

Sitthisa, S., An, W. & Resasco, D. E. Selective conversion of furfural to methylfuran over silica-supported NiFe bimetallic catalysts. *J. Catal.* **284**, 90-101 (2011).

Somorjai, G. A. & Kliewer, C. J. Reaction selectivity in heterogeneous catalysis. *React Kinet Catal L* **96**, 191-208 (2009).

Strong, L. & Whitesides, G. M. Structures of Self-Assembled Monolayer Films of Organosulfur Compounds Adsorbed on Gold Single-Crystals - Electron-Diffraction Studies. *Langmuir* **4**, 546-558 (1988).

Studer, M., Blaser, H. U. & Exner, C. Enantioselective hydrogenation using heterogeneous modified catalysts: An update. *Adv Synth Catal* **345**, 45-65 (2003).

Sun, L. & Crooks, R. M. Indirect Visualization of Defect Structures Contained within Self-Assembled Organomeraptan Monolayers - Combined Use of Electrochemistry and Scanning-Tunneling-Microscopy. *Langmuir* **9**, 1951-1954 (1993).

Taguchi, T., Isozaki, K. & Miki, K. Enhanced Catalytic Activity of Self-Assembled-Monolayer-Capped Gold Nanoparticles. *Adv. Mater.* **24**, 6462-6467 (2012).

Tenney, S. A., Lu, D., He, F., Levy, N., Perera, U. G. E., Starr, D. E., Müller, K., Bluhm, H. & Sutter, P. submitted for publication.

Tiwari, P. M., Vig, K., Dennis, V. A. & Singh, S. R. Functionalized gold nanoparticles and their biomedical applications. *Nanomaterials*. **1**, 31-63 (2011).

Unterhalt, H., Galletto, P., Morkel, M., Rupprechter, G. & Freund, H. J. Sum frequency generation study of CO adsorption on palladium model catalysts. *Phys Status Solidi A* **188**, 1495-1503 (2001).

van Druten, G. M. R. & Ponc, V. Hydrogenation of carbonylic compounds Part I: Competitive hydrogenation of propanal and acetone over noble metal catalysts. *Appl Catal a-Gen* **191**, 153-162 (2000).

Vogtle, F., Gestermann, S., Hesse, R., Schwierz, H. & Windisch, B. Functional dendrimers. *Prog Polym Sci* **25**, 987-1041 (2000).

von Arx, M., Wahl, M., Jung, T. A. & Baiker, A. Adsorption and surface mobility of cinchonidine on Pt(111) studied by STM. *Phys Chem Chem Phys* **7**, 273-277 (2005).

Vorotnikov, V. & Mpourmpakis, G.; Vlachos, D. G. DFT study of furfural conversion to furan, furfuryl alcohol, and 2-methylfuran on Pd(111). *ACS Catal.* **2**, 2496-2504 (2012).

Werpy, T. & Petersen, G. "Top Value Added Chemicals from Biomass: Volume 1 – Results of Screening for Potential Candidates from Sugars and Synthesis Gas." U.S. Department of Energy (2004).

Wilke, S. & Scheffler, M. Poisoning of Pd(100) for the dissociation of H₂: a theoretical study of co-adsorption of hydrogen and sulfur. *Surf. Sci.* **329**, L605-L610 (1995).

Wood, J., Alldrick, M. J., Winterbottom, J. M., Stitt, E. H. & Bailey, S. Diffuse reflectance infrared Fourier transform spectroscopy (DRIFTS) study of ethyne hydrogenation on Pd/Al₂O₃. *Catal. Today* **128**, 52-62 (2007).

- Willey, T. M. *et al.* Near-edge X-ray absorption fine structure spectroscopy of diamondoid thiol monolayers on gold. *J Am Chem Soc* **130**, 10536-10544 (2008).
- Wu, B. H., Huang, H. Q., Yang, J., Zheng, N. F. & Fu, G. Selective Hydrogenation of alpha,beta-Unsaturated Aldehydes Catalyzed by Amine-Capped Platinum-Cobalt Nanocrystals. *Angew. Chem.-Int. Edit.* **51**, 3440-3443 (2012).
- Xian, J. Y., Hua, Q., Jiang, Z. Q., Ma, Y. S. & Huang, W. X. Size-Dependent Interaction of the Poly(N-vinyl-2-pyrrolidone) Capping Ligand with Pd Nanocrystals. *Langmuir* **28**, 6736-6741 (2012).
- Xu, Y. Decomposition of furan on Pd(111). *Top. Catal.* **55**, 290-299 (2012).
- Yang, G. H. & Liu, G. Y. New insights for self-assembled monolayers of organothiols on Au(111) revealed by scanning tunneling microscopy. *J Phys Chem B* **107**, 8746-8759 (2003).
- Yang, Y.-C., Lee, Y.-L., Yang, L.-Y. O. & Yau, S.-L. In situ scanning tunneling microscopy of 1,6-hexanedithiol, 1,9-nonanedithiol, 1,2-benzenedithiol, and 1,3-benzenedithiol adsorbed on Pt(111) electrodes. *Langmuir* **22**, 5189-5195 (2006).
- Yeo, Y. Y., Vattuone, L. & King, D. A. Calorimetric investigation of NO and CO adsorption on Pd{100} and the influence of preadsorbed carbon. *J Chem Phys* **106**, 1990-1996 (1997).
- Zaera, F. Mechanisms of hydrocarbon conversion reactions on heterogeneous catalysts: analogies with organometallic chemistry. *Top Catal* **34**, 129-141 (2005).
- Zhang, H., Jin, M., Xiong, Y., Lim, B & Xia, Y. Catalysing sustainable fuel and chemical synthesis. *Acc. Chem. Res.* **46**, 1783-1794 (2013).
- Zhang, J. Z., Tsai, Y. T., Sangkaewwattana, K. L. & Goodwin, J. G. Structure sensitivity of cyclopropane hydrogenolysis on carbon-supported platinum. *J Catal* **280**, 89-95 (2011).
- Zhang, W., Zhu, Y., Niu, S. & Li, Y. A study of furfural decarbonylation on K-doped Pd/Al₂O₃ catalysts. *J. Mol. Catal. A: Chem.* **335**, 71-81 (2011).

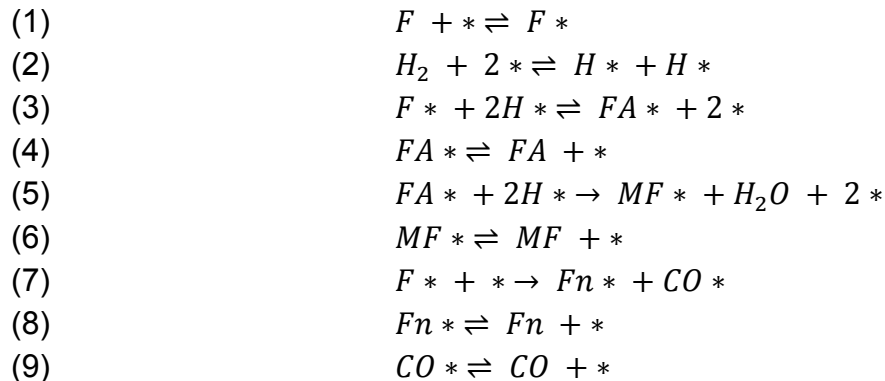
Appendix A

Langmuir-Hinshelwood Model of Furfural Reaction Network

In order to gain additional insight into the specific kinetic processes that were altered with increasing monolayer coverage, the rate data from the reaction order studies were fit to a simplified Langmuir-Hinshelwood model with the following assumptions:

1. Surface reactions were rate limiting
2. DC and HDO reactions were irreversible
3. Furfural and furfuryl alcohol adsorbed molecularly

With these assumptions, the following steps for the furfural reaction network were proposed:



Surface species and vacant sites are indicated by *. The rate limiting steps were assumed to be (3), (5), and (7) for production of furfuryl alcohol (or furfural, from furfuryl alcohol), methylfuran, and furan, respectively. Addition or removal of only a single H was considered to be rate limiting in steps (3) and (5) even though two are needed stoichiometrically. With these assumptions, explicit rate expressions for the production of F, FA, MF, Fn, and CO were derived as follows:

$$\begin{aligned}
(10) \quad & \text{Rate}_F = -k_3\theta_F\theta_H + k_{-3}\theta_{FA}\theta_V - k_7\theta_F \\
(11) \quad & \text{Rate}_{FA} = k_3\theta_F\theta_H - k_{-3}\theta_{FA}\theta_V - k_5\theta_{FA}\theta_H \\
(12) \quad & \text{Rate}_{MF} = k_5\theta_{FA}\theta_H \\
(13) \quad & \text{Rate}_{Fn} = k_7\theta_F \\
(14) \quad & \text{Rate}_{CO} = k_7\theta_F \\
(15) \quad & \text{Rate}_H = -k_3\theta_F\theta_H + k_{-3}\theta_{FA}\theta_V - k_5\theta_{FA}\theta_H
\end{aligned}$$

$$\begin{aligned}
(16) \quad & \theta_F = K_F P_F \theta_V \\
(17) \quad & \theta_H = (K_H P_H)^{0.5} \theta_V \\
(18) \quad & \theta_{FA} = K_{FA} P_{FA} \theta_V \\
(19) \quad & \theta_{MF} = K_{MF} P_{MF} \theta_V \\
(20) \quad & \theta_{Fn} = K_{Fn} P_{Fn} \theta_V \\
(21) \quad & \theta_{CO} = K_{CO} P_{CO} \theta_V
\end{aligned}$$

$$(22) \quad \theta_F + \theta_H + \theta_{FA} + \theta_{MF} + \theta_{Fn} + \theta_{CO} + \theta_{SAM} + \theta_V = 1$$

Because rate constants k_n and adsorption equilibrium constants K_n appeared as paired products in these expressions, they could not be solved for independently. We then proposed the following substitutions:

$$\begin{aligned}
(23) \quad & \varphi_{AH} = k_3 \times K_F \times (K_H)^{1/2} \\
(24) \quad & \varphi_{HDO} = k_5 \times K_{FA} \times (K_H)^{1/2} \\
(25) \quad & \varphi_{DC} = k_7 \times K_F \\
(26) \quad & \varphi_{ADH} = k_{-3} \times K_{FA}
\end{aligned}$$

These expressions represented the combined rate and adsorption equilibrium constants for a particular reaction step and were therefore subscripted with the associated reaction process where k_{-3} denoted the reverse process in (3). With these substitutions, the rate equations became:

$$\begin{aligned}
(27) \quad & \text{Rate}_F = -\varphi_{AH} P_F P_{H_2}^{1/2} \theta_V^2 + \varphi_{ADH} P_{FA} \theta_V^2 - \varphi_{DC} P_F \theta_V \\
(28) \quad & \text{Rate}_{FA} = \varphi_{AH} P_F P_{H_2}^{1/2} \theta_V^2 - \varphi_{ADH} P_{FA} \theta_V^2 - \varphi_{HDO} P_{FA} P_{H_2}^{1/2} \theta_V^2 \\
(29) \quad & \text{Rate}_{MF} = \varphi_{HDO} P_{FA} P_{H_2}^{1/2} \theta_V^2 \\
(30) \quad & \text{Rate}_{Fn} = \varphi_{DC} P_F \theta_V \\
(31) \quad & \text{Rate}_{CO} = \varphi_{DC} P_F \theta_V \\
(32) \quad & \text{Rate}_H = -\varphi_{AH} P_F P_{H_2}^{1/2} \theta_V^2 + \varphi_{ADH} P_{FA} \theta_V^2 - \varphi_{HDO} P_{FA} P_{H_2}^{1/2} \theta_V^2
\end{aligned}$$

The ϕ terms were then determined by performing a non-linear least squares fit to the kinetic data from the reaction order experiments. Without independent adsorption equilibrium constants, the coverage of individual species involved in the site balance could not be directly determined. Experimental reaction orders on the uncoated catalyst suggested that the surface coverage of furfural-derived intermediates was low. In this low coverage regime, we approximated Θ_V as the number of vacant sites excluding SAM coverage. SAM coverage was estimated using peak areas from CO DRIFTS experiments using the relationship $\theta_{SAM} = 1 - CO_{uncoated}/CO_{SAM}$ and was calculated separately for coverage on terrace sites ($\sim 1895 \text{ cm}^{-1}$) vs. edge sites ($\sim 2050 \text{ cm}^{-1}$). In order to account for different reaction processes occurring on different types of sites, Θ_V was replaced by the fraction of available sites estimated for each reaction process. Comparison on the peak areas from CO DRIFTS on the uncoated catalyst suggested that $\sim 10\%$ of the sites are edges and steps while 90% on particle terraces which is reasonable for particles of this size. If DC occurred primarily on terrace sites, HDO on edge sites, and AH and ADH on both, the rate equations then become:

$$(33) \quad Rate_F = -\phi_{AH} P_F P_{H_2}^{1/2} (1.0 * \theta_V^2) + \phi_{ADH} P_{FA} (1.0 * \theta_V^2) - \phi_{DC} P_F (0.9 * \theta_V^2)$$

$$(34) \quad Rate_{FA} = \phi_{AH} P_F P_{H_2}^{1/2} (1.0 * \theta_V^2) - \phi_{ADH} P_{FA} (1.0 * \theta_V^2) - \phi_{HDO} P_{FA} P_{H_2}^{1/2} (0.1 * \theta_V^2)$$

$$(35) \quad Rate_{MF} = \phi_{HDO} P_{FA} P_{H_2}^{1/2} (0.1 * \theta_V^2)$$

$$(36) \quad Rate_{Fn} = \phi_{DC} P_F (0.9 * \theta_V^2)$$

$$(37) \quad Rate_{CO} = \phi_{DC} P_F (0.9 * \theta_V^2)$$

$$(38) \quad Rate_H = -\phi_{AH} P_F P_{H_2}^{1/2} (1.0 * \theta_V^2) + \phi_{ADH} P_{FA} (1.0 * \theta_V^2) - \phi_{HDO} P_{FA} P_{H_2}^{1/2} (0.1 * \theta_V^2)$$

Figure A-1 shows the best fit values for ϕ terms using this approximation. Error bars are the standard error calculated from the nonlinear fit to reaction order data.

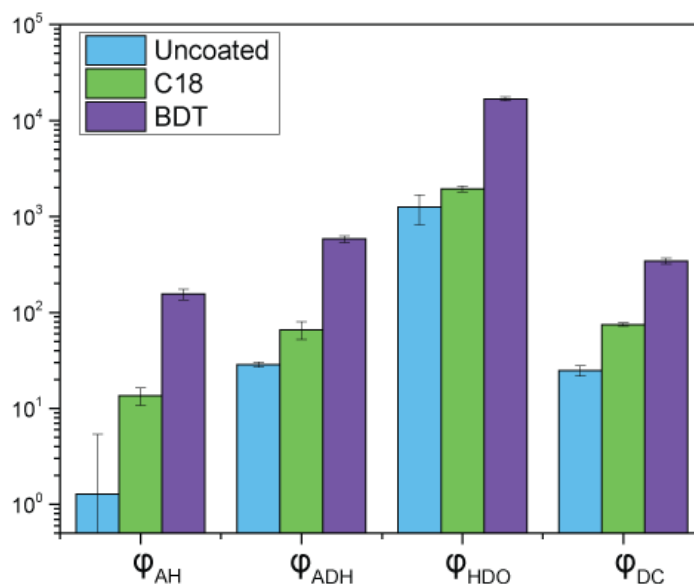


Figure A-1. Best fit rate parameters for ϕ terms. ϕ_{AH} and ϕ_{HDO} have units of ($s^{-1} \times atm^{-3/2}$) and ϕ_{ADH} and ϕ_{DC} have units of ($s^{-1} \times atm^{-1}$).

From the model, ϕ values were found to increase with increasing thiolate coverage. This result could be due to two major effects: 1) the presence of the thiols actually improved either the inherent rate constant and/or equilibrium constants for each of the reaction processes, or 2) the number of vacant sites was over-predicted by using CO adsorption areas from CO DRIFTS. Because the high reaction orders on the uncoated catalyst suggested a relatively low coverage of adsorbates for the surface, it is not likely that SAMs increased adsorption affinity of the reactants. In addition, for processes where the SAMs apparently shut down the reaction as in DC, it is not likely that the SAMs increased the inherent rate constant. Thus, this effect is likely due to over-prediction of the available adsorption sites using CO DRIFTS. This is not unexpected since the size of CO is much smaller than the reactants involved in this reaction, and it does not necessarily bind on the same ensemble of Pd atoms as the furanic reactants. Thus, an improved “titration” approach utilizing molecules the same size as the reactants would be needed for determining the available vacant sites on these catalysts.